

Davey et al, 2004

# **The Effectiveness of Transient Electromagnetics and Ground Penetrating Radar for Investigating Regolith**

**Honours Thesis**

Adam Davey<sup>1</sup>

**Supervisors**

John Joseph<sup>1</sup>, Graham Heinson<sup>1</sup>

<sup>1</sup>CRC LEME, School of Earth and Environmental Sciences, University of Adelaide, Adelaide SA 5005.

## Contents:

<a href="#">Abstract:</a> .....	3
<a href="#">Introduction:</a> .....	3
<a href="#">Methodology:</a> .....	4
<a href="#">Time Domain Electromagnetics (TEM)</a> .....	4
<a href="#">Fast Turn Off TEM</a> .....	5
<a href="#">TEM Data Processing</a> .....	6
<a href="#">GPR:</a> .....	6
<a href="#">Ground Penetrating Radar (GPR)</a> .....	6
<a href="#">GPR Survey Types:</a> .....	7
<a href="#">Wave Types:</a> .....	8
<a href="#">Frequencies of GPR:</a> .....	9
<a href="#">The Physics of GPR</a> .....	9
<a href="#">GPR Data Processing:</a> .....	14
<a href="#">Suitability of GPR:</a> .....	15
<a href="#">Experiments and Results:</a> .....	16
<a href="#">White Dam:</a> .....	16
<a href="#">TEM Survey in White Dam</a> .....	16
<a href="#">GPR Survey in White Dam</a> .....	17
<a href="#">Girilambone:</a> .....	20
<a href="#">TEM Survey in Girilambone:</a> .....	20
<a href="#">Discussion:</a> .....	25
<a href="#">White Dam:</a> .....	25
<a href="#">Girilambone:</a> .....	26
<a href="#">Conclusions:</a> .....	27

[Acknowledgements:](#).....28

[References:](#).....28

[List of Tables:](#) .....32

[List of Figures:](#).....33

## **Abstract:**

Regolith can be mapped at the surface using a variety of landform mapping methods. Subsurface regolith structures can be investigated by excavating costeans through the profile, but non-invasive geophysical methods, such as Ground Penetrating Radar (GPR) and shallow focussed Transient Electromagnetics (TEM), are much less destructive techniques that can be used to provide information on the physical properties of the subsurface. GPR offers exceptional resolution imagery of the subsurface, and TEM can be used to produce exceptional resistivity sections of the top several tens of metres. White Dam, Curnamona province, is a gold and copper prospect and is home to a regolith case study. The two geophysical methods were used here to investigate how well each performs in such an environment, and results were compared with the regolith landform map. Paleochannels in the Girilambone-Cobar area, New South Wales, were investigated using transient EM. Sets of non-magnetic and magnetic channels were selected, and TEM was undertaken in a single transect over each set, coincident with lines of drill holes. Both transects were approximately 2km in length, and passed 2 or 3 drill holes, allowing direct comparison of TEM resistivity plots with drill derived cross sections.

## **Introduction:**

Australia is a continent blanketed by a veneer of regolith\*, which has enormous impact on mining in the country, as it tends to cloak major economic mineral deposits, and may also host secondary deposits. The science of regolith is relatively new, and approaches in this field are steadily progressing through their developmental phases. The ability to understand the regolith is assisted by the growing understanding of regolith landforms structures, and how they interact with each other, and the subsurface. Landform mapping is one of the primary approaches, and provides a host of

## The Effectiveness of Transient Electromagnetics and Ground Penetrating Radar for Investigating Regolith

information but is limited by the exposure of regolith features. Subsurface regolith layers may be realised using other approaches, such as geophysics. Ground penetrating radar (GPR), for example, has been used to indicate and investigate subsurface regolith layers (Robertson et al, 2003). In environments where hands-on observations are not viable, such as on Mars, GPR could be useful for investigating the regolith profile (Grimm et al, 2003), as shown in mars-analogue environments (Campbell et al, 2002). Currently, studies are underway to assess the application of transient electromagnetics (TEM) to assess and manage dryland salinity in Australia, investigate groundwater with TEM and GPR (among other geophysical methods), and investigate regolith on Mars, using GPR and low frequency EM. Ground penetrating radar (GPR) and transient electromagnetics are both non-invasive techniques, so they may be undertaken with minimal environmental impacts. They are both straightforward enough that they can be used without rigorous expertise. Both techniques may be scaled for different survey requirements. GPR has a highly variable depth of investigation, of up to tens of metres. TEM can provide us with information from deep within the earth to depths as shallow as 2 metres and has traditionally seen extensive use as a minerals exploration tool. TEM can provide good vertical resolution in layered earth environments (Carlson and Zonge, 1996). The approach of this project is to assess how effectively TEM can be used to delineate paleochannels in the Girilambone-Cobar area in New South Wales, as well as to assess the effectiveness of GPR and TEM for providing information about the regolith in White Dam, South Australia.

### **Methodology:**

#### ***Time Domain Electromagnetics (TEM)***

TEM has seen extensive use as a minerals exploration tool, and can provide good vertical resolution in layered earth environments (Carlson and Zonge, 1996). TEM surveys tend to involve the transmission of a 50% duty cycle, time domain, square wave signal (alternating between positive,

## The Effectiveness of Transient Electromagnetics and Ground Penetrating Radar for Investigating Regolith

zero, and negative voltages (as shown in figure 1) into an ungrounded insulated loop of wire (known as a transmitting loop, which is laid out on the surface of the ground, as shown in figure 2 (Carlson and Zonge, 1996). Measurements are made, using a receiving loop, also shown in figure 2, whilst the transmitter is turned off, during which decaying secondary magnetic fields from subsurface conductors can be measured. The measured ground response is shown in figure 1. Shallow information is contained in the early part of the decay, with increasing time corresponding to increasing depth. TEM can be operated using a number of different configurations. Two common configurations are the vertical sounding mode and profiling mode using a fixed loop configuration, as shown in figure 3. The vertical sounding mode is less complex, but is more time consuming, as both loops and both units must be moved between readings. However, the transmitting and receiver units may be synchronised using a direct connection as both units do not have to be separated. For the fixed loop configuration, the transmitting loop remains connected to the transmitting unit, whilst the receiver unit is moved with the receiving loop. In this case, the receiver unit and the transmitting unit are synchronised using a highly accurate low-drift crystal clock in each unit. The vertical sounding configuration is most useful in a layered earth environment. The profiling (fixed loop) configuration is more effective for investigating 3D features; particularly steeply dipping or sub-vertical dike-like features (Zonge, 1992).

### **Fast Turn Off TEM**

In a fast turn off TEM system, the transmitted signal decays to zero very rapidly, without "ringing" or oscillations of either the electronics or the wire loops themselves, such that decay information from the very shallow subsurface may be measured. An example of a fast turn off TEM system, named NanoTEM, can collect data at depths of less than 2 metres.

## **TEM Data Processing**

TEM data is easily forward modelled, matching theoretical decay curves to those calculated for a given model, but the data must be prepared for optimum results. Data points which make up the decay curves for each station can be compared, and those which may be noise can be removed. This is known as trimming of the data and although subjective, is essential to remove noise and other spurious data which would otherwise misguide the modelling process. The aim of trimming is to increase the signal-to-noise ratio. There is a balance between the level of noise which should be removed, and the level of signal which needs to be retained. Sometimes, the signal may not be easily distinguished from noise, so the task of trimming becomes highly subjective. Points that do not seem (upon visual inspection) to lie within the trend of a decay curve, or data points with large error bars (showing variation between readings in a stack) tend to be removed. Modelling of TEM data is usually undertaken by calculating a forward model, and then refining it to suit the data. TEM data tends to be modelled under the premise that smooth transitions exist between blocks of contrasting conductivity. There are modelling techniques which use sharp contacts between bodies of varying conductivity, but these seem to be less common. Models produced through inversion of the data can be presented in the form of a conductivity vs depth pseudo-section for the vertical plane beneath the survey line.

## ***GPR:***

### **Ground Penetrating Radar (GPR)**

GPR is a geophysical method used to gain insights into the structure of the shallow subsurface. It has seen use as a non-destructive evaluation (NDE) method for a considerable period of time (Clemena, 1991 and Bungey et al, 1991) and is used in a variety of applications, including soil stratigraphy, groundwater flow studies, mapping bedrock fractures and determining depth to the water table (Davis and Annan, 1989). GPR works by sending a pulsed electromagnetic (EM) signal

## The Effectiveness of Transient Electromagnetics and Ground Penetrating Radar for Investigating Regolith

into the ground, and then measuring the reflections produced from certain interfaces within the subsurface. The signal is transmitted into the ground by the transmitting antenna. The receiving antenna picks up the reflections from the subsurface. Figure 4 shows the path of a reflected wave from the transmitting antenna to the receiving antenna. The data recorded for any given reflection is its relative intensity, and the time which the wave took to travel from the transmitter, reflect from the reflector and travel to the receiver (two way travel time, twt). The twt can be used to pinpoint the location of the reflector, and the intensity of a reflection provides some indication of the physical contrast over the reflector. The data can be displayed as an individual wavelet (also known as a Wave Train), or as a radarplot (also known as a radargram or waterfall plot)

### **GPR Survey Types:**

Reflection Profiling: The most common type of GPR survey, “reflection profiling”, involves moving both antennae along a survey line. For a step survey, the antennae are moved by a certain increment along the survey line, before a measurement is taken, and then antennae are moved again. For a continuous survey, the antennae are continuously moving, with measurements taken repeatedly at a constant rate. Continuous surveys may be conducted from the back of a vehicle, and are hence quicker. Step surveys can involve the stacking of several readings at each measurement point, increasing the quality, and hence clarity, of the data. Figure 5 shows how the ray paths differ for each of the different readings, and how the resulting data can be presented as a radarplot. It is important to note that the radarplot is a distorted image of the subsurface, as the reflections are plotted vertically below the antenna. The process of migration moves these reflections to the positions of reflectors from which they were produced. If the data is successfully migrated, then the reflections will all lie on the retrospective reflectors, and the plot will be a pseudo- image of the structures present in the subsurface. A depth conversion may be used to plot the reflectors with depth, so that a depth profile may be produced.



## The Effectiveness of Transient Electromagnetics and Ground Penetrating Radar for Investigating Regolith

Common Mid Point: To allow analysis of GPR velocity in the subsurface, A common mid-point (CMP) survey is often undertaken with reflection profiling surveys, and allows a NMO (Normal Move Out) correction to be applied to the data (Yilmaz, 1987). The antennas are moved apart, so that the point half way between the two antennas remains stationary, as shown in Figure 6a. Velocity analysis can be undertaken using CMP plots.

Transillumination: An innovation of GPR, transillumination involves placing the transmitter and receiver on opposite sides of the material to be surveyed, as shown in figure 6b. GPR waves can travel directly from the transmitter to the receiver, or can be reflected or refracted during transit. This may be especially useful in underground mining operations, where it has been used for tomography of blocks in between passageways

Drill Hole Surveys: If the transmitter is located at depth in a drill hole, the receiver can be moved around the surface, or in mine shafts, and a tomographical image of the subsurface can be gradually developed.

Ground Wave Surveys: Because the ground wave (the wave which travels through the top most component of the ground between the transmitter and receiver) has been exposed to part of the subsurface, it contains some information about it. A ground wave survey records only the ground wave to highlight the physical attributes of the top most portion of the subsurface.

Synthetic Aperture radar (SAR): This innovative form of GPR involves using a single antenna at multiple locations, or multiple antennae, to drastically improve the resolution of the resulting data. (Geo-Centres EFGPR information page)

### **Wave Types:**

There are several different types of waves evident on a GPR radarplot. Two large artefacts in the data are the air wave (a wave which travels directly from the transmitting antenna to the receiving antenna, through the air), and the ground wave (a wave which travels from the transmitting antenna to the receiving antenna through the top most portion of the subsurface. The waves that propagate

## The Effectiveness of Transient Electromagnetics and Ground Penetrating Radar for Investigating Regolith

down into the subsurface and reflect back up to the receiver are known as reflected waves. While ground waves can provide us with information about some of the physical attributes of the surface layer, the reflected wave provides us with far more detailed information about some of the physical attributes of the subsurface. (Oswald et al, 2003). The air wave arrives first, at a time dependent by the separation between the antennae. The ground wave arrives second, at a time dependent on the electrical properties of the thin surface layer through which it propagates.

### **Frequencies of GPR:**

One of the main factors distinguishing various GPR systems is the frequency of GPR signal. This frequency is dependent upon the length of antenna. Typical frequencies in use today range from 10MHz to 1GHz, and the corresponding antennae range in length from 10 centimetres to 10 metres. An antenna consists of a looped wire, and tends to be encased in a medium not detrimental to the GPR signal. Antennae may be shielded to reduce the “above ground” input. The frequency of GPR used will determine a range of survey attributes, including the resolution of the data, the depth to which useful information may be extracted, and the step size necessary to ensure that aliasing does not occur. Table 1 shows a table of frequencies and how they compare with each other.

### **The Physics of GPR**

An electromagnetic pulse, with orthogonal electric and magnetic field components, as shown in figure 8 (figure 7 does not exist), is emitted from the transmitting antenna. Both the magnetic and electric components are related by the dielectric permittivity,  $\epsilon$ , of the propagation medium, as shown in the following equation, which has been derived from Maxwell’s third equation,

$$- \frac{dH}{dx} = \epsilon \frac{dE}{dt} \quad (4)$$

For any given medium, the permittivity is the ratio of electric displacement (in coulombs per square metre) to the electric field strength (in volts per metre). Permittivity is specified in farads per metre,

## The Effectiveness of Transient Electromagnetics and Ground Penetrating Radar for Investigating Regolith

but can be represented as relative permittivity (a ratio of the permittivity to the absolute permittivity of a vacuum ( $\epsilon_0 = 8.854 \times 10^{-12} \text{Fm}^{-1}$ )). Table 2 shows a table of relative permittivity for a range of given materials (in ideal conditions), with corresponding EM velocity. When a medium is subjected to an applied electric field, a current is produced. This current has two components. Conduction currents involve the flow of free electrons, while displacement currents do not, as shown in figure 9. A perfect dielectric is a material that exhibits displacement currents, but no conduction currents. The velocity of propagation of an EM wave through the ground can be represented in terms of the dielectric permittivity and the magnetic permeability. The dielectric permittivity varies for different lithologies, and different physical conditions. A variation in the dielectric permittivity will produce a dielectric boundary. In general, EM energy incident on such a boundary will be partly reflected, and partly transmitted through the boundary. Fresnel equations provide the ratio of the electric field amplitudes of the reflected and transmitted waves.

## The Effectiveness of Transient Electromagnetics and Ground Penetrating Radar for Investigating Regolith

The intensity of reflections can be quantified using power (or intensity) coefficients, which are given by:

$$R = |r|^2 \quad (11) \quad T = |t|^2 \quad (13)$$

$$R_{\perp} = |r_{\perp}|^2 \quad (12) \quad T_{\perp} = |t_{\perp}|^2 \quad (14)$$

R represents the intensity of the reflected wave, while T represents the intensity of the transmitted wave. The subscripts represent the mode of the wave. The two parallel vertical lines indicate TM (Transverse magnetic field mode), while the pair of perpendicular lines indicates TE (Transverse electric field mode). Transmitted waves are refracted, as the propagation velocity varies on either side of the interface. Figure 10 illustrates TE and TM modes. For TE mode, the transmission and reflection coefficients are respectively given in terms of the angle of incidence ( $\theta$ ), by

$$t_{\perp} = \frac{2\sin\theta' \cos\theta}{\sin(\theta+\theta')} \quad (15)$$

and

$$r_{\perp} = -\frac{\sin(\theta-\theta')}{\sin(\theta+\theta')} \quad (16)$$

For TM mode, the transmission and reflection coefficients are respectively given by

$$t_{\parallel} = \frac{2\sin\theta' \cos\theta}{\sin(\theta+\theta')\cos(\theta-\theta')} \quad (17)$$

and

$$r_{\parallel} = \frac{\tan(\theta-\theta')}{\tan(\theta+\theta')} = \frac{\sin\theta' \cos\theta' - \sin\theta \cos\theta}{\sin\theta' \cos\theta' + \sin\theta \cos\theta} \quad (18)$$

## The Effectiveness of Transient Electromagnetics and Ground Penetrating Radar for Investigating Regolith

The TE component of the electric field may be phase shifted upon reflection, with phase shift,  $\Delta\phi$ , given by

$$\Delta\phi = \begin{cases} \pi, & \epsilon_2 > \epsilon_1 \\ 0, & \epsilon_2 < \epsilon_1 \end{cases} \quad (19)$$

At normal incidence (when  $\theta=90^\circ$ ), with  $\epsilon_2 > \epsilon_1$ , the reflection and transmission coefficients for both TE and TM modes are respectively given by

$$\mathbf{r}_\perp = - \frac{\epsilon_2 - \epsilon_1}{\epsilon_2 + \epsilon_1} \quad (20)$$

and

$$\mathbf{t}_\perp = \frac{2\epsilon_1}{\epsilon_2 + \epsilon_1} \quad (21)$$

from which the reflectance and transmittance coefficients for a given interface can be respectively

given as

$$R_\perp = \left| \frac{\mathbf{E}_r}{\mathbf{E}_i} \right|^2 = \left( \frac{\epsilon_2 - \epsilon_1}{\epsilon_2 + \epsilon_1} \right)^2 \quad (22)$$

and

$$T_\perp = \left| \frac{\mathbf{E}_t}{\mathbf{E}_i} \right|^2 = \frac{4\epsilon_1^2}{(\epsilon_2 + \epsilon_1)^2} \quad (23)$$

See Figure 10 for notation in above diagram.

The reflectance and transmittance coefficients are denoted R and T respectively and are the ratio of the reflected or transmitted electric field amplitude, respectively, to the incident electric field

## The Effectiveness of Transient Electromagnetics and Ground Penetrating Radar for Investigating Regolith

amplitude. The two modes, TE and TM, each relate to a specific orientation of antennas. Figure 11 shows the relationship of the relative orientation of the antennae and the corresponding mode.

The transmitting and receiving antennae are usually separate, but they may be integrated into a single antenna. Each antenna contains a loop of wire, through which a current is conducted to produce the EM waves. Different sized antennae consist of different sized loops, and hence produce EM radiation of different frequencies. GPR systems generally use frequencies somewhere in between 10MHz and 1GHz. The corresponding wavelengths vary from approximately 10cm to 10m. The frequency of GPR is fixed for any antenna (except, intuitively enough, for innovative multi-frequency antennae). The depth to which GPR can image the subsurface depends on both the GPR frequency, and the physical properties of the subsurface. The choice of antenna depends largely on the aim of the survey, and the suitability of various antenna to achieving this aim. Generally, higher frequency antenna are used for smaller, higher resolution surveys, whilst lower frequency antenna tend to be used on a much broader scale to yield much lower resolution data. The size of the antennas is characteristic of the GPR frequency that it will produce. A 10MHz antenna, for example, is approximately 10 metres in length. The antenna size may be critical if surface conditions (ie vegetation or topography) inhibit the use of equipment of such size. Increased lateral resolution is achieved by decreasing the spacing between readings. As this is at the expense of the speed of the survey, it is also at the expense of survey length which can be accomplished in a given period of time. The penetration depth is the depth to which GPR can resolve information. This depth is primarily dependent upon the rate at which the GPR signal is attenuated by the subsurface. The rate of attenuation is controlled primarily by the conductivity of the propagation medium (Cai and McMechan, 1999). Highly conductive (ie saline) fluids and clay are generally responsible for high attenuation rates. Quartz rich mediums, with a low saturation of conductive fluids tend to exhibit quite low attenuation, as they tend to be highly resistive. The lower the attenuation rate, the deeper the penetration depth, and vice versa. In addition to conduction losses, attenuation is also a

## The Effectiveness of Transient Electromagnetics and Ground Penetrating Radar for Investigating Regolith

result of scattering and geometrical spreading. Small scale heterogeneities can scatter the propagating signal, attenuating higher frequency data to a greater degree.

Because of their highly attenuating nature, clay rich profiles, as well as those saturated with saline fluid tend to be detrimental to GPR, and penetration depths into such mediums can be severely decreased (Olhoeft, 1984). Quartz rich sedimentary profiles lend themselves to GPR, and surveys have been successfully carried out to image the sedimentary structures present within these units. Table 3 shows typical values for a range of materials. The most conductive of these materials (clay and seawater), have the highest attenuation rates. Below the penetration depth, any reflections are attenuated to below noise levels before they reach the surface (Smith et al, 1995). In quartz rich sandstones, this depth may be many tens of metres (Jol et al, 2003), whereas in clay rich environments, it may be as low as several centimetres (Smith et al, 1995). Zones of increased conductivity along a survey line should show up as patches of blurred signal, indicating an increase in the rate of signal attenuation.

### **GPR Data Processing:**

GPR data processing is being developed as its applications increase. A vast number of software packages are available to process the data, and because of the similarities between GPR and seismic data, seismic processing techniques can sometimes be used. There are several aims of data processing. For the analysis of data, processing may aim to differentiate (and possibly remove) noise from signal within the data. Data processing can also be used to make the data more visually appealing. Whilst data can be interpreted without any processing, this is highly subjective, and would be very similar to interpreting seismic depth sections without first processing the data. Like seismic data, it is possible to transform the dataset into a different domain (such as using a Fourier transform to shift the data into the frequency domain), such that noise and signal, or different components of signal may be distinguished, and perhaps separated. Common processing steps for GPR are filters to remove noise produced by the survey itself, horizontal (adjacent trace) and

## The Effectiveness of Transient Electromagnetics and Ground Penetrating Radar for Investigating Regolith

vertical (down trace) averaging, static corrections (to factor topography into the twt (two way time) sections), gains (to normalise the amplitudes for easy viewing), and various other filters which highlight certain features. The processing steps used will depend on the intended output. Obvious sources of noise need to be kept in mind during processing, as noise can be processed to make it appear more like signal than noise.

### **Suitability of GPR:**

GPR has been shown to be effective in delivering high resolution imagery of the subsurface (Jol et al, 2003, Van Dam et al, 2003, Harari, 1996 , McMechan et al, 1998, Kruse et al, 2000). The performance of the technique will depend greatly on the site at which it is to be used, as well as the design (and implementation) of the survey. Providing the subsurface is not too conductive, reasonable penetration depths of at least several metres, and possibly up to several tens of metres may be achieved. Two main advantages of GPR over other techniques is in its resolving power, and ease of use, and if a site is suited, then it may be imaged and otherwise investigated using GPR (David et al, 1995). A wide range of structures may be delineated using a range of various GPR methods. Structure such as cm scale cross bedding may be imaged such that the orientation of successive beds can be measured, and this information can be used to interpret the depositional history of these cross bed sets. Much larger scale structures, such as the interface between transported cover, in situ cover, and bed rock may also be imaged over large distances, and the continuity of such lateral structures may be investigated, providing there are suitable contrasts in the electrical properties of the structure compared to the medium in which the structure is located.



## **Experiments and Results:**

### ***White Dam:***

White Dam is a gold and copper prospect located approximately 31 km NE of Olary, in South Australia, as shown in figure 13 (figure 12 does not exist). Detected first by a regional geochemical soil survey, the deposit is blanketed by up to 2 metres of recent sediments. Although the topography is very subdued, there are several distinct types of regolith in and around the area of mineralisation. The area is due to be excavated, and as such, provides a unique opportunity for a regolith case study, angled at providing further insights into such deposits, with a focus on how they are related to the regolith. Six large costeans (rectangular pits or trenches) have been excavated at the site, as shown in figure 14 and the profiles exposed in these costean walls are being closely studied. Regolith landform mapping has been undertaken, with each landform investigated thoroughly. The objective of these surveys were to assess the viability of GPR for characterising the regolith as part of the much broader White Dam regolith case study. A regolith landform map, shown in figure 15, kindly provided by Aaron Brown, was used to plan the survey lines for both the NanoTEM and GPR surveys in White Dam.

### **TEM Survey in White Dam**

Two days of field work (out of a total of four ) were designated to the NanoTEM surveys at White Dam. The survey lines were orientated as shown in figure 16, and would be coincident with 25MHz GPR survey lines. The two lines undertaken in the time allowed were positioned to cross several of the landform units (the first cut through a number of varying landforms, and the second crossed over a boundary between depositional and erosional plains. Figure 17 does not exist.

For the survey, the receiving loop (a 5 x 5 metre square wire loop) was located in the middle of the transmitting loop (a 20 x 20 metre square wire loop), and readings were taken at 20 metre intervals. The wires were easily threaded around the abundant low lying vegetation and excessive care was

## The Effectiveness of Transient Electromagnetics and Ground Penetrating Radar for Investigating Regolith

taken to ensure the sides of both transmitting and receiving loops were parallel to each other. Time was the greatest limiting factor. Consideration was given to the location of the vehicle (an obvious source of noise), far enough away as to minimise its impact on the survey.

The data were processed at Zonge Engineering, in Adelaide, with smooth-edge inversion used to produce a smooth 2 dimensional contoured resistivity depth sections for each line. Figures 18a and 18b show the resistivity plots for line 1 and line 2 respectively. Figure 19 shows the same profiles overlaid on the regolith landform map. Line 1 shows the erosional plain as a resistive zone, and the northern depositional plain as a more conductive zone. Line 2 shows a distinctive contrast over the boundary between the depositional and erosional plains. The erosional plain overlies more resistive bedrock, and the depositional plane is dominated by sediments consolidated to a much lesser degree. These unconsolidated sediments would be relatively permeable, so a build up of fluid in the shallow subsurface would be expected after rains. Because rains were noted in several of the weeks leading up to the surveys, and the track we used to access the site was still boggy in parts, it may be reasonable to expect that the conductivity contrast between the two regolith landforms might decrease significantly if the survey was undertaken during much dryer weather.

### **GPR Survey in White Dam**

The objectives of the GPR surveys in White Dam were to investigate the suitability of the technique in delineating and/or providing information about subsurface interfaces, such as that between transported and in-situ regolith, and to investigate links between GPR signal behaviour and conductivity of the propagation medium, as well as to investigate the effectiveness of two different frequencies of GPR. Our choices of GPR frequency were limited by the availability of antennae. The two frequencies used in White Dam were 25 and 50MHz, for which the antennae are shown in figure 20. The antennae were used in the TE configuration only, as this is the most common setup. The survey lines were planned on-site, with particular consideration given to the regolith landform map, and to the location of costeans from which much information has been and is being extracted.

## The Effectiveness of Transient Electromagnetics and Ground Penetrating Radar for Investigating Regolith

The costeans, which are orientated almost exactly North-South, would have caused difficulties with surveys of any other orientation so all survey lines were aligned North-South, parallel to the costeans. The higher frequency (50MHz) surveys, shown in figure 21 were marginally longer than the costeans themselves, with the intention of drawing direct correlations to the geology observed in the walls of the costeans. The lower frequency (25MHz) survey lines, shown in figure 22, extended much further through the area. The data from these surveys was not expected to allow for much correlation directly to the costeans, but rather correlation to the higher frequency data, and then to geology further away from the costeans. Two transmitting units were available for use with the antennae, with voltages of 400 and 1000 volts. We used the 1000V transmitter with both frequencies of antennae. Tape measures were used to ensure consistency in the placement of the antennae for each reading. Once the equipment had been set up from boxes in the vehicle, the vehicle was relocated away from the survey line, and the first reading was taken. An antenna mounted switch was used to trigger a reading. After the first reading, both antennae were moved along the tape measure by a distance equal to the step size, and the trolley (in which the equipment was carried) was also moved forward along the line so that it was far as possible from the antennae, but not so far as to put tension on the optic fibre cables through which the signals were being carried between the control unit and the antennae. The data were occasionally monitored using a laptop computer located in the trolley, as it was being taken. Equipment malfunction was indicated by the lack of discernible GPR signal. When this happened, the survey was stopped and the problem was overcome before continuing with the survey. Occasionally, the measuring tapes were brought forward of the equipment, and laid out to continue the survey line. The vegetation at White Dam, which consisted primarily of saltbush and bluebush, was extremely detrimental to the placement of the antennae flat against the ground, as illustrated in figure 23. The bushes themselves acted to hold the antennas away from the ground, while their roots have preferentially protected the ground below from erosion, leading to soil being raised, under the bushes. In the case of white dam, some sort of

## The Effectiveness of Transient Electromagnetics and Ground Penetrating Radar for Investigating Regolith

system could presumably be engineered to overcome the obstacle of the plants but this was far beyond the scope of this project. In the field, the possible effects of the costeans was considered, but was greatly underestimated. Due to space restrictions, the same trolley was used for both the NanoTEM and GPR surveys. This particular trolley, constructed from steel, was an excellent GPR reflector, and the distance between it and the antennae was not kept constant, so in addition to its presence in the data set as noise, it is variable, and hence not easy to differentiate and remove. Previous work in the area has utilised steel markers, at 25 and 50 metre intervals. There were also drill holes at similar spacings. Parabolic reflections produced by point reflectors in the data (such as figure 24) can be attributed to either the drill holes, the steel markers, or possibly to both. Large-scale horizontal reflectors throughout all data sets collected in most certainly noise due to the equipment, which the Dewow filter was ineffective in removing. This horizontal nature of these features, and the similarity between their frequency and that of the transmitting antenna, suggests this is systematic noise (noise produced by the survey itself). Where the line passes a costean, the reflections produced can be seen as large amplitude hyperbolic features in the data. Costeans 1 and 2 are shown as reflectors in figure 25. Line 4 (figure 26) is least affected by the costean reflections as it is a long line, and only passes by a costean at its southern-most end. Patches where the radar plot is blurred seem to indicate zones of increased conductivity. In White Dam, we collected both the NanoTEM and GPR data. The two lines of NanoTEM were coincident with 2 (out of 4) lines of 25MHz GPR. The conductivity pseudo-sections could be used to estimate the conductivity, and hence to differentiate structurally controlled events in the GPR data from attenuation due to increased conductivity. The resistivity plot, in the case of NanoTEM Line 2, at White Dam, simply showed what would have been expected from interpretation of the regolith landforms present in the area. The GPR data shows patches of attenuation which seem to correlate roughly with the more conductive regions within the subsurface, and the difference between data in the conductive and resistive areas is shown in figure 27. The first trace is through the more conductive depositional

## The Effectiveness of Transient Electromagnetics and Ground Penetrating Radar for Investigating Regolith

plane to the north of the line, and the second is through the more resistive bedrock (with very shallow cover). A GPR antenna is designed to output a single frequency, but as this frequency is pulsed, a range of frequencies is transmitted. The signal consists of a range of frequencies, and these frequencies are attenuated at different rates. The higher frequency data is more easily attenuated than the lower frequency data (which in this case seems to be larger amplitude horizontal noise events). The signal through the more conductive medium has been subjected to a higher level of attenuation, and hence exhibits suppression of higher frequency data. The signal through the more resistive medium has been subjected to a much smaller degree of attenuation, and hence exhibits much less suppression of the higher frequency data. The character or appearance of the waves relative to each other could be used to estimate relative conductivities (which is more conductive than the other).

### ***Girilambone:***

The Girilambone-Cobar region is located in between the towns of Girilambone and Cobar in New South Wales, approximately 400km East of Broken Hill. The area, which is part of the Sussex-Coolabah sheet, has extensive regolith cover and is dominated by erosional plains with colluvium and alluvium as well as alluvial valleys associated with the Darling River (Gibson, 1999), and is shown in figure 28. The area, which is home to several large economic mineral deposits, is currently being investigated from several different angles. Several airborne geophysical methods have been flown over the area, including radiometrics and magnetics. A comprehensive drilling program has been carried out through the region, and a suite of detailed regolith and landform evolution studies are also underway.

### **TEM Survey in Girilambone:**

The NanoTEM surveys were undertaken in Girilambone, with the objectives of delineating paleochannels as part of the much more extensive CRC-LEME project framework within the

## The Effectiveness of Transient Electromagnetics and Ground Penetrating Radar for Investigating Regolith

region, and to demonstrate the effectiveness of NanoTEM in completing such a task. The Sussex-Coolabah drilling program involved drilling along Booroomugga, Elmore and Coolabah roads, as shown in figure 29. The drill holes are located at approximately 1-3 kilometre intervals and reach an average depth of 18.6 metres. This drilling program provided data that was used in conjunction with remotely sensed data sets (eg. Radiometrics, magnetics, and a DEM) to produce geological cross sections cross cutting the area.

Three sets of paleochannels were selected as possible locations for the NanoTEM surveys, and two were chosen as they were suitable given the time constraint of 3-4 days in the field area. The third set was deemed far too complex, and would have mandated a much longer survey. Each set of paleochannels contained a channel with a strong magnetic signature, and one with a much weaker magnetic signature. Planned survey lines 1 and 2 were chosen because there is a distinctive magnetic anomaly with each. Figures 30 and 31 show the 1.5vd (vertical derivative) magnetics image and drill-derived geological section for line 1. Figures 32 and 33 show the 1.5vd magnetics image and drill-derived geological section for line 2.

We used a 5m x 5m receiving loop, centred in a 20m x 20m transmitting loop. The transmitting loop consisted of four segments of lightly insulated electrical wire, arranged to form a square. Three corners of this square were joined, at the remaining corner, the two loose ends were connected to the transmitter unit to form the transmitting circuit. The length of wire joining the receiving loop to the receiving unit was measured such that when it was (carefully) pulled taught, the receiving loop was centred in the transmitting loop. In addition, three 20 metre long segments of wire were used to allow the construction of a second transmitting loop while the first loop was being used. After sufficient readings had been taken at the first station, the transmitter was connected to the second loop, which had already been set up, and the receiving loop was carried into the centre of the second loop, while the trolley with the transmitting and receiving loops remained at the same position. While this was taking place, the segments of the first transmitting loops (with the exception of the

## The Effectiveness of Transient Electromagnetics and Ground Penetrating Radar for Investigating Regolith

segment shared by the two adjacent transmitting loops) was moved to the opposite side of the second transmitting loop. This movement of the survey is shown in figure 34. After sufficient readings had been taken using this second transmitting loop, both this loop and the trolley (into which the receiving loop was bundled) was moved along to allow for the following two readings, in an identical fashion to the first two readings. This method was repeated throughout the day. A handheld GPS receiver was used at the first station, and then at ten station (approximately 200 metre) intervals, to record the spatial progression of the survey and to account for bends in the road. At several points, 2 different GPS receivers were compared to ensure consistency of readings. Each night, data was 'dumped' onto two laptop computers, and all data was also backed up on floppy disks. Although the memory capacity of the receiving unit was sufficient to hold all the data collected over the 4 days, backed up copies were kept to avoid the corruption or other irreconcilable loss of data. On the last day, the "alias filter" was accidentally turned off, which altered the way in which the data was recorded, and provided several problems when we attempted to invert this section of the survey. The raw data consists of a decay curve for each reading, with error bars showing variations between readings taken at the same station. For each reading, we had the receiving unit set so that 256 readings were stacked to form one average reading. Three of these stacked readings were taken at each station. These three readings were compared with error bars, using the plotting capability of the receiving unit, and when observed to be satisfactory, the loops were moved for the next reading. Each reading was stored in a data block. Each data block is allocated a unique integer, incremented 1 from the previous data block. Stored in each data block was such information as the station number. For each station, an arbitrary station number was assigned. Hand written notes allow for these block numbers and station numbers to be reconciled to reconstruct the path of the survey. If one or several readings were found to be unusual, the equipment was checked and the affected data blocks were flagged electronically and noted in the written notes, so that it would not be used in any processing, and may even be removed.. The road

## The Effectiveness of Transient Electromagnetics and Ground Penetrating Radar for Investigating Regolith

could have been a significant source of noise, but fortunately, any such noise was not excessive. The road was unsealed, and lay along an old fence line, of which we found buried metal remnants (fence wire of various thicknesses and lengths, and metal spacers) along the entirety of both survey lines. This metal within the top few tens of centimetres, would have provided the noise in the 'early time' data. The batteries for the transmitter lasted for the entire day, but a spare 12 volt lead acid (car-type) battery was carried in case the primary battery went flat. Each night, the battery for the transmitter and the receiver's internal power source were recharged using a mains-powered charger. This was deemed sufficient for a days usage. However, on one occasion, the receiver's internal power source dropped below a certain voltage which flagged several error messages. Unfortunately, we did not have the appropriate cable, so we had to abandon the survey until the following day. A 4 digit binary number represented an amplification factor. Where the transmitting loop had been accidentally left disconnected, an amplification reading of 0400 was observed, indicating that something untoward had happened. A similar reading would be likely if the ground was particularly resistive, resulting in a poor electrical coupling with the ground. In much more conductive terrains, where there is a good EM coupling with the ground, the secondary field measured with the receiving loop is strong, and an amplification factor of 0000 is observed, which indicates that amplification is not required. On a laptop, the downloaded data was saved into a raw data file, which was 'shredded'. This step is the reformatting of the data into a more processing friendly form so that it may be inverted and a model produced. The inversion program used favours smooth contrasts, rather than sharp contacts, such as those between paleochannel sediments and the rock into which the channel was incised. Sharp boundary inversion would have been desirable, but was not available for this project. Several assumptions are used to greatly simplify the inversion process, such as that the magnetic permeability of the subsurface remains constant. This leads to the relation of the intensity of the induced field to the conductivity of the propagation medium. In many cases, this assumption is reasonable, but particularly where there are concentrations of maghemite, this



## The Effectiveness of Transient Electromagnetics and Ground Penetrating Radar for Investigating Regolith

assumption can lead to overestimation of conductivity. The magnetic susceptibility of magnetite and maghemite is three orders of magnitude greater than that of other iron-bearing minerals within the regolith profile. A reasonable concentration of these minerals within the regolith profile would perhaps increase the modeled conductivity by up to 400%, if the magnetic susceptibility is not accounted for when modeling the TEM data. Where Magnetic information is available, such as over our survey lines, it should be possible to use these magnetic profiles to determine the concentrations of maghemite in the stratigraphic profile, and to account for the effects of changes in the magnetic permeability.

Resistivity plots for lines 1 and 2 are shown in figures 35 and 36, respectively. Line 1 shows a paleochannel, which is filled with sediments which are more conductive than the host material into which the channel was cut. Although the interface between the channel and the host rock is quite well defined in the data, the smoothed transition is an artefact of the inversion process, and the actual contact would presumably be much sharper. If this channel contained maghemite, the associated conductivity anomaly would have been over-estimated by the inversion process, and hence the actual values for conductivity would be lower. Line 2 is over a much more complex set of paleochannels, the data is much less clear, but with the aid of other datasets, can be interpreted to define the outlines of the various distinct channels. In line 2, several of the stations near the end of this line did not have an alias filter, so there is some discontinuity between these and prior stations. In Girilambone, the other datasets include drilling data, cross sections derived from this data, and a range of airborne geophysical data (such as magnetics, and radiometrics). To correct the conductivity profile for the presence of maghemite, a magnetic profile along the same line would be used to model the spatial distribution of the maghemite, and this would be taken into account when re-modelling or interpreting the conductivity pseudo-sections. More within the scope of this paper, the cross sections derived from the drilling data (and other information such as magnetic lineaments) can be refined using the conductivity plots. Whilst the boundaries modelled between

## The Effectiveness of Transient Electromagnetics and Ground Penetrating Radar for Investigating Regolith

blocks of contrasting conductivity are excessively smooth, the approximate shape, orientation, and location of these boundaries can be approximated, although the depth of these boundaries will be affected by the smoothing effect of the inversion process. In 37a to 37g, drilling-information lithology information has been plotted against the resistivity depth sections to see how well the two sets of data correlate vertically. Figure 38a and 38b show the drill holes and survey lines 1 and 2 respectively. In line 1 of the Girilambone NanoTEM data, the paleochannel seems to be very well defined in the data, and there is good correlation between the cross section and the resistivity section, but the conductivity anomaly which appears to correlate with the paleochannel has been modelled several tens of metres deeper in the resistivity section. If the inversion was biased towards sharper boundaries, which would suit these paleochannels, then perhaps the modelled conductivity would correlate vertically with the features observed in the drilling data. Line 2 from the Girilambone data also shows interesting correlation, but again the depths seem to have been overestimated by the inversion process. The plots show good lateral correlation with the drill-derived sections, but it seems the depth to the more conductive bodies has been overestimated.

### **Discussion:**

#### ***White Dam:***

The resistivity plots showed conductive zones consistent with a build up of moisture in the regolith profile, particularly as it was a matter of days since rains had been noted in the area. Such contrasts between the different regolith landforms may not have been prominent without such a build up of moisture. As with the Girilambone NanoTEM data, the plots seem to finger out below approximately 10 metres, and the depths for the conductivity anomalies may have been overestimated. NanoTEM is able to, in exceptional circumstances, provide data from a depth as shallow as 2 metres, so the information shown for depths shallower than this may not be realistic. Patches of increased attenuation in the GPR data are more prominent and abundant in the conductive zones

## The Effectiveness of Transient Electromagnetics and Ground Penetrating Radar for Investigating Regolith

shown in the NanoTEM data. It may have been appropriate to try several configurations with the GPR antennae. The sensitivity of different configurations to different noise sources and different subsurface interfaces and structures would have been different, as the regolith profile is not a homogenous half-space. With the benefit of after sight, I would plan the surveys at White Dam differently. Two survey lines, each of approximately 1 kilometre in length, orientated NW-SE transecting the various regolith landforms, but sufficiently distanced from the costeans, would have been used for several geophysical techniques. Such a pair of survey lines would avoid noise from the costeans, and may provide insights not available from the costeans of surface expression of the regolith profile. The obvious noise sources could be removed simply by giving such factors more consideration prior to undertaking such surveys. Different configurations of GPR used along the lines may highlight different features in the regolith profile.

### ***Girilambone:***

NanoTEM was easy to use, especially as the road was almost wide enough for the entire array. Sources of noise near the survey lines were minimal, and the road did not seem to have a significant impact, though the buried remnants of a fence line along the entirety of both survey lines were a possible source of early-time noise. The drill hole and airborne geophysical data was used to construct the drill-derived geological sections through the area. The plots of resistivity show the paleochannels observed in the sections. The NanoTEM plots compare very well with these sections, laterally along the profile, even despite the apparent excessive depths estimated for the conductivity anomalies. Below depths of approximately 30 metres, the resistivity depth sections seem to show downward fingering, suggesting that data below this depth is not realistic. Although their depths seem to have been overestimated, the paleochannels in both lines have been resolved, at least laterally, to a greater level than with the drilling and airborne geophysics data. Even without remodelling the data using sharp-edge inversion methods, the resistivity plots could be used to constrain existing sections. Unlike the field work at White Dam, the benefit of after sight would not

## The Effectiveness of Transient Electromagnetics and Ground Penetrating Radar for Investigating Regolith

have made such a dramatic difference. NanoTEM seems to be a much more resilient technique than GPR, even despite the challenges (excessive smoothing, depth inconsistencies) resulting from the method of inversion used to model the data.

### **Conclusions:**

Both NanoTEM and GPR are simple to use. Although NanoTEM is a more resilient technique, both can be adapted to many different environments, and can provide a host of information without the need for invasive methods. GPR was more sensitive to errors in the implementation of the surveys, but with more thorough planning, and more attention paid to obvious sources of noise, it can be very effective at providing high resolution images of the shallow sub surface. GPR surveys can be greatly affected by the presence of structures such as costeans. GPR would have shown much better correlation with the profiles observed in the costean walls, if the survey had been undertaken prior to the excavation of those costeans. In the case of White Dam, this was not possible, but in studies where it is, the full potential of GPR may be greater realised. NanoTEM was shown to provide data from depths as shallow as several metres, with excellent lateral correlation with the other datasets available. In White Dam, the data collected shows the value of regolith landform mapping, as the regolith landforms are related to what we saw, using the two geophysical methods. In Girilambone, the two techniques were shown to be effective in imaging sub-surface regolith structure.

## **Acknowledgements:**

Particular thanks go to CRC-LEME for project funding and support throughout the project.

Thanks also go to:

-Zonge Engineering, for the loan of their equipment, remote assistance and troubleshooting, and for their support in data processing.

-Benjamin Alan Campbell for his assistance in the entirety of the White Dam field work.

-Jessie Davey and Rachel Maier for their assistance throughout the Girilambone field work.

-Jessie Davey for her work on the White Dam data.

-Ken G. McQueen, and his honours student, Dougle C. Munro, for their support particularly in Girilambone and for introducing us to the more classy establishments in the city of Cobar.

-My supervisors, John Joseph and Graham Heinson for their exceptional support and assistance throughout.

## **References:**

Bungey, J.H., Millard, S.G. and Shaw, M.R., 1991. "The use of sub-surface radar for structural assessment of insitu concrete", A.C.I., SP128/31, Vol. 2, pp. 497-514.

Cai, J. and McMechan, G.A. (1999) "2-D ray-based tomography for velocity, layer shape, and attenuation from GPR data.", Geophysics, 64, p 1579–1593

Campbell, B.A., Grant, J.A., and Maxwell, T., (2002) "Radar Penetration in Mars Analog Environments" Lunar and Planetary Science XXXIII

## The Effectiveness of Transient Electromagnetics and Ground Penetrating Radar for Investigating Regolith

Carlson, N. R. and Zonge, K.L., 1996 “Case Histories of Buried Borehole Detection: An Exercise in Flexibility”, Presented at the Environmental and Engineering Geophysical Society SAGEEP '96, Keystone, Colorado.

Chan, R.A., Greene, R.S.B., de Souza Kovacs, N., Maly, B.E.R, McQueen, K.G. and Scott, K.M., (2003) “Regolith, geomorphology, geochemistry and mineralisation of the Sussex-Coolabah area in the Cobar-Girilambone region, North-western Lachlan Fold Belt, NSW - a joint project between CRC LEME and NSW DMR”, CRC LEME Open File Report 148

Clemena, G.G., 1991. “Short pulse radar methods, Chapter 11 in Handbook on Non-Destructive Testing of Concrete,” Malhotra, V.M. and Carino, N.J. (eds.), CRC Press, Boston, pp. 253-274.

David F. Dominic, K. E., Cindy Carney, Paul J. Wolfe and Mark R. Boardman (1995). “Delineation of shallow stratigraphy using ground penetrating radar.” Journal of Applied Geophysics **33**(1-3): 167-175.

Davis, .L. and Annan, A.P., 1989. “Ground-penetrating radar for high-resolution mapping of soil and rock stratigraphy.” Geophysical Prospecting, 37, 531-551.

George A. McMechan, R. G. L., Xiaoxian Zeng and Paul Mescher (1998). “Ground penetrating radar imaging of a collapsed paleocave system in the Ellenburger dolomite, central Texas.” Journal of Applied Geophysics **39**(1): 1-10.

Gibson, D.L., 1999. “Explanatory notes for the 1:5000 000 Cobar Regolith Landform map.” CRC LEME Open File Report 76. 53pp.

## The Effectiveness of Transient Electromagnetics and Ground Penetrating Radar for Investigating Regolith

Grimm, R.E. and Harrison, K.P. (2003) "Rheological Constraints on Martian Landslides", p163, 347-362

Harari, Z. (1996). "Ground-penetrating radar (GPR) for imaging stratigraphic features and groundwater in sand dunes." Journal of Applied Geophysics **36**(1): 43-52.

In Papp, É. (Editor), 2002, "Geophysical and Remote Sensing Methods for Regolith Exploration", CRC LEME Open File Report 144, pp 53-79.

Jol, H.M., Bristow, C.S., Smith, D.G., Junick, M.B., and Putnam, P. (2003) "Stratigraphic Imaging of the Navajo Sandstone using Ground-Penetrating Radar." The Leading Edge **22**: 882-887

Kruse, S.E., J.C. Schneider, D.J. Campagna, J.A. Inman, and T.D. Hickey (2000). "Ground penetrating radar imaging of cap rock, caliche and carbonate strata." Journal of Applied Geophysics **43**(2-4): 239-249.

Lane, R, Green, A, Golding, C, Owers, M, Pik, P, Plunkett, C, Sattel, D and Thorn, B, (2000) "An example of 3D conductivity mapping using the TEMPEST airborne electromagnetic system" Exploration Geophysics **31**, 162-172

Liu, L and Arcone, S.A. (2003) "Numerical Simulation of the Wave-Guide Effect of the Near-Surface Thin Layer on Radar Wave Propagation" Journal of Environmental & Engineering Geophysics **8**(2):133-141

The Effectiveness of Transient Electromagnetics and Ground Penetrating Radar for Investigating  
Regolith

McMechan G.A., Loucks R.G., Zeng X.X., and Mescher P., (1998) “Ground penetrating radar imaging of a collapsed paleocave system in the Ellenburger dolomite, central Texas”, Journal of Applied Geophysics, 39

Olhoeft, G.R., (1984). “Applications and limitations of ground penetrating radar”.

SEG 54th Annu. Int. Meeting, Atlanta, GA, pp. 147-148

Oswald, B., Wollschläger, U. and Roth, K.(2003) “Ground penetrating radar (GPR) for mapping subsurface structures” lecture notes

<http://www.iup.uni-heidelberg.de/institut/forschung/groups/ts/projects/gpr/gpr.html>

Phil Mill (Ecophyte Technologies) pers. comm.

Robertson, C., 2003, “Regolith investigations and tree survival in a Eucalyptus plantation”: CRC LEME Western Regolith Symposium.

Smith, Derald G. and Jol, Harry M. (1995). “Ground penetrating radar: antenna frequencies and maximum probable depths of penetration in Quaternary sediments.” Journal of Applied Geophysics **33**(1-3): 93-100.

Van Dam, Remke L., Nichol, Scott L., Augustinus, Paul C., Parnell, Kevin E., Hosking, Peter L., and Mclean, Roger F. (2003) “GPR stratigraphy of a large active dune on Parengarenga Sandspit, New Zealand” The Leading Edge **22**: 865-870, 881



## The Effectiveness of Transient Electromagnetics and Ground Penetrating Radar for Investigating Regolith

Yilmaz, O., 1987. Seismic Data Processing. Edited by Doherty S., M., Society of Exploration Geophysics, Series: Investigation in Geophysics, Vol. 2.

Zonge, K.L. (1992), "INTRODUCTION TO TEM", Zonge Engineering and Research Organization, Inc. Extracted from Practical Geophysics II, Northwest Mining Association, 1992.

Webpages:

Geo-Centers "Why EFGPR is Different from Other GPR Mine Detection Technologies"

<http://www.geo-centers.com/GPR/Capabilities1b.htm>

"Application of Ground Penetrating Radar"

[http://www.dage.co.kr/dage\\_english1/method/gpr/gpr.htm](http://www.dage.co.kr/dage_english1/method/gpr/gpr.htm)

Copyright 2000. All rights reserved by Dong-A Geological Engineering Co., Ltd

### **List of Tables:**

Table 1: Comparison of different GPR frequencies.

Table 2: Ideal values for relative permittivity and EM velocity for a range of materials.

Table 3: Typical Values of dielectric constant, conductivity, velocity, and attenuation rates for a range of ideal materials.

Table 4a: Locations of Girilambone Line 1 stations with drill holes

Table 4b: Locations of Girilambone Line 2 stations with drill holes

## List of Figures:

Figure 1: Transmitted waveform and measured ground response for typical time domain EM (Lane et al, 2000), showing square wave nature of transmitter current waveform, and the decay curve nature of the measured ground response.

Figure 2: TEM transmitter loops and receiver coil configuration for typical in-loop time domain ground EM (CRC LEME Open File Report 144, page 60), showing size of array and relative positions of transmitting and receiving loops.

Figure 3: Field setup for vertical sounding (in-loop TEM (a)) and profiling (Fixed-Loop TEM (b)), (Zonge, 1992)

Figure 4: The path of a reflected wave from the transmitting antenna to the receiving antenna, passing down into the subsurface and being reflected from a target body.

Figure 5: Reflection Profiling: The Movement of a GPR array over a set of reflectors, and a corresponding radarplot of the reflectors. (Application of GPR webpage).

Figure 6: Schematic representations of CMP (a) and Transillumination (b) configurations (Application of GPR webpage).

Figure 7: Omitted

Figure 8: Electric and Magnetic fields, orthogonal to each other.

Figure 9: Conduction vs. displacement currents, showing nature of electron movement (pers. comm. Phil Mill, 2003)

Figure 10: Relative field orientations for TE and TM modes (modified from Liu et al, 2003).

Figure 11: Relative orientation of antennae and corresponding TE or TM mode (Liu et al, 2003).

Figure 12: Omitted

Figure 13: Locality map of White Dam, South Australia.

Figure 14: Location of costeans and outline of mineralisation in White Dam, South Australia (modified from Aaron Brown, 2003).

## The Effectiveness of Transient Electromagnetics and Ground Penetrating Radar for Investigating Regolith

Figure 15: Regolith Landform Map, White Dam, South Australia (Aaron Brown, 2003).

Figure 16: NanoTEM Survey Lines overlaid over White Dam regolith landform map.

Figure 17: Omitted

Figure 18: Smooth inverted resistivity depth sections for White Dam, Line 1 (a) and Line 2 (b), resistive areas shown in blue (cooler colours), more conductive areas shown as orange and pinks (warmer colours).

Figure 19: Resistivity depth sections overlaid on regolith landform map

Figure 20: GPR antennae, including 25MHz and 50MHz GPR as used in White Dam

Figure 21: 50MHz GPR survey lines, White Dam

Figure 22: 25MHz GPR survey lines, White Dam

Figure 23: Placement of 50MHz (left) and 25MHz (right) antennae during a survey, showing increased difficulty with the longer 25MHz antennae.

Figure 24: Radarplot showing parabolic events at 25m intervals and vertical striping from static shifts produced by inconsistent placing of antennae.

Figure 25: Reflections of costeans in radarplot

Figure 26: White Dam 25MHz GPR line 4, showing more prominent patches of attenuation towards the northern end of the line.

Figure 27: GPR traces in resistive and conductive terrains, showing attenuation of higher frequency components with increase in attenuation (by conduction losses)

Figure 28: Locality map of Girilambone-Cobar study area, New South Wales.

Figure 29: Drilling transects along roads in the Girilambone-Cobar study area (CRC LEME Open File Report 148)

Figure 30: 1.5 vd magnetics image showing planned survey line 1 in Girilambone-Cobar area, crossing paleochannel with strong magnetic signature

Figure 31: Drill-derived geological section showing paleochannel crossed by line 1

## The Effectiveness of Transient Electromagnetics and Ground Penetrating Radar for Investigating Regolith

Figure 31b: Key to drill derived sections.

Figure 32: 1.5 vd magnetics image showing planned survey line 2 in Girilambone-Cobar area, crossing 2 magnetic features, each of a different scale.

Figure 33: Drill-derived geological section showing paleochannels crossed by line 2

Figure 34: Movement of NanoTEM loops in survey.

Figure 35: Smooth inverted 2D resistivity depth section for Girilambone Line 1, showing a pair of conductivity anomalies, the strongest correlating with the strongly magnetic paleochannel, and the other correlating to the weakly magnetic paleochannel.

Figure 36: Smooth inverted 2D resistivity depth section for Girilambone Line 2. plot along coincident line, showing more complex structure than for line 1. Vertical axis of lower plots is Elevation, with 5m increments on the scale. Colour Scale: blue (resistive) through to purple (much less resistive). Figure 37 a) Key for Drill info summaries, b)-g) Drill info summaries plotted with resistivity vs depth

Figure 38a: Plot of Line 1, Girilambone, with drill holes indicated

Figure 38b: Plot of Line 2, Girilambone, with drill holes indicated

Frequency of GPR (MHz)	Approximate Depth (m)	Resolution (cm)	Measurement Spacing (cm)
1000	0.5-2	1	5
200	2.5-10	5	25
50	10-25	20	100
25	Greater than 25	40	200

Table 1

Table 2 Relative permittivity for a range of given materials (in ideal condition with corresponding EM velocity. (from provided lecture material))

Material	$\epsilon_r$		from lecture notes	V(m/hrs)
	measured at 10			
	from Davis and Arman, 1989	from Daniels, 1996	from lecture notes	
Air	1	1	1	300
Distilled water	80			33
Fresh water	80	81	81	33
Sea water	80		81	33
Fresh water ice	3-4	4	4	190
Sea water ice		4-8	2.5-8	78-157
Snow		8-12	1.4-3	194-252
Permafrost		4-8	1-8	106-300
Sand, dry	3-5	4-6	3-6	120-170
Sand, wet	20-30	10-30	25-30	55-80
Sandstone, dry		2-3		
Sandstone, wet		5-10	6	112
Limestone	4-8		7-9	100-113
Limestone, dry		7		
Limestone wet		8		
Shales	5-15			
Shale, wet		6-9	7	113
Silts	5-30		10 (wet silt)	95 (wet silt)
Clays	5-40			
Clay, dry		2-6		
Clay, wet		15-40	8-15	86-110
Soil, sandy dry		4-6		
Soil, sandy wet		15-30		
Soil, loamy dry		4-6		
Soil, loamy wet		10-20		
Soil, clayey dry		4-6	3	173
Soil, clayey wet		10-15		
Coal, dry		3-5		
Coal, wet		8		
Granite	4-6		5-8	106-120
Granite, dry		5		
Granite, wet		7		
Basalt (wet)			8	106
Dolomite			6.8-8	106-115
Salt, dry	5-6	4-7		
PVC, Epoxy, Polyesters			3	173
Asphalt			4.5	134-173
Concrete			6-30	55-112
Quartz			4.3	145
Coal			4.5	134-150
Marsh			12	86
Agricultural Land			15	77
Pastoral land			13	83
Average 'soil'			16	75

Table 2

Table 3: typical values for given materials (Davis et al, 1989)

Material	Dielectric constant	Conductivity (mS/m)	Velocity (m/ns)	Attenuation (dB/m)
Air	1	0	0.3	0
Distilled water	80	0.01	0.033	0.002
Fresh water	80	0.5	0.033	0.1
Sea water	80	30,000	0.01	1,000
Dry sand	3-5	0.01	0.15	0.01
Saturated sand	20-30	0.1-1.0	0.06	0.03-0.3
Limestone	4-7	0.5-2	0.12	0.4-1
Shale	5-15	1-100	0.09	1-100
Silt	5-30	1-100	0.07	1-100
Clay	4-40	2-1,000	0.06	1-300
Granite	4-6	0.01-1	0.13	0.01-1
Salt (dry)	5-6	0.01-1	0.13	0.01-1
Ice	3-4	0.01	0.16	0.01

Table 3

Table 4a

Girilambone Line 1			Station	Eastings	Northings	Station	Eastings	Northings
Station	Eastings	Northings	54	55448516	6565733	108	55449605	6565841
1	55447472	6565625	55	55448537	6565733	109	55449625	6565844
			56	55448558	6565733			
2	55447492	6565630	57	55448579	6565733	110	55449646	6565847
3	55447512	6565636	58	55448599	6565733	111	55449664	6565850
4	55447532	6565641	59	55448620	6565733	112	55449684	6565853
5	55447552	6565646	60	55448641	6565733	113	55449704	6565856
6	55447571	6565652	61	55448662	6565734	114	55449724	6565859
7	55447591	6565657				CB AC88	55450516	6565996
8	55447611	6565662	62	55448682	6565734			
9	55447631	6565668	63	55448703	6565735			
10	55447651	6565673	64	55448723	6565736			
11	55447670	6565679	65	55448744	6565737			
12	55447690	6565685	66	55448764	6565737			
13	55447709	6565691	67	55448785	6565738			
14	55447729	6565697	68	55448805	6565739			
15	55447748	6565603	69	55448826	6565739			
16	55447767	6565609	70	55448846	6565740			
17	55447787	6565615	71	55448866	6565741			
18	55447806	6565621	72	55448886	6565742			
19	55447826	6565627	73	55448906	6565743			
20	55447845	6565633	74	55448926	6565744			
21	55447865	6565638	75	55448947	6565746			
22	55447884	6565643	76	55448967	6565747			
23	55447904	6565648	77	55448987	6565748			
24	55447924	6565653	78	55449007	6565749			
25	55447944	6565659	79	55449027	6565750			
26	55447963	6565664	80	55449047	6565751			
27	55447983	6565669	81	55449067	6565754			
28	55448003	6565674	82	55449087	6565757			
29	55448022	6565679	83	55449106	6565760			
30	55448042	6565684	84	55449126	6565763			
31	55448062	6565688	85	55449146	6565767			
32	55448081	6565692	86	55449166	6565770			
33	55448101	6565696	87	55449186	6565773			
34	55448120	6565700	88	55449205	6565776			
35	55448140	6565705	89	55449225	6565779			
36	55448159	6565709	90	55449245	6565782			
37	55448179	6565713	91	55449265	6565786			
38	55448198	6565717	92	55449285	6565789			
39	55448218	6565721	93	55449305	6565793			
40	55448237	6565725	94	55449325	6565796			
41	55448257	6565726	95	55449346	6565800			
42	55448276	6565727	96	55449366	6565803			
43	55448296	6565727	97	55449386	6565807			
44	55448315	6565728	98	55449406	6565810			
45	55448335	6565729	99	55449426	6565814			
46	55448355	6565730	100	55449446	6565817			
47	55448374	6565731	101	55449466	6565820			
48	55448394	6565731	102	55449486	6565823			
49	55448413	6565732	103	55449506	6565826			
50	55448433	6565733	104	55449525	6565829			
51	55448454	6565733	105	55449545	6565832			
52	55448475	6565733	106	55449565	6565835			
53	55448495	6565733	107	55449585	6565838			



Girilambone Line 2							
Station	Easting	Northing			Station	Easting	Northing
CBAC130	55411262	6556288			53	55412440	6556955
1	55411526	6556429			54	55412457	6556965
2	55411544	6556439			55	55412474	6556975
3	55411562	6556449			56	55412492	6556985
4	55411580	6556459			57	55412509	6556995
5	55411598	6556469			58	55412526	6557006
6	55411617	6556478			59	55412543	6557016
7	55411635	6556488			60	55412560	6557026
8	55411653	6556498			61	55412578	6557036
9	55411671	6556508			62	55412595	6557046
10	55411689	6556518			63	55412613	6557057
11	55411706	6556529			64	55412631	6557067
12	55411724	6556539			65	55412649	6557077
13	55411741	6556550			66	55412666	6557087
14	55411759	6556560			67	55412684	6557097
15	55411776	6556571			68	55412702	6557108
16	55411793	6556581			69	55412719	6557118
17	55411811	6556592			70	55412737	6557128
18	55411828	6556602			71	55412754	6557137
19	55411846	6556613			72	55412772	6557147
20	55411863	6556623			73	55412789	6557156
21	55411880	6556633			74	55412807	6557166
22	55411897	6556643			75	55412824	6557175
23	55411914	6556653			76	55412841	6557184
24	55411931	6556663			77	55412859	6557194
25	55411948	6556674			78	55412876	6557203
26	55411965	6556684			79	55412894	6557213
27	55411982	6556694			80	55412911	6557222
28	55411999	6556704			81	55412929	6557233
29	55412016	6556714			82	55412947	6557243
30	55412033	6556724			83	55412966	6557254
31	55412051	6556734			84	55412984	6557264
32	55412070	6556744			85	55413002	6557275
33	55412088	6556754			86	55413020	6557286
34	55412106	6556764			87	55413038	6557296
35	55412125	6556775			88	55413057	6557307
36	55412143	6556785			89	55413075	6557317
37	55412161	6556795			90	55413093	6557328
38	55412179	6556805			CBAC 128	55413249	6557434
39	55412198	6556815			CBAC 127	55414350	6558041
40	55412216	6556825					
41	55412233	6556835					
42	55412251	6556845					
43	55412268	6556855					
44	55412285	6556865					
45	55412302	6556875					
46	55412320	6556884					
47	55412337	6556894					
48	55412354	6556904					
49	55412372	6556914					
50	55412389	6556924					
51	55412406	6556934					
52	55412423	6556944					
CBAC129	55412426	6556959					

Table 4b

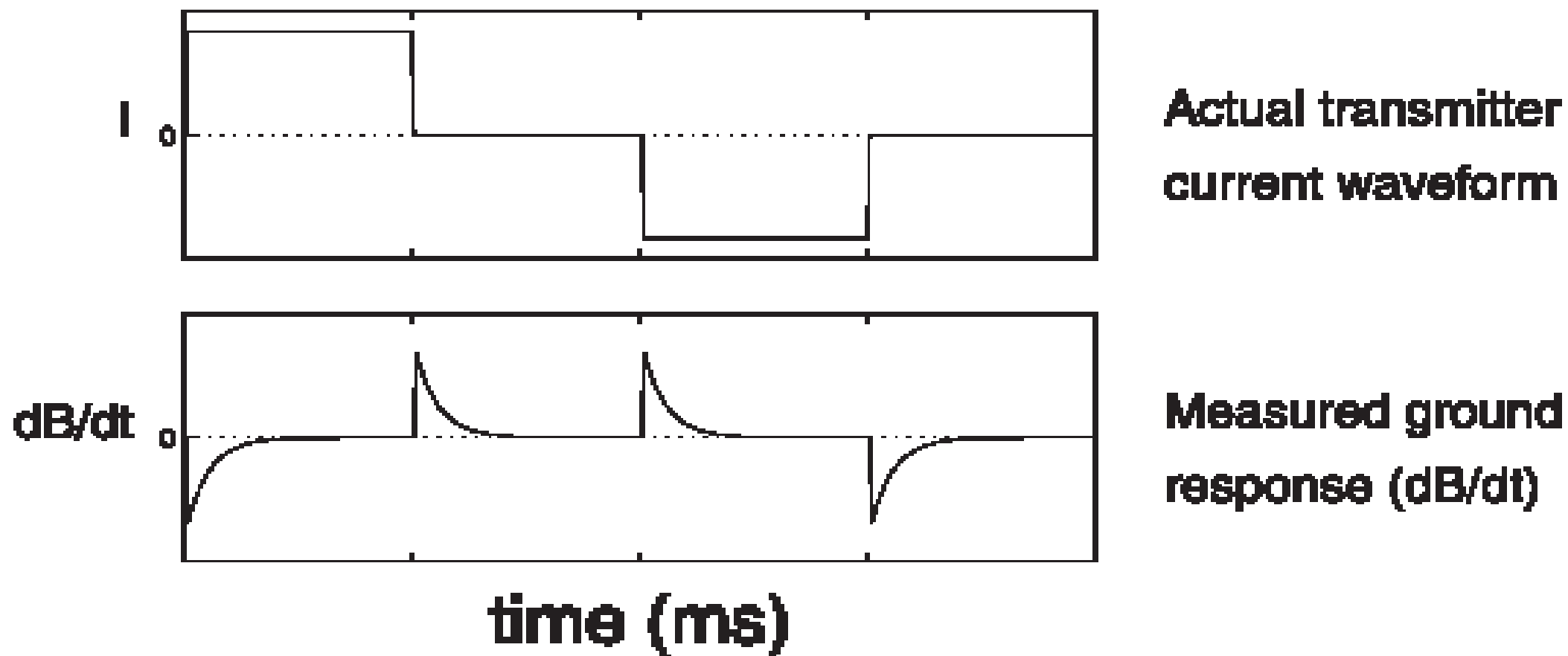


Figure 1

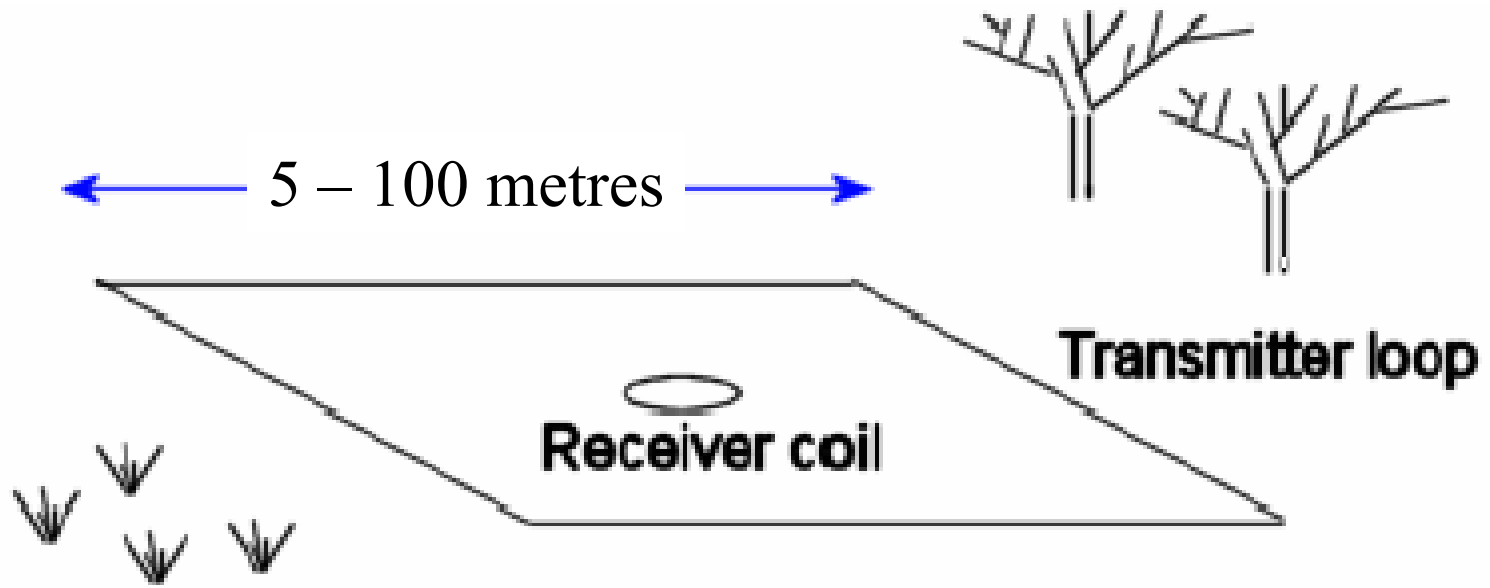
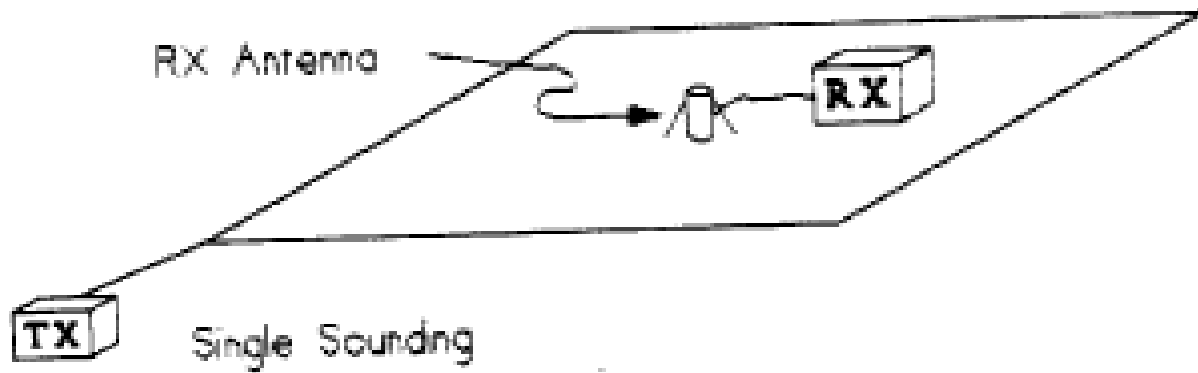
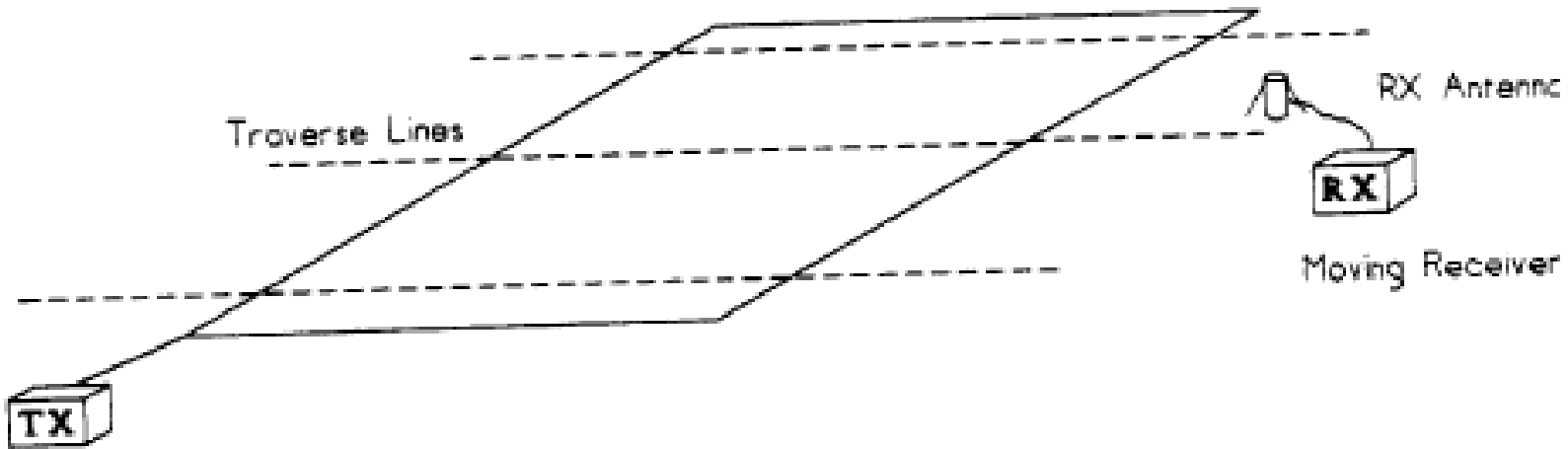


Figure 2



a) In-Loop TEM



b) Fixed-Loop TEM

Figure 3

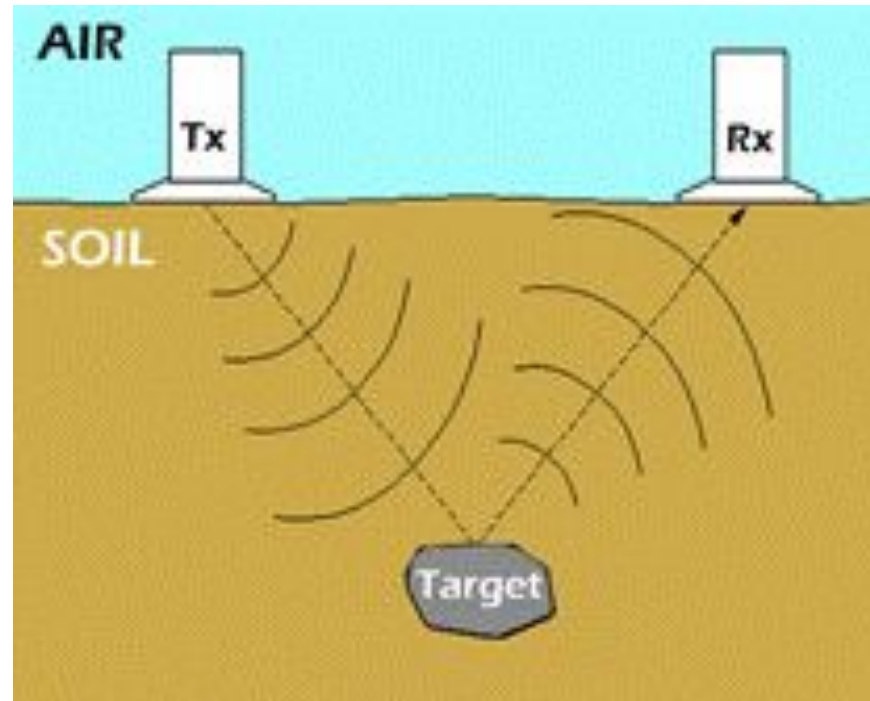
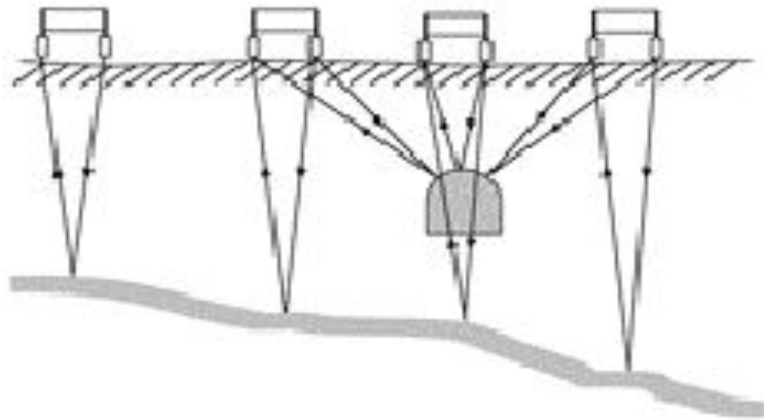
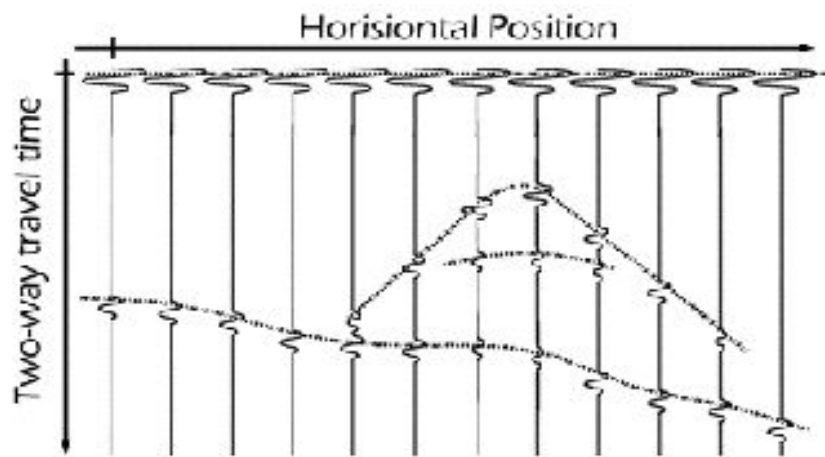


Figure 4



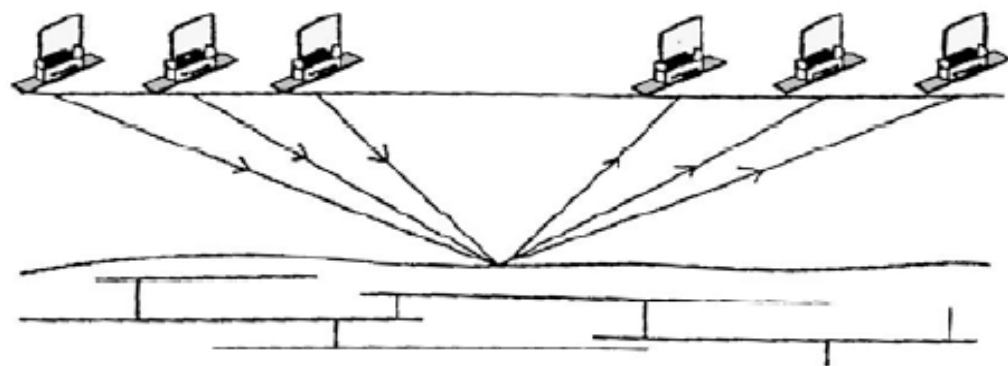
Movement of GPR array over set of reflectors, showing ray path differences.



A radarplot of the reflectors  
(Application of GPR  
webpage)

Figure 5

a) COMMON MID POINT (CMP)



b) TRANSILLUMINATION

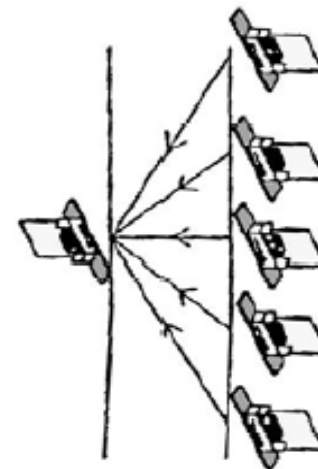


Figure 6

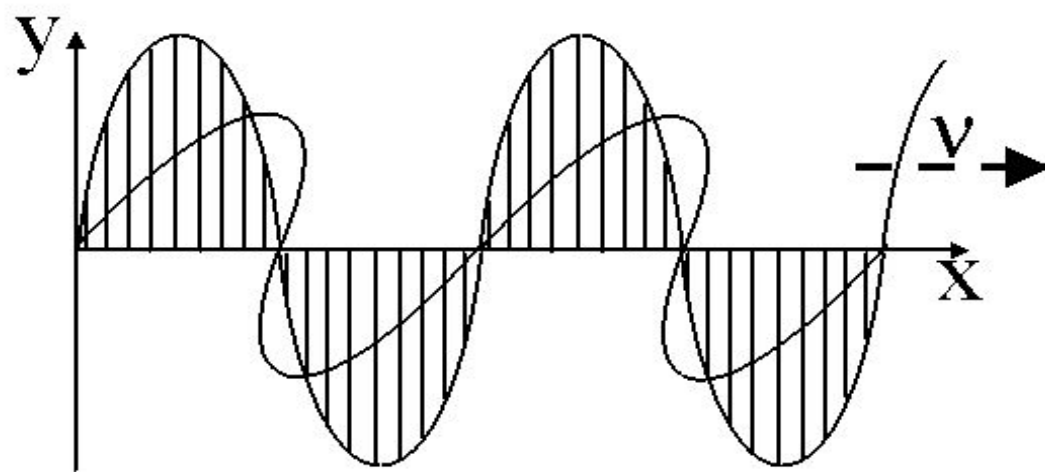
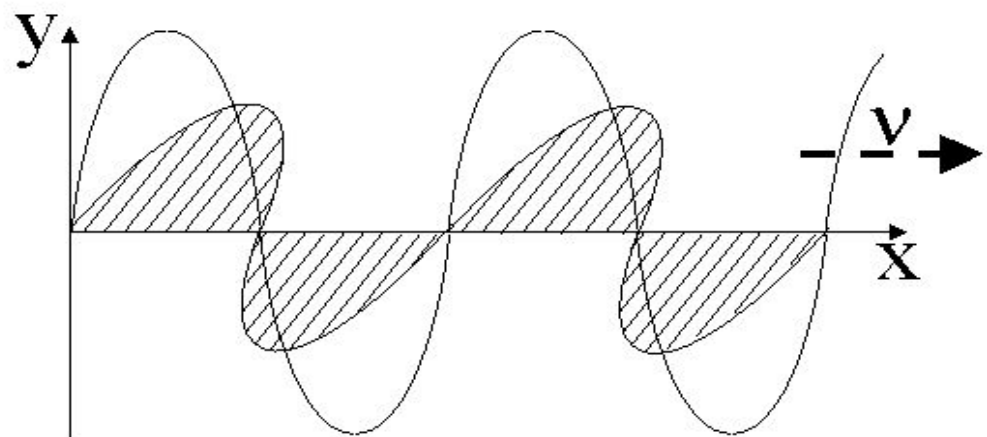


Figure 8



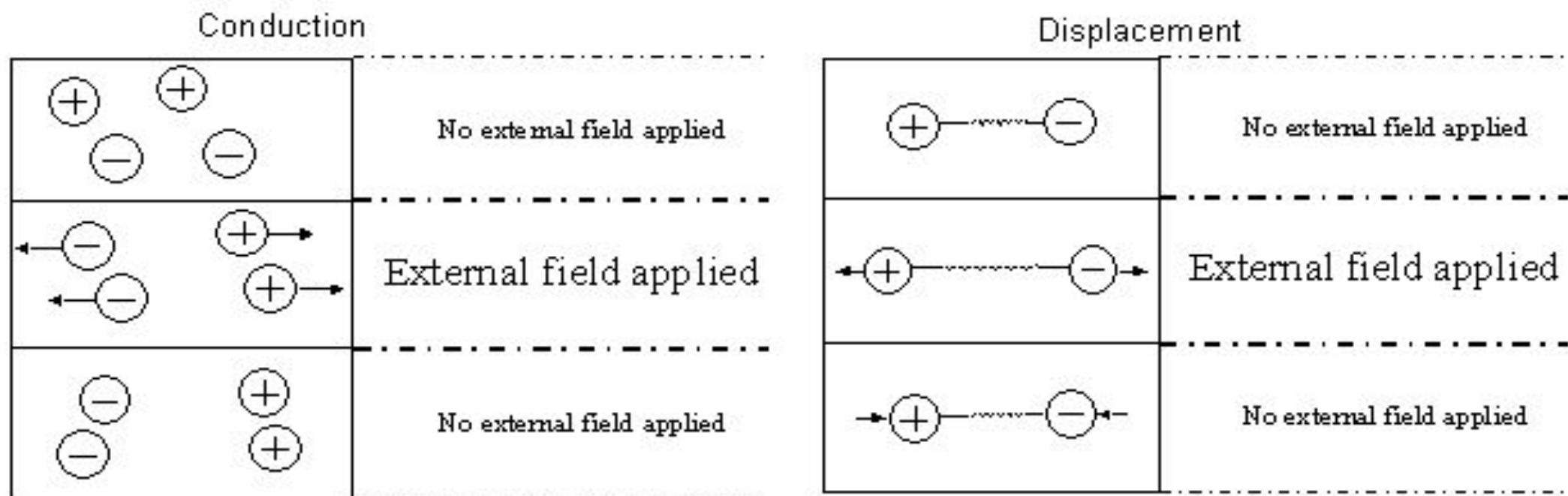


Figure 9

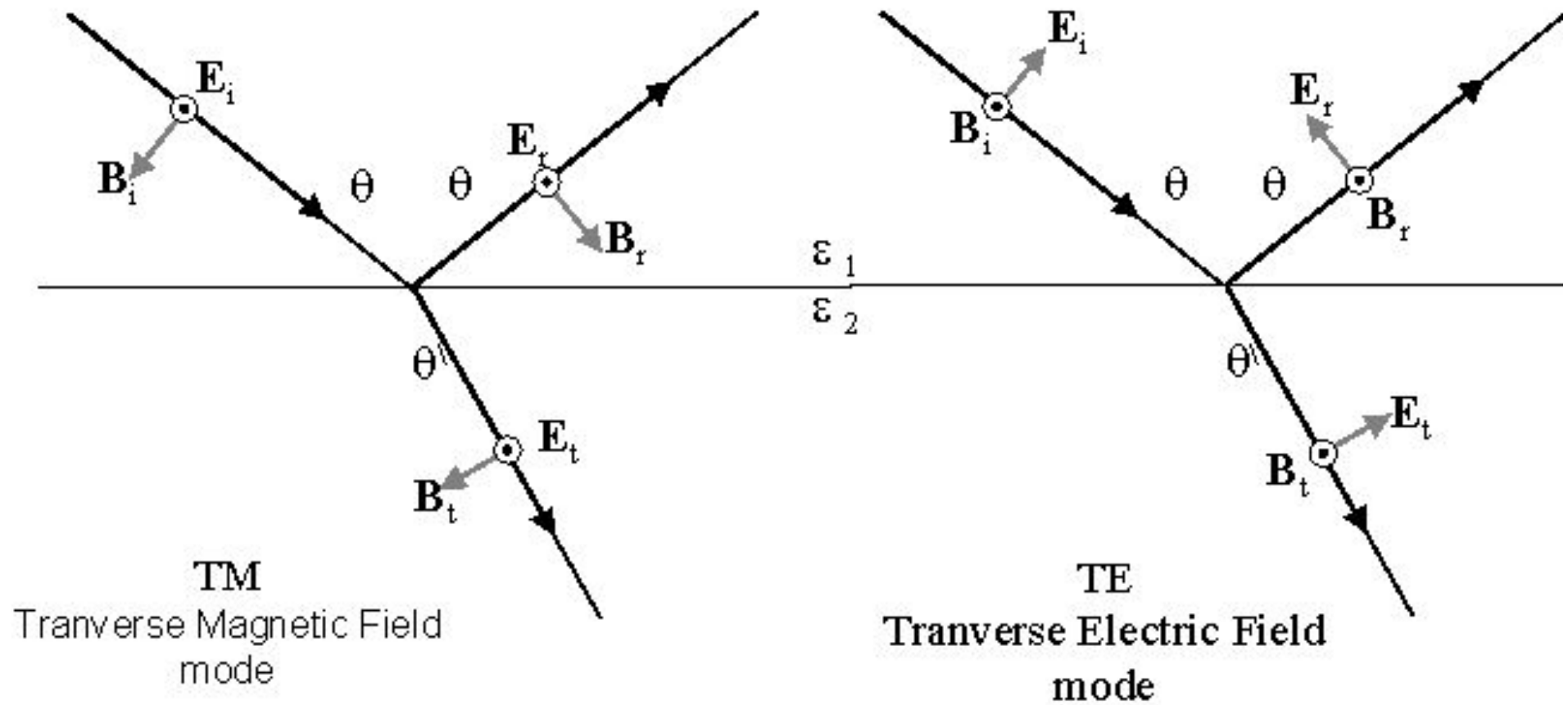


Figure 10

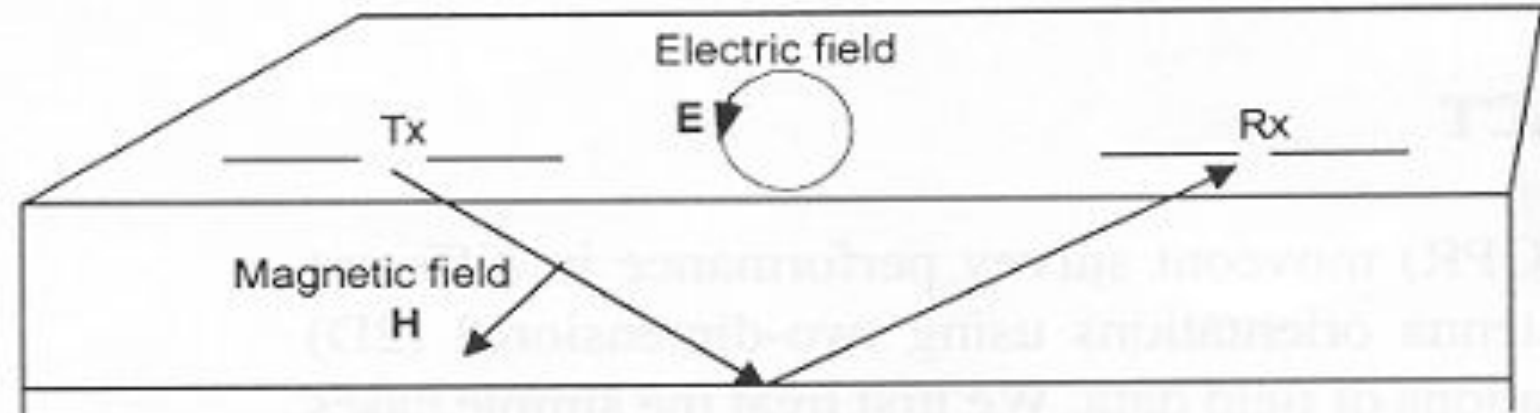
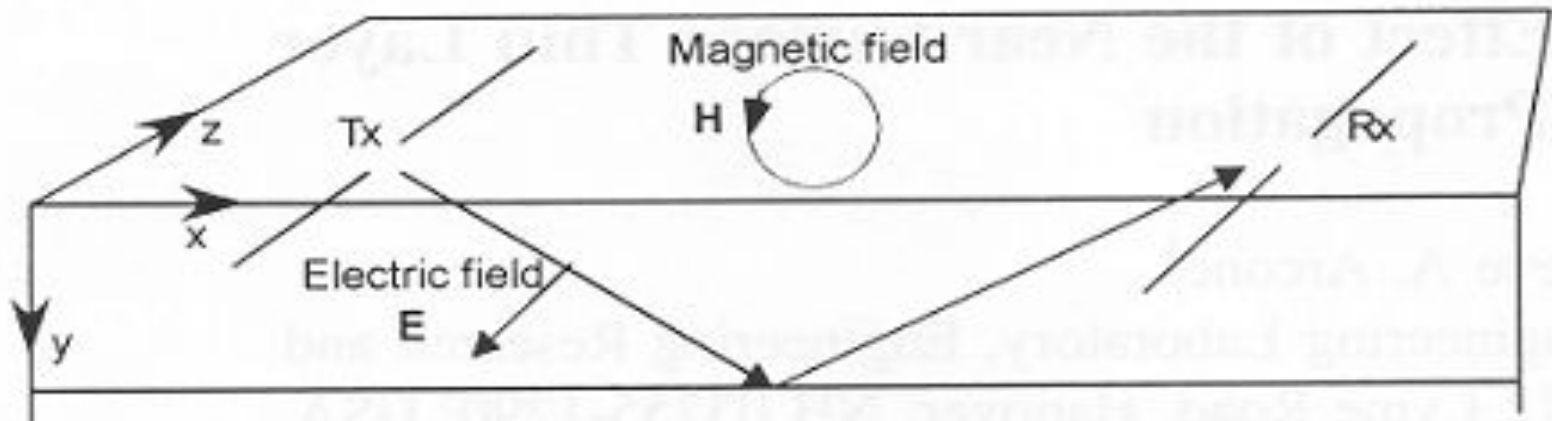


Figure 11

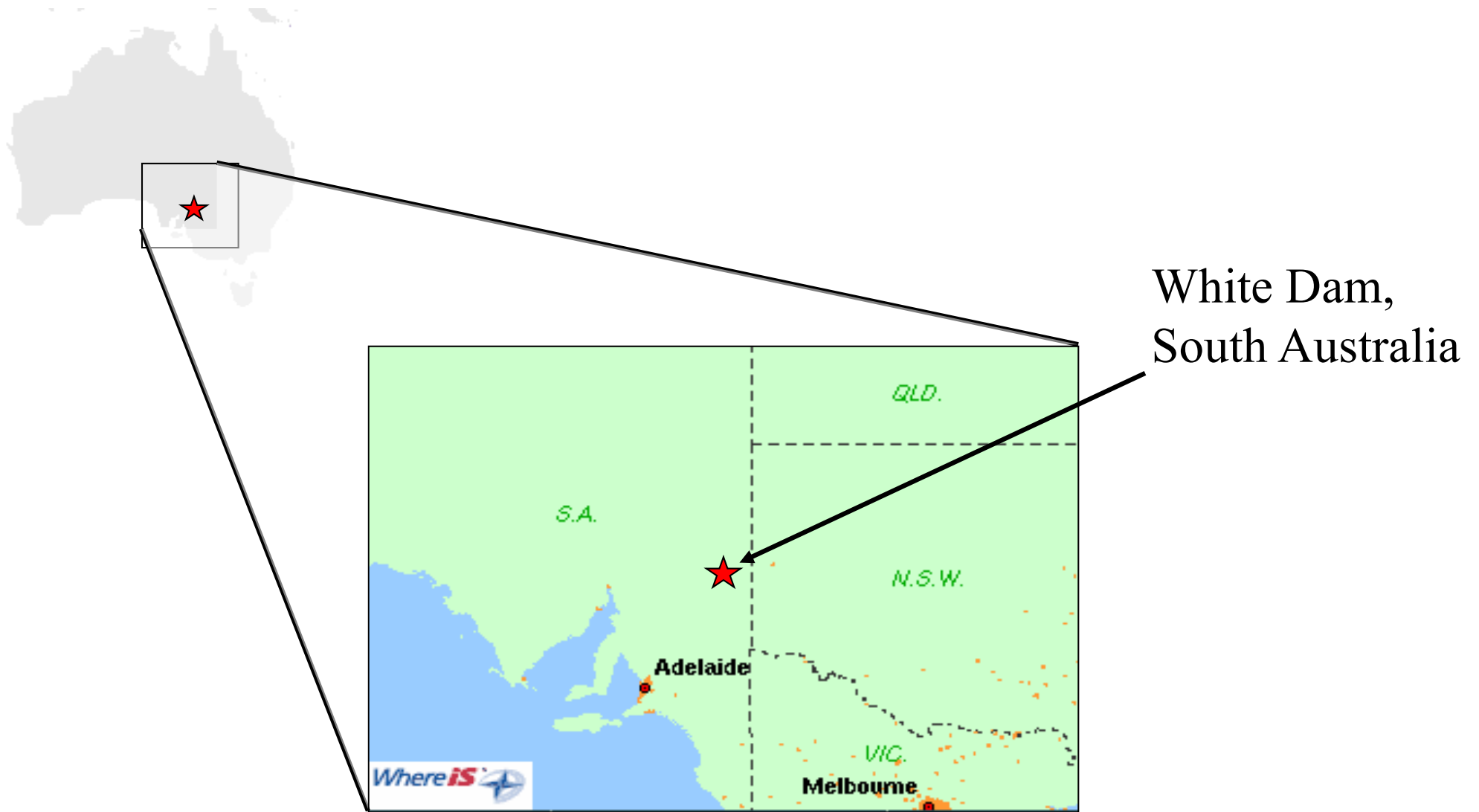


Figure 13

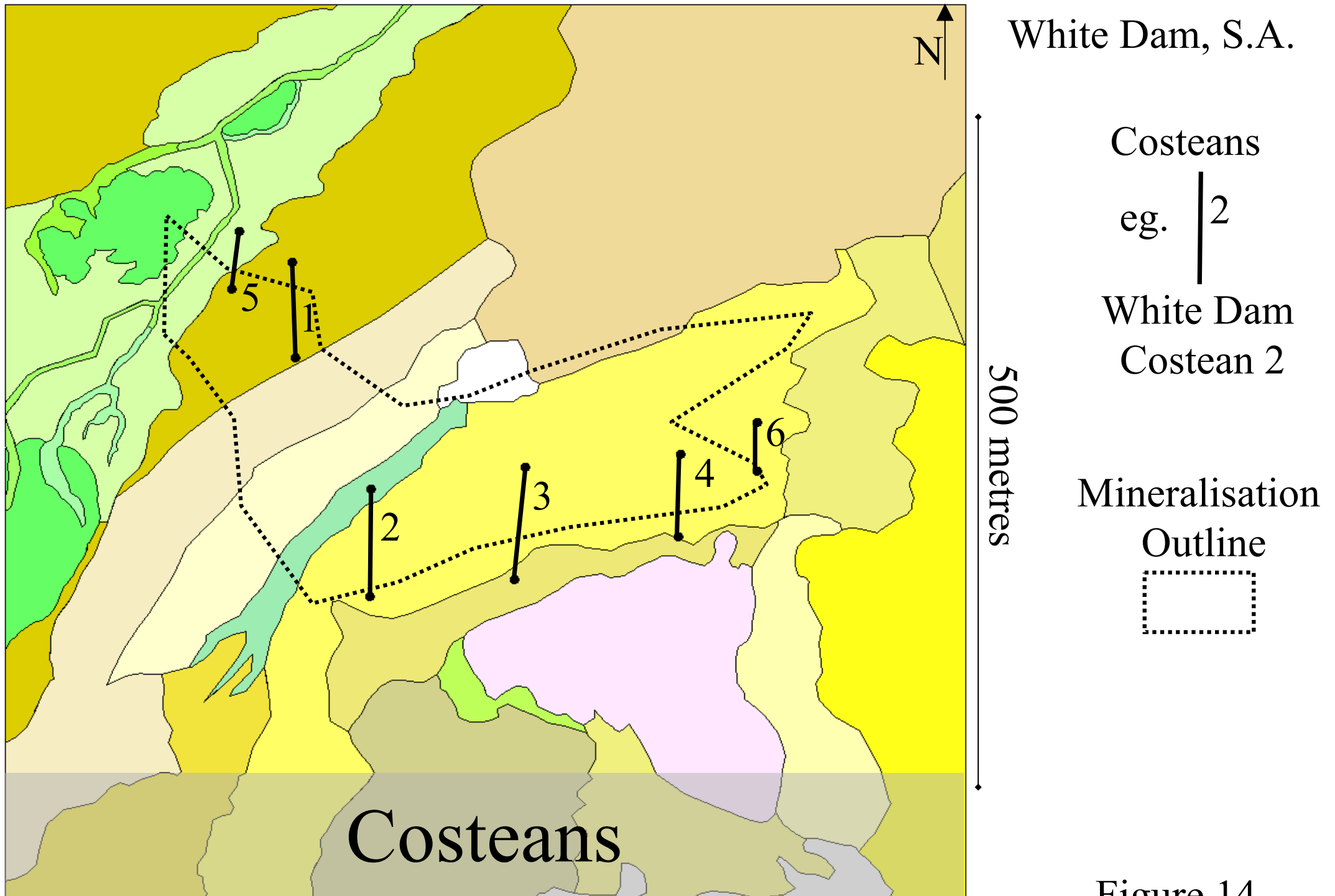


Figure 14

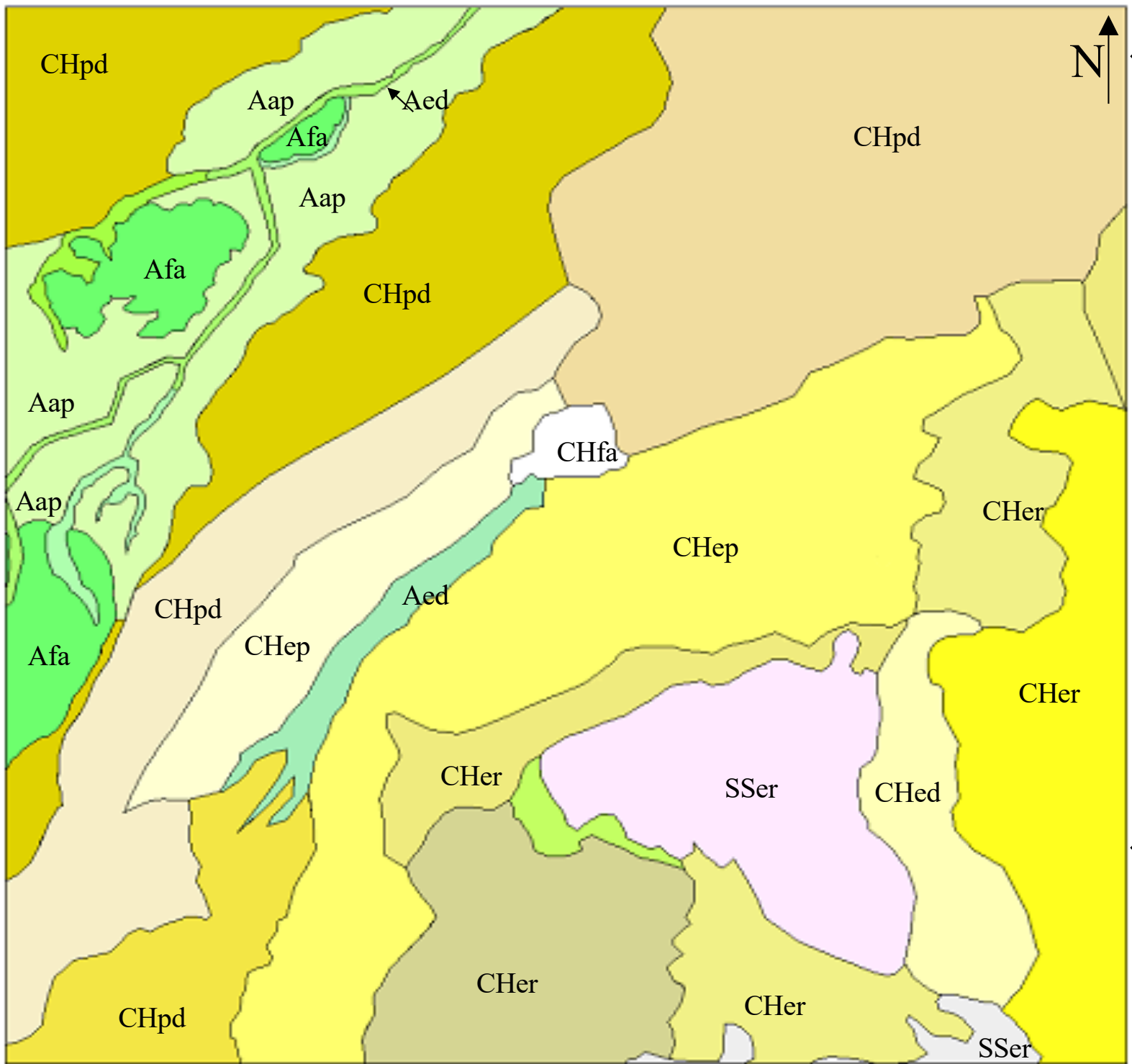
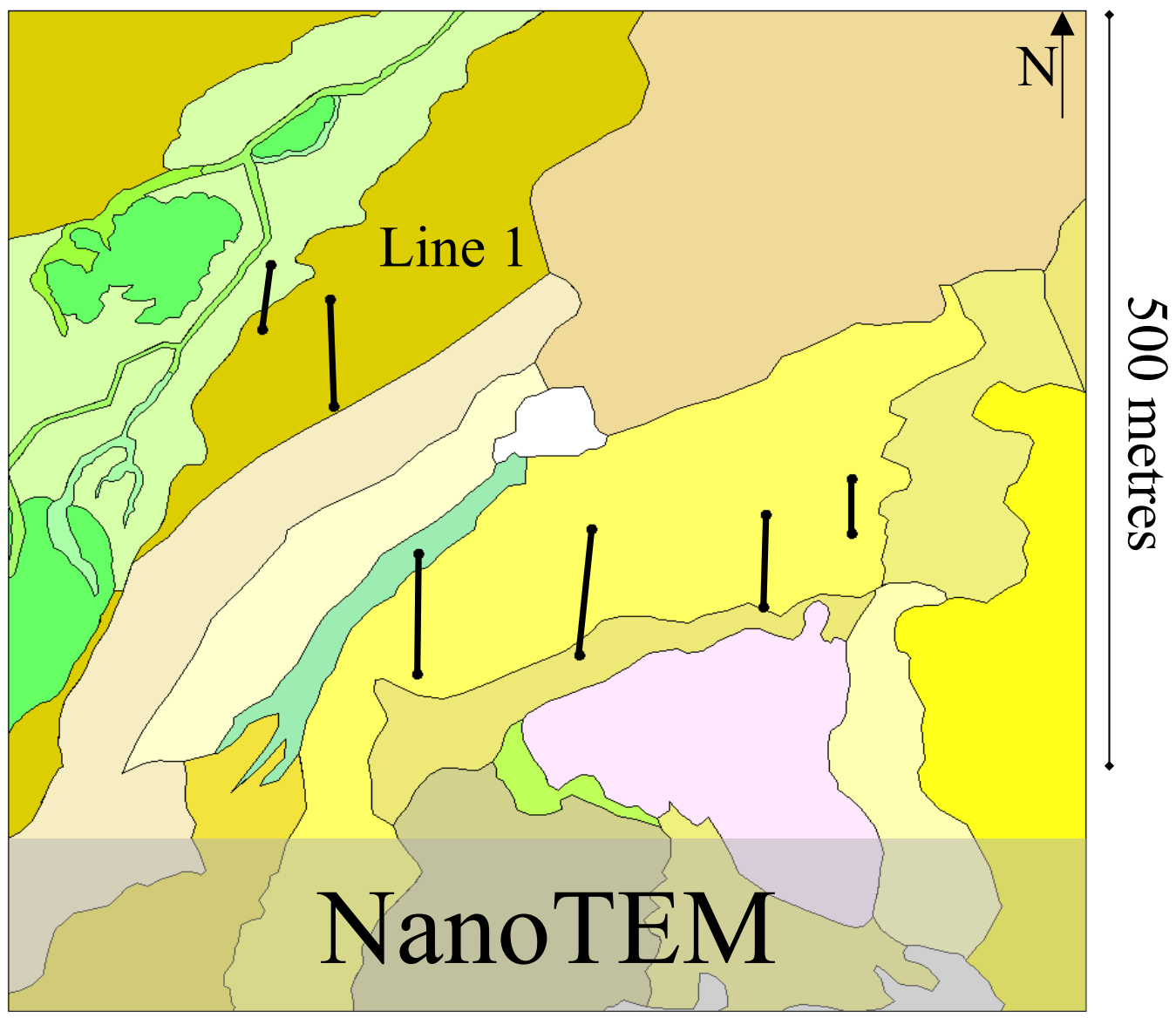


Figure 15

500 metres

- Landforms:**
- Depositional:
  - ap** Alluvial Plain
  - ed** Drainage Depression
  - fa** Alluvial Fan
  - pd** Depositional Plain
  - Erosional:
  - ep** Erosional Plain
  - er** Erosional Rise

Line 2



500 metres

NanoTEM

Figure 1

Figure 16



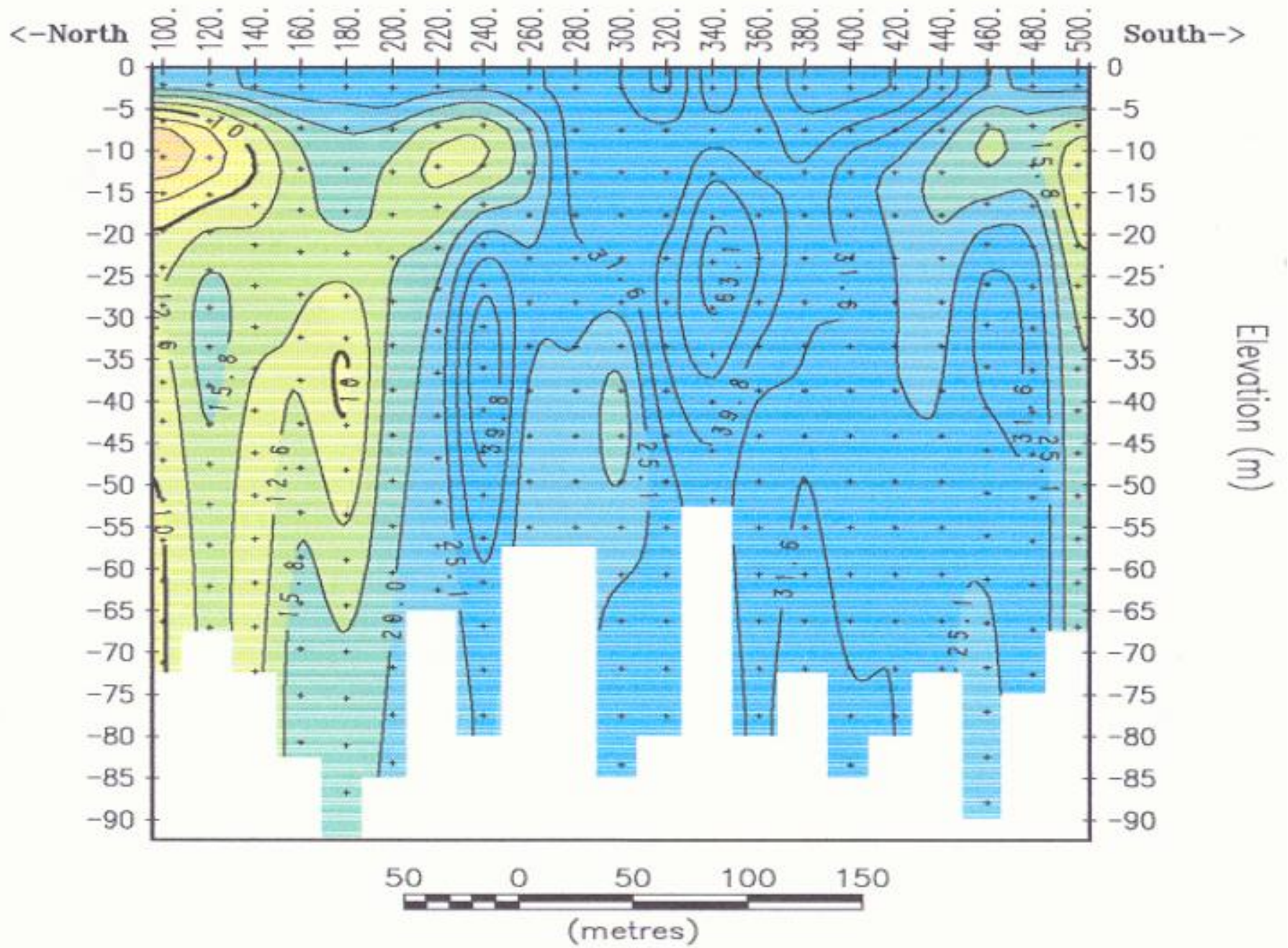


Figure 18a



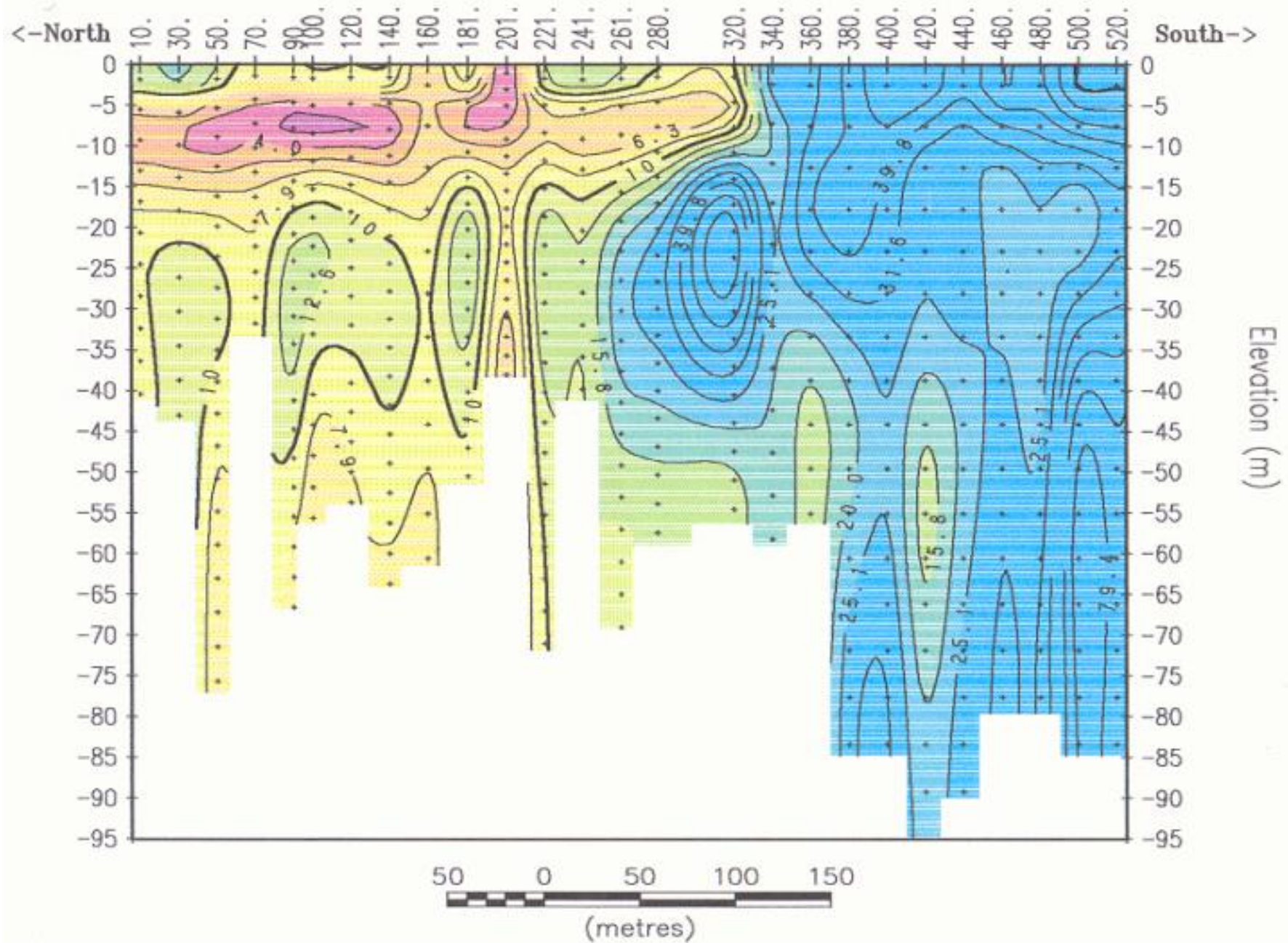


Figure 18b

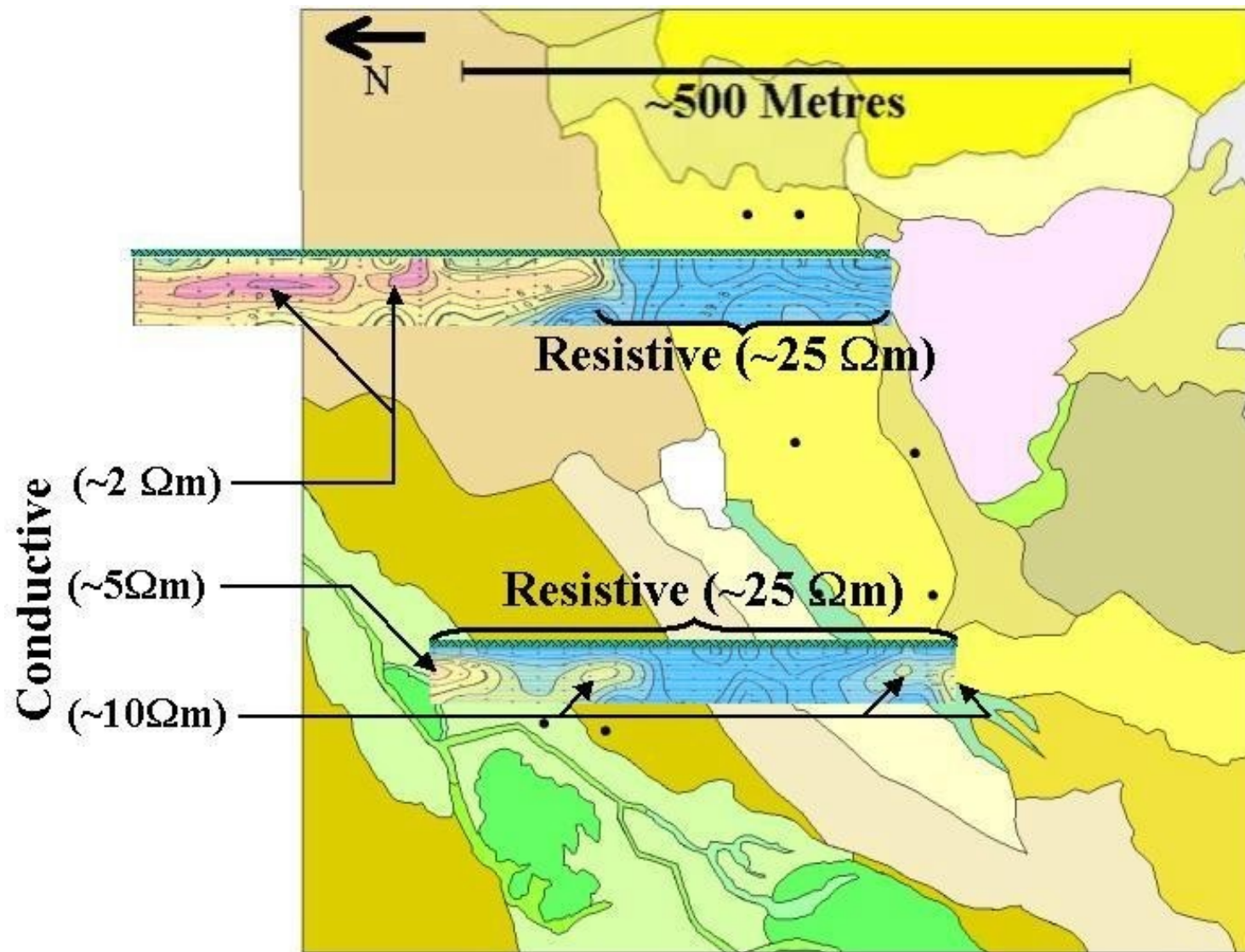


Figure 19



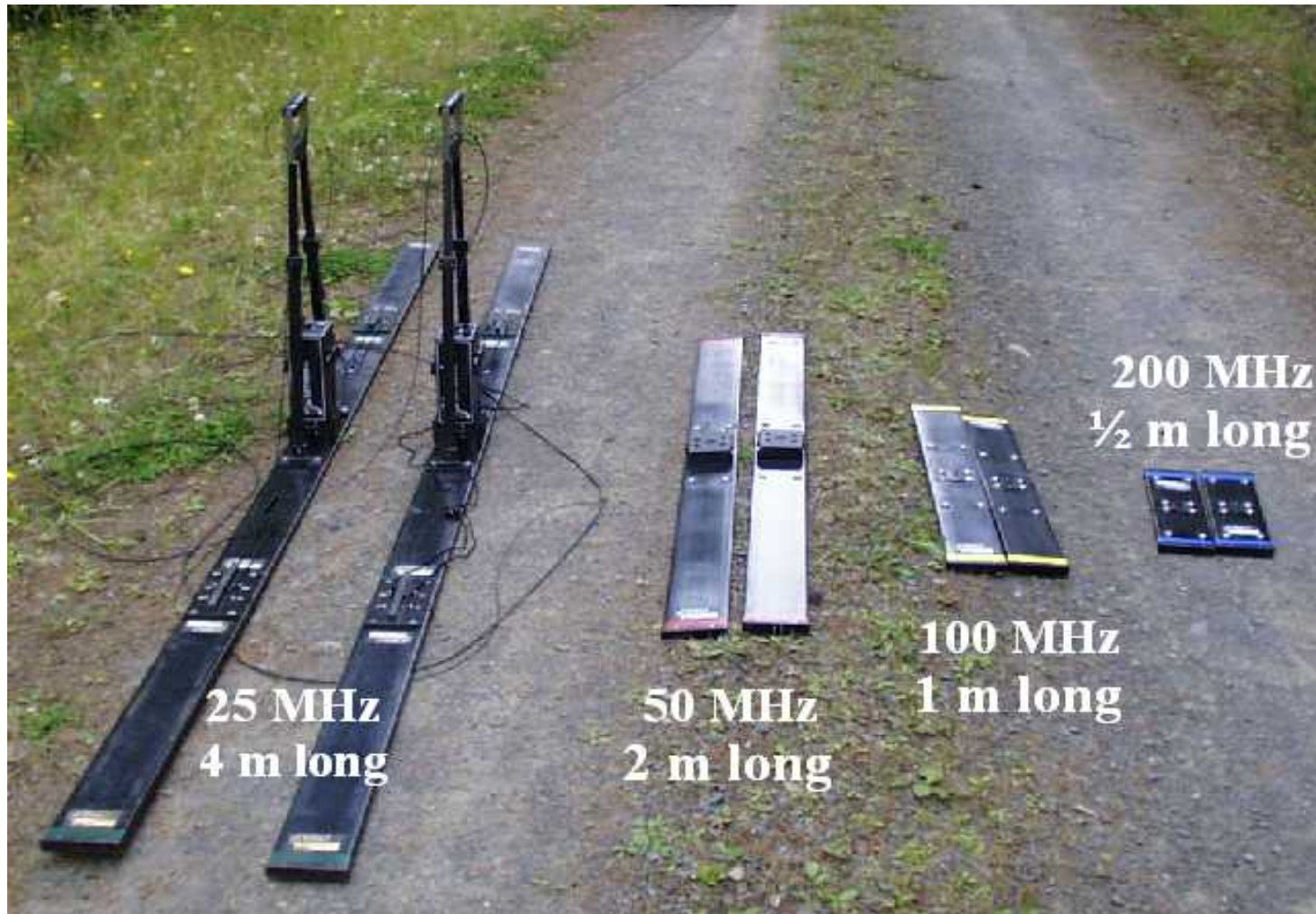


Figure 20

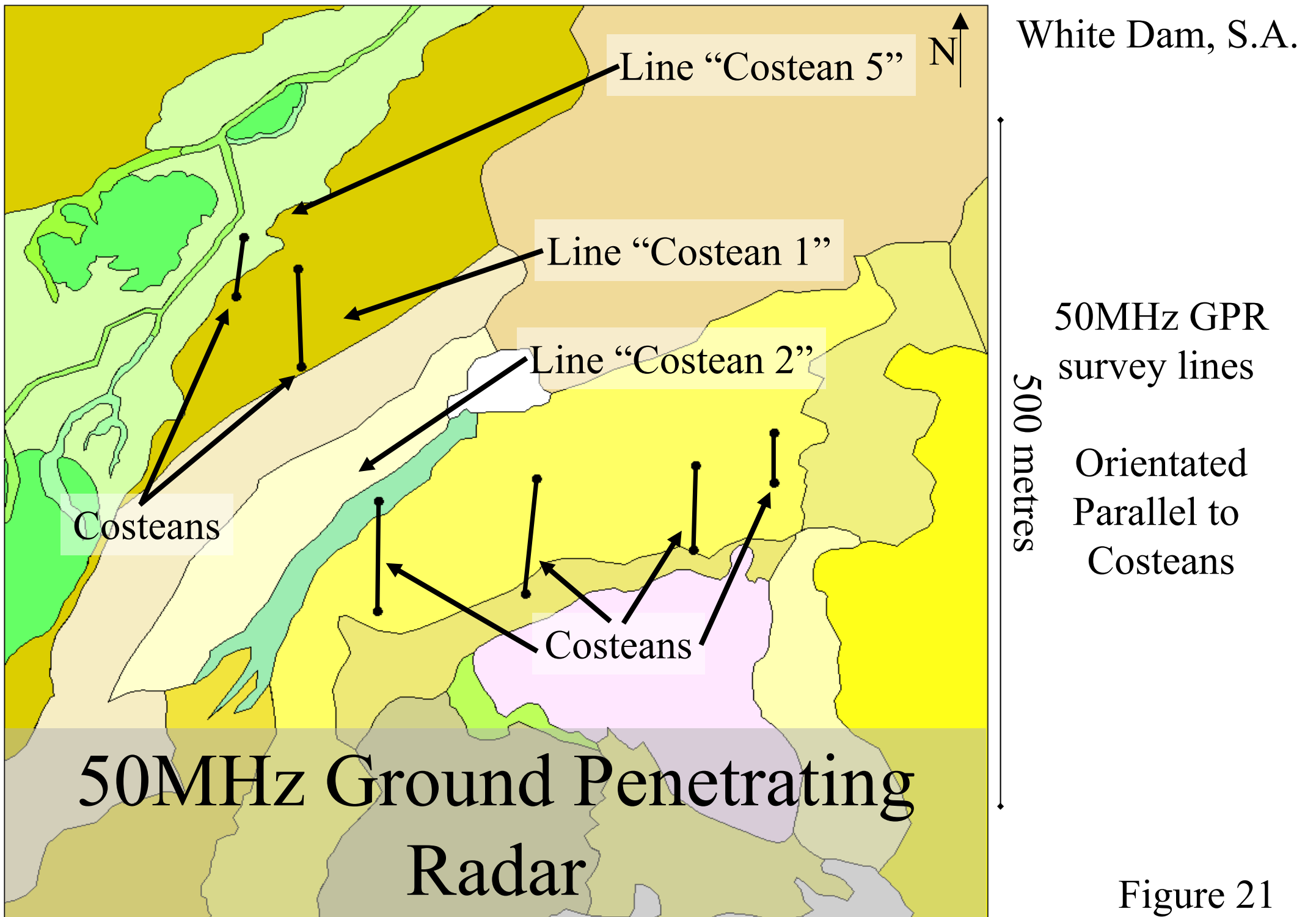


Figure 21

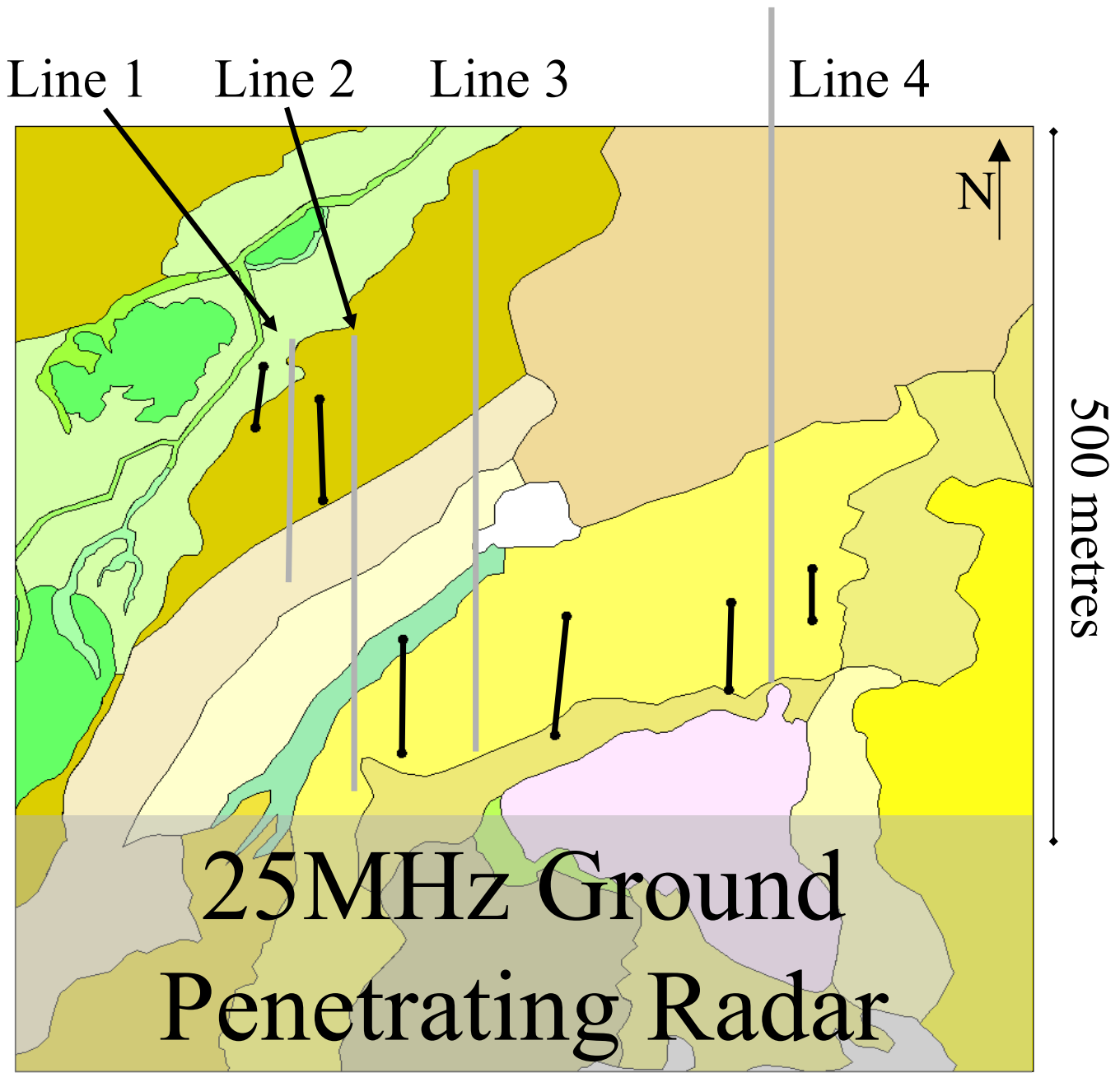


Figure 22





a



b

Figure 23

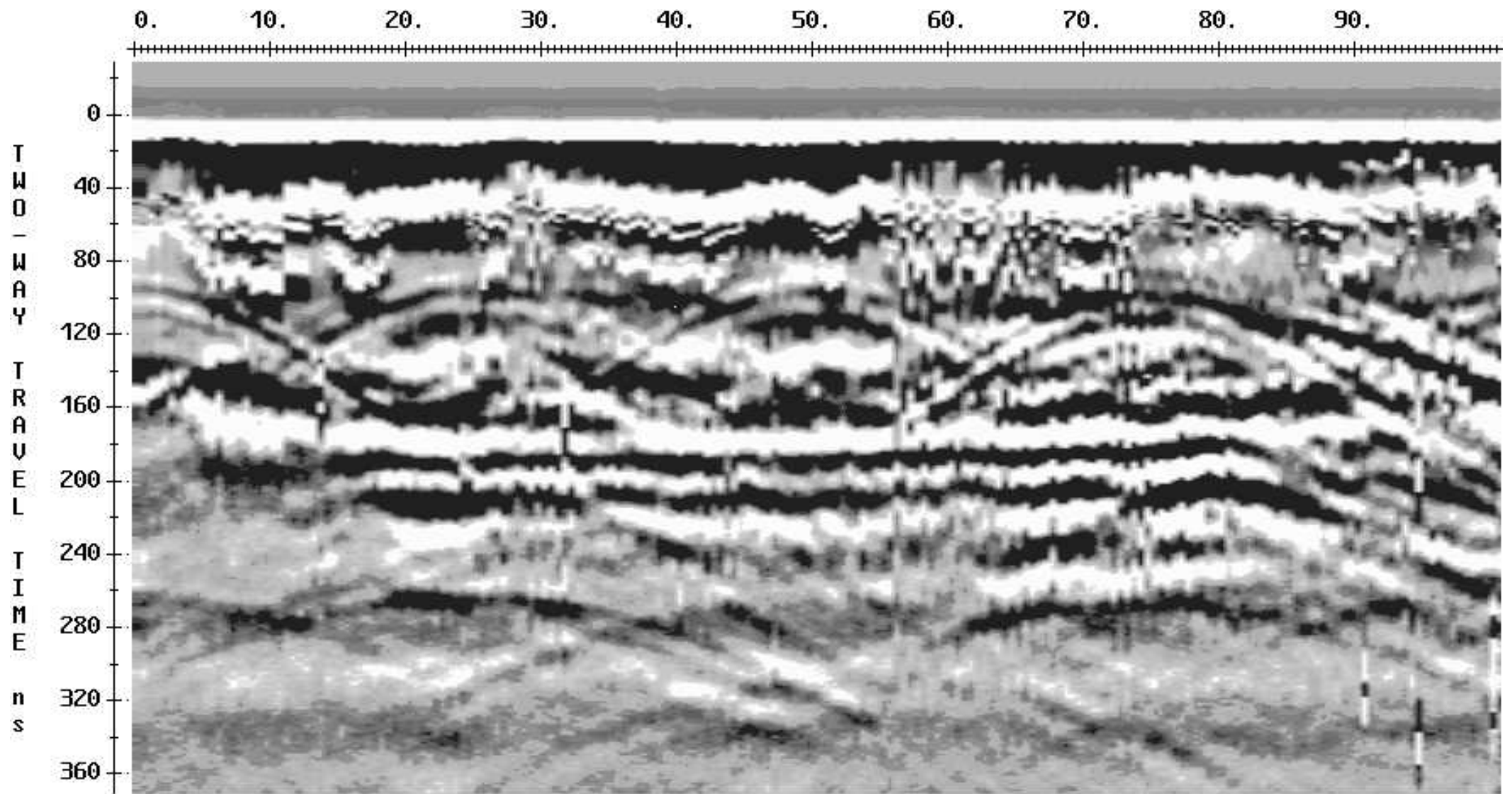


Figure 24

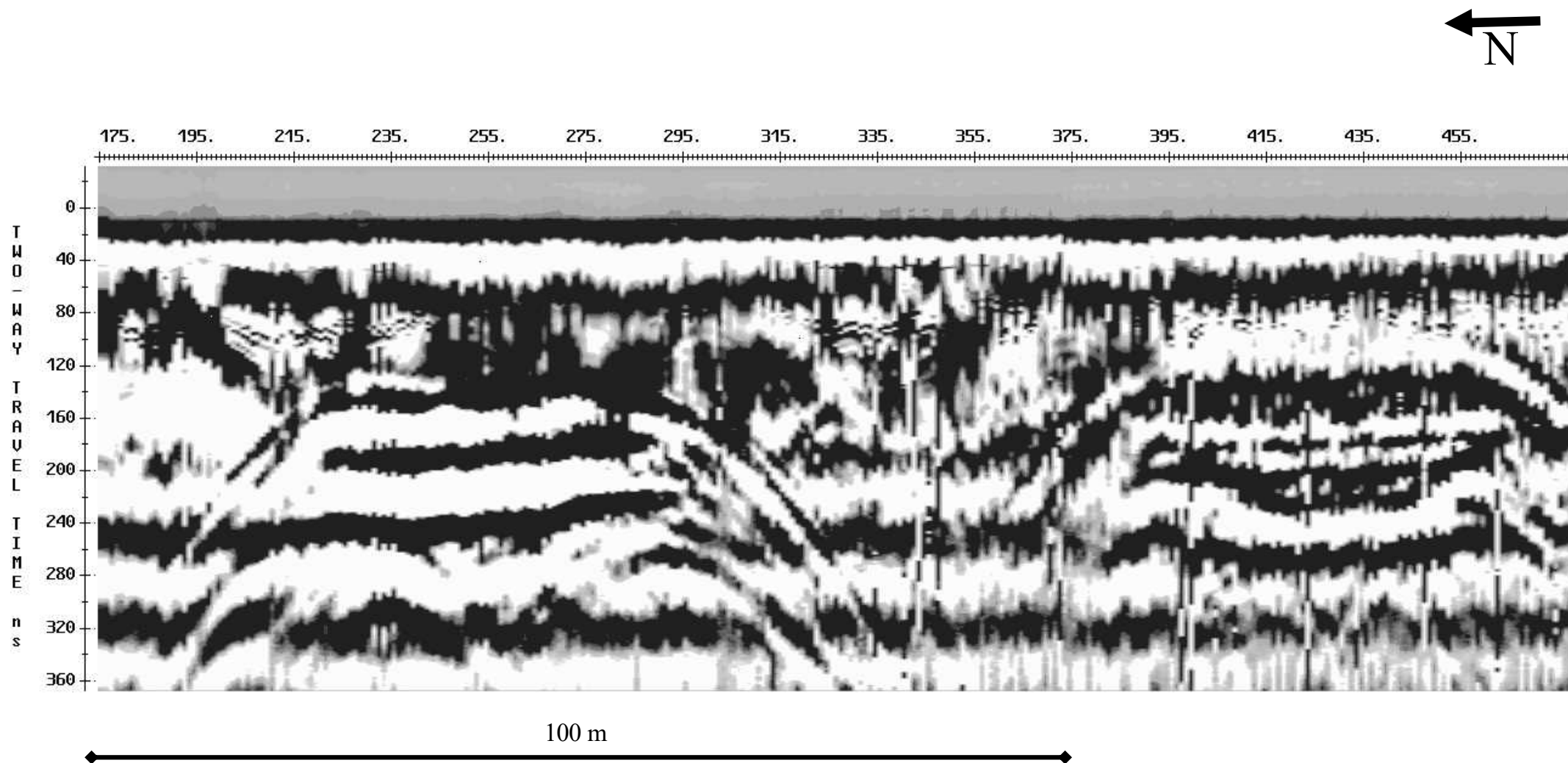


Figure 25



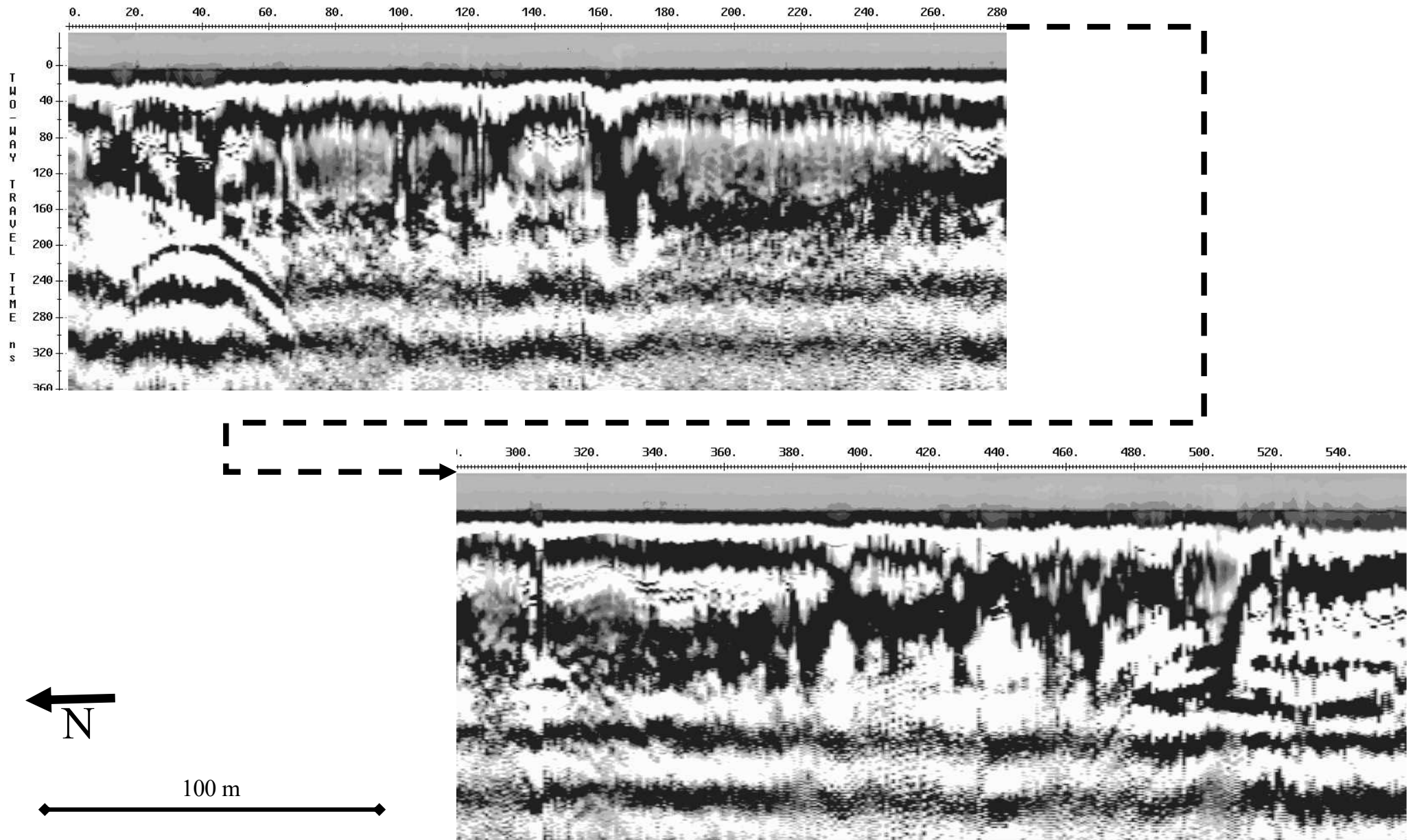
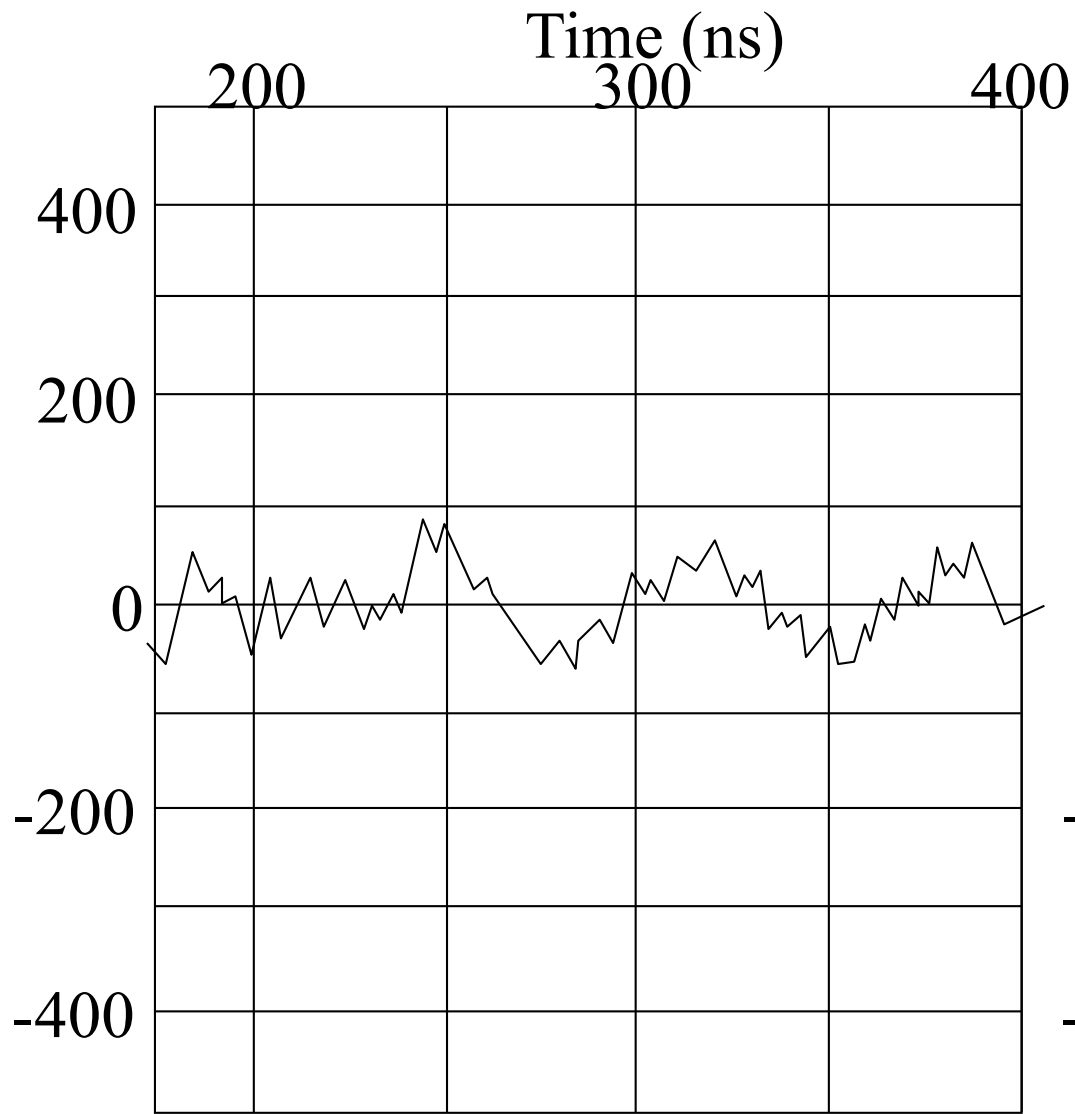
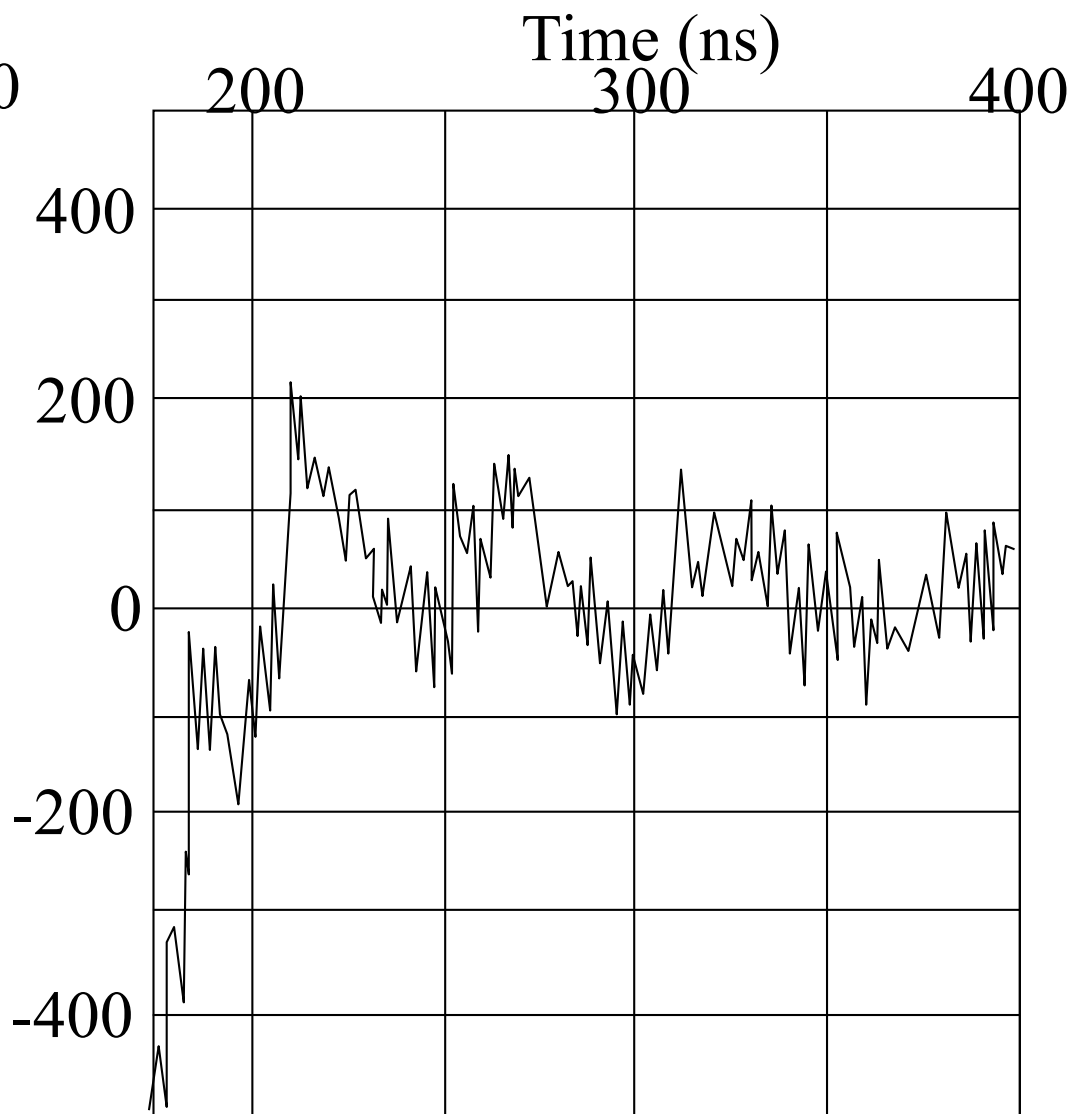


Figure 26

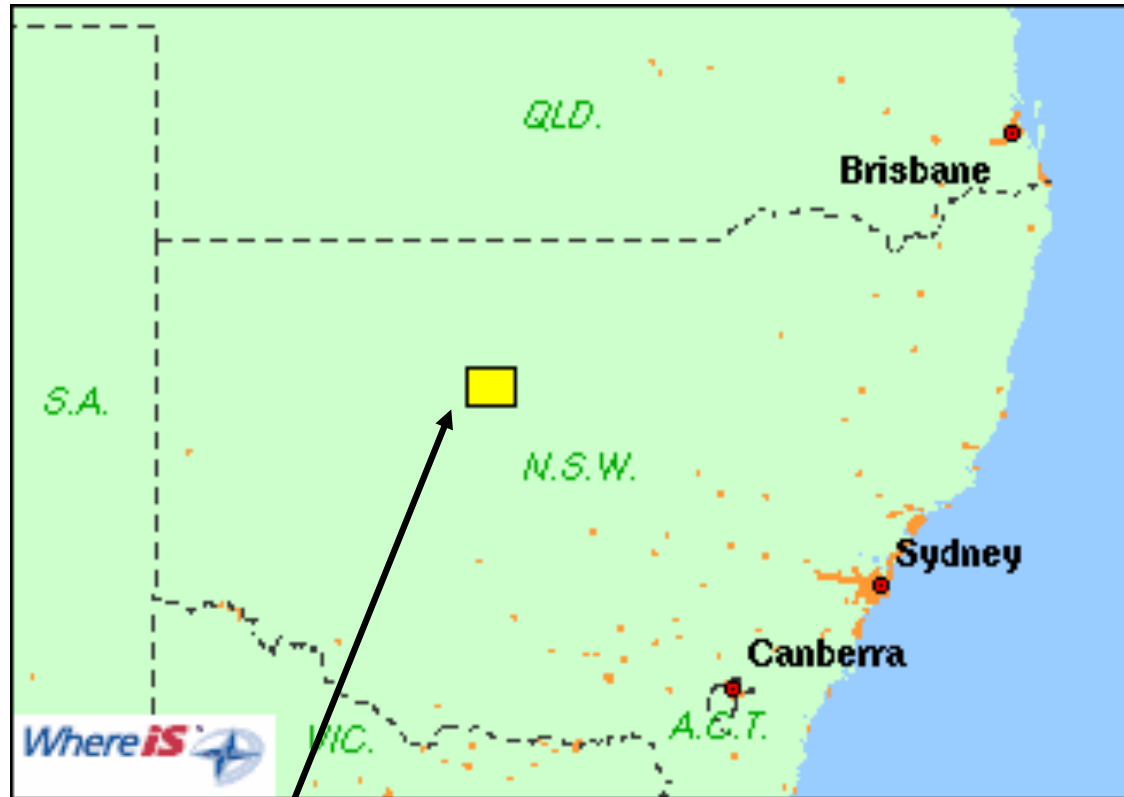


Trace#004  
Apparent resistivity =  $10\Omega\text{m}^{-1}$



Trace#471  
Apparent resistivity =  $40\Omega\text{m}^{-1}$

Figure 27



Girilambone-Cobar  
Study Area

**Figure 28**

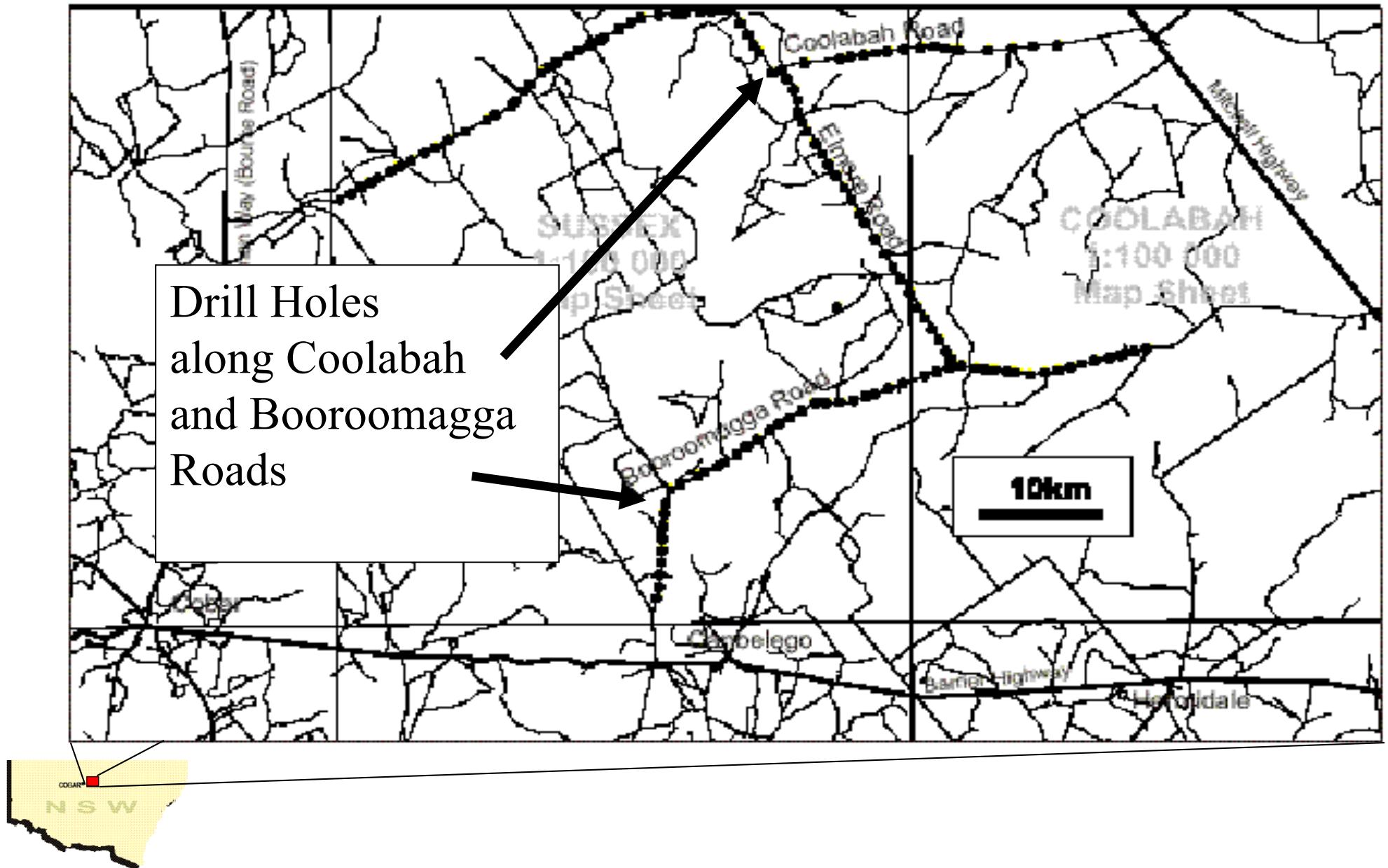
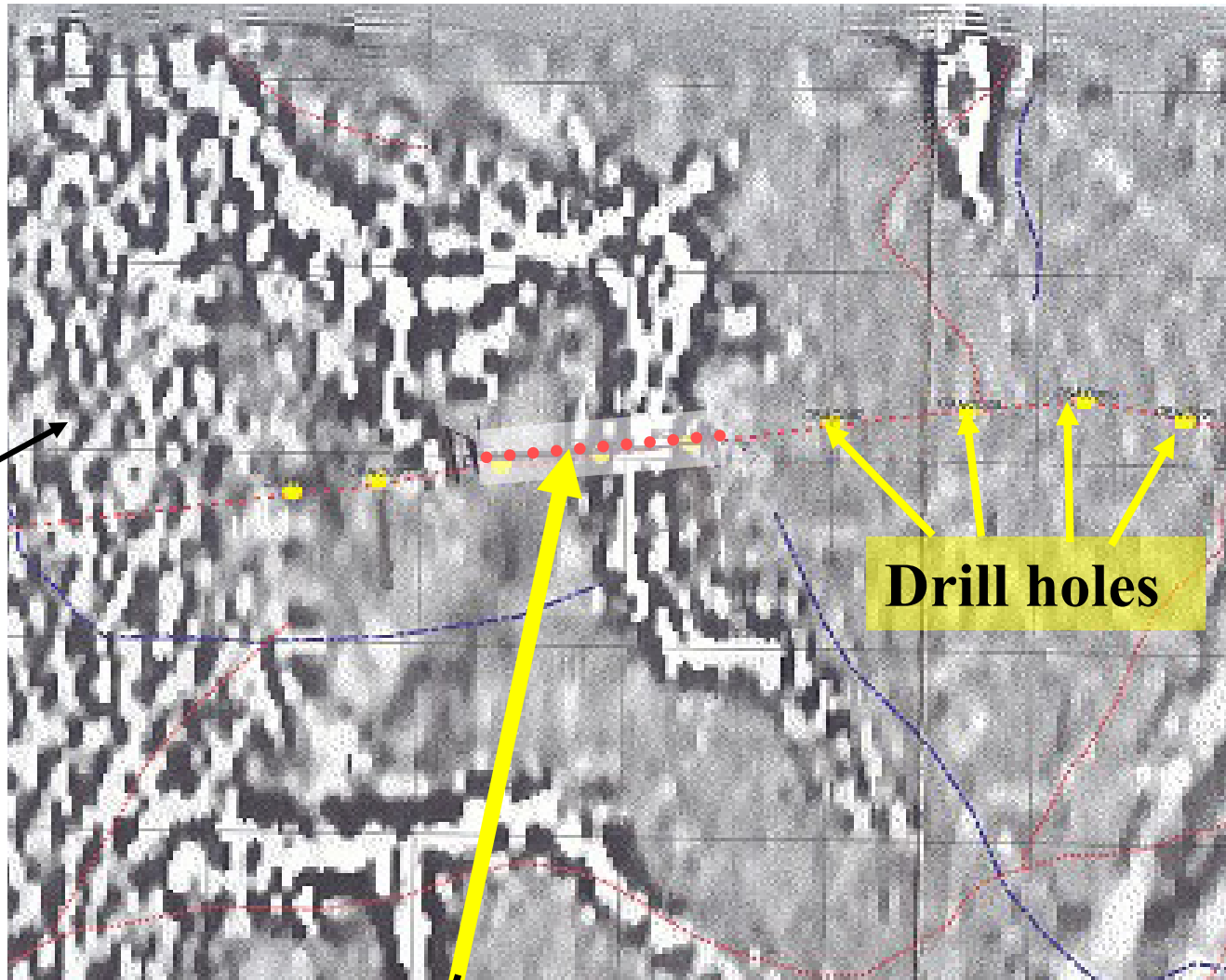


Figure 29

Magnetic features



road

**Drill holes**

Planned Survey Line 1

Figure 30

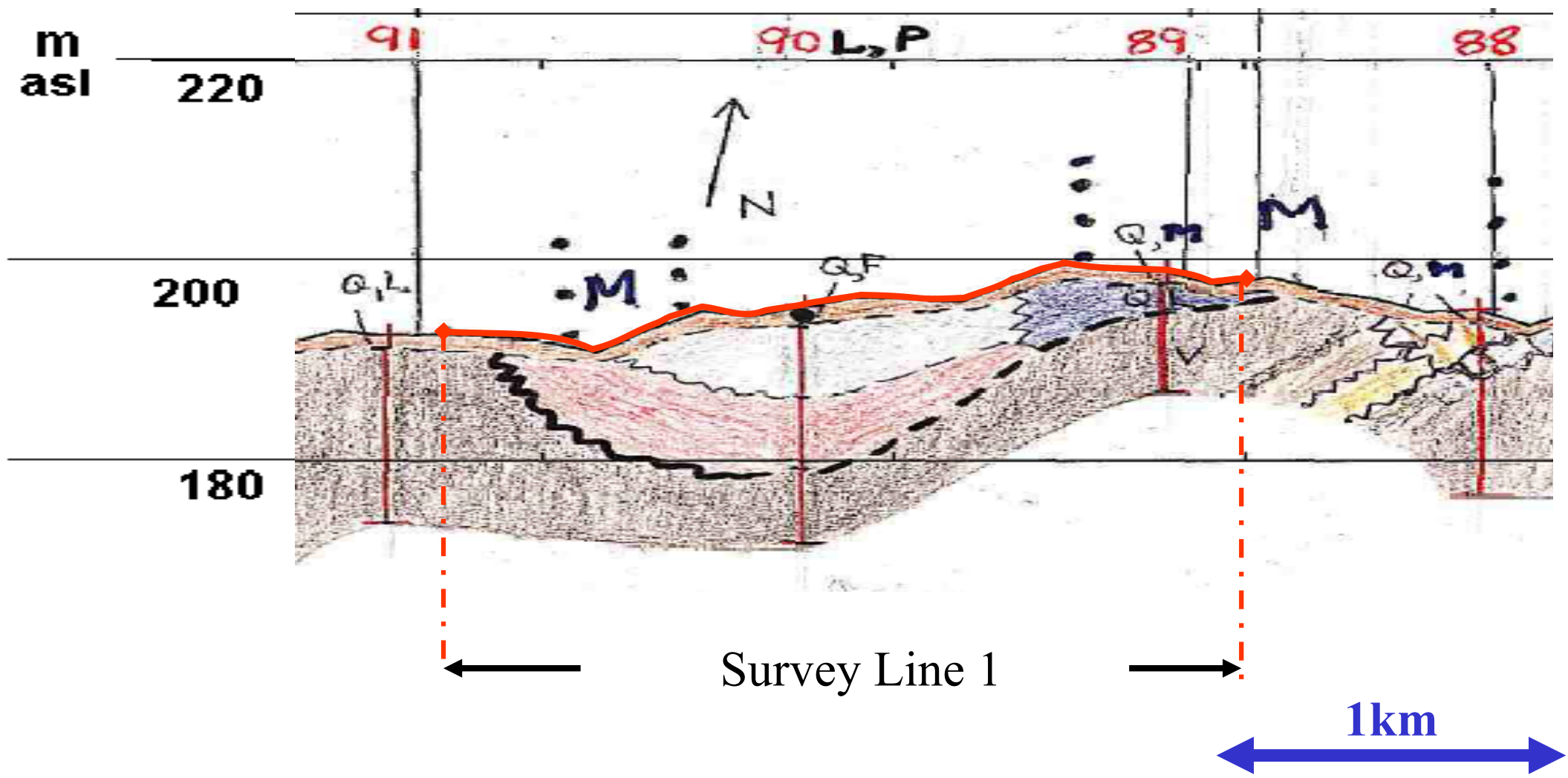


Figure 31

















# LEGEND


## REGOLITH LEGEND FOR DRILL HOLE PROFILES

--- --- Transported - In Site boundary








### TRANSPORTED

-  Gravel
-  Gravel; sand
-  Sand, gravel
-  Sand
-  Sand, clay
-  Sand, clay, gravel
-  Clay, gravel
-  Clay, sand
-  Clay
-  Clay: grey → white
-  Clay: pink
-  Clay: green → yellow
-  Clay: yellow → brown
-  Gravel: coarse sands (1-2mm) → gravels → pebbles (2-4mm) (4-6mm)

### Mixed

 Barren: ochre silt/clay incorporated into existing residual and transported soils

### IN-SITU

-  Saprolite: multicoloured
-  Saprolite: bleached
-  Saprolite: sandstone
-  Saprolite: micaceous sandstone
-  Saprolite: siltstone
-  Saprolite: siltstone, sandy in places
-  Saprolite: conglomerate

### INDUCATED





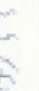
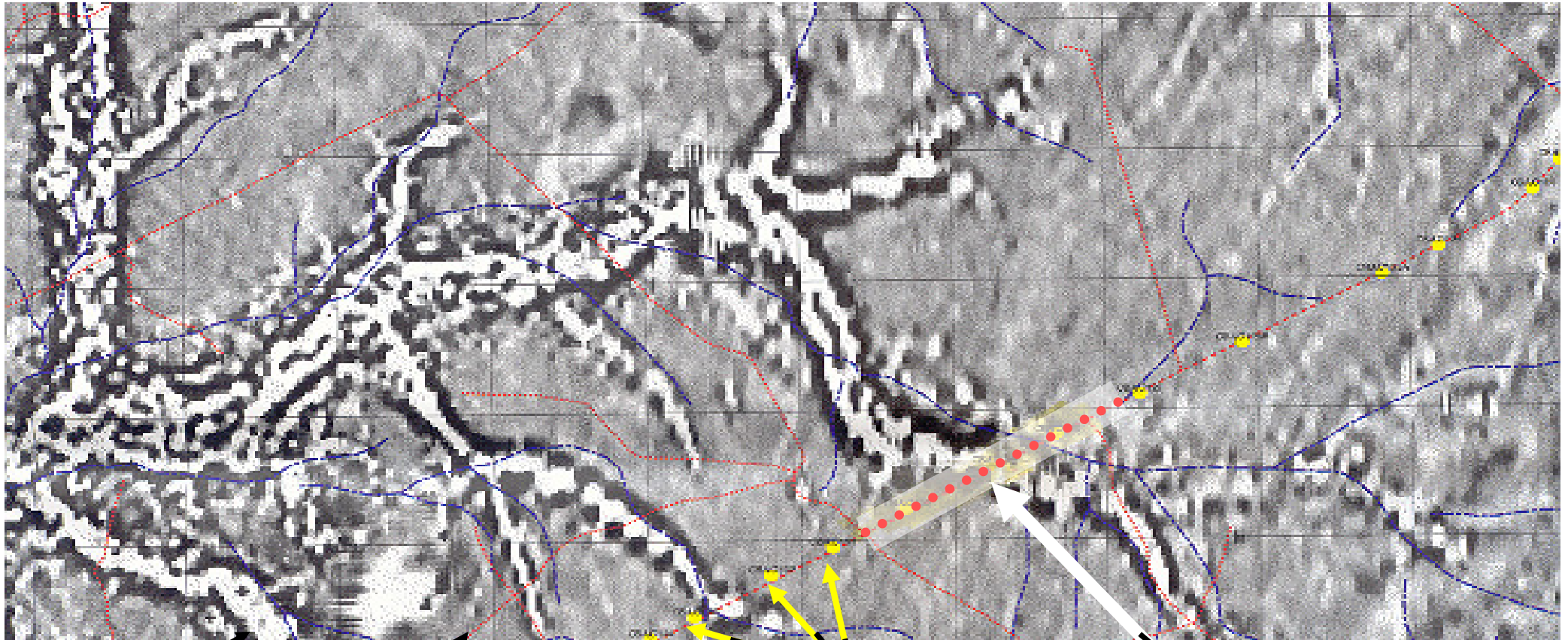
-  Siliceous
  -  Ferruginous
  -  Mottles
  -  Fe staining
  -  Carbonate
- CLASTS
- |   |                               |   |                           |
|---|-------------------------------|---|---------------------------|
| C | Chart                         | Q | Quartz                    |
| F | Ferruginous & red fragments   | L | Little fragments          |
| M | Magnetic particles            | ∩ | Flattening rounded quartz |
| o | Rounded quartz grains/pebbles | V | Vein quartz               |

Figure 31b



Magnetic features

road

Drill holes

Planned Survey Line 2

Figure 32



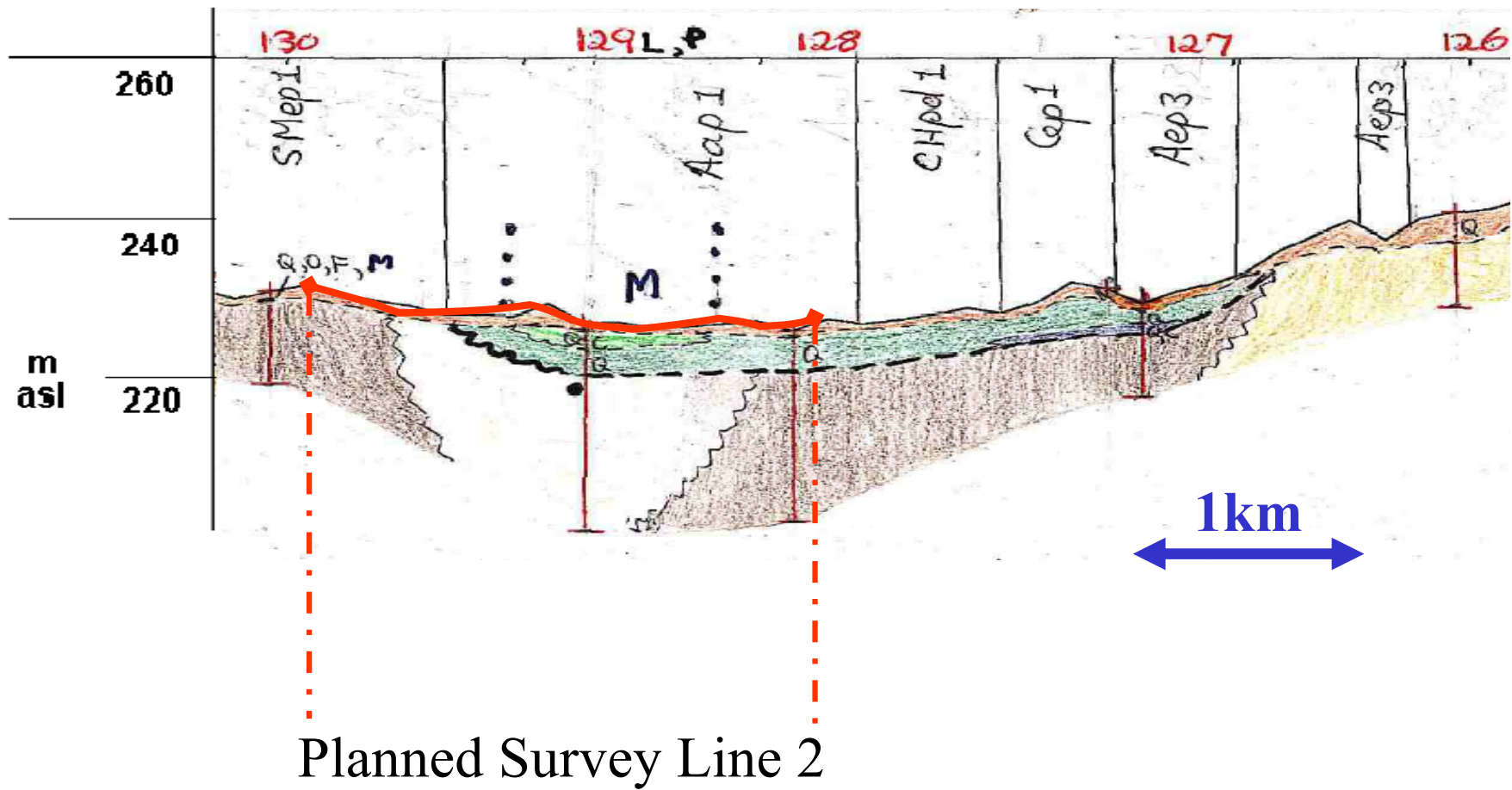


Figure 33

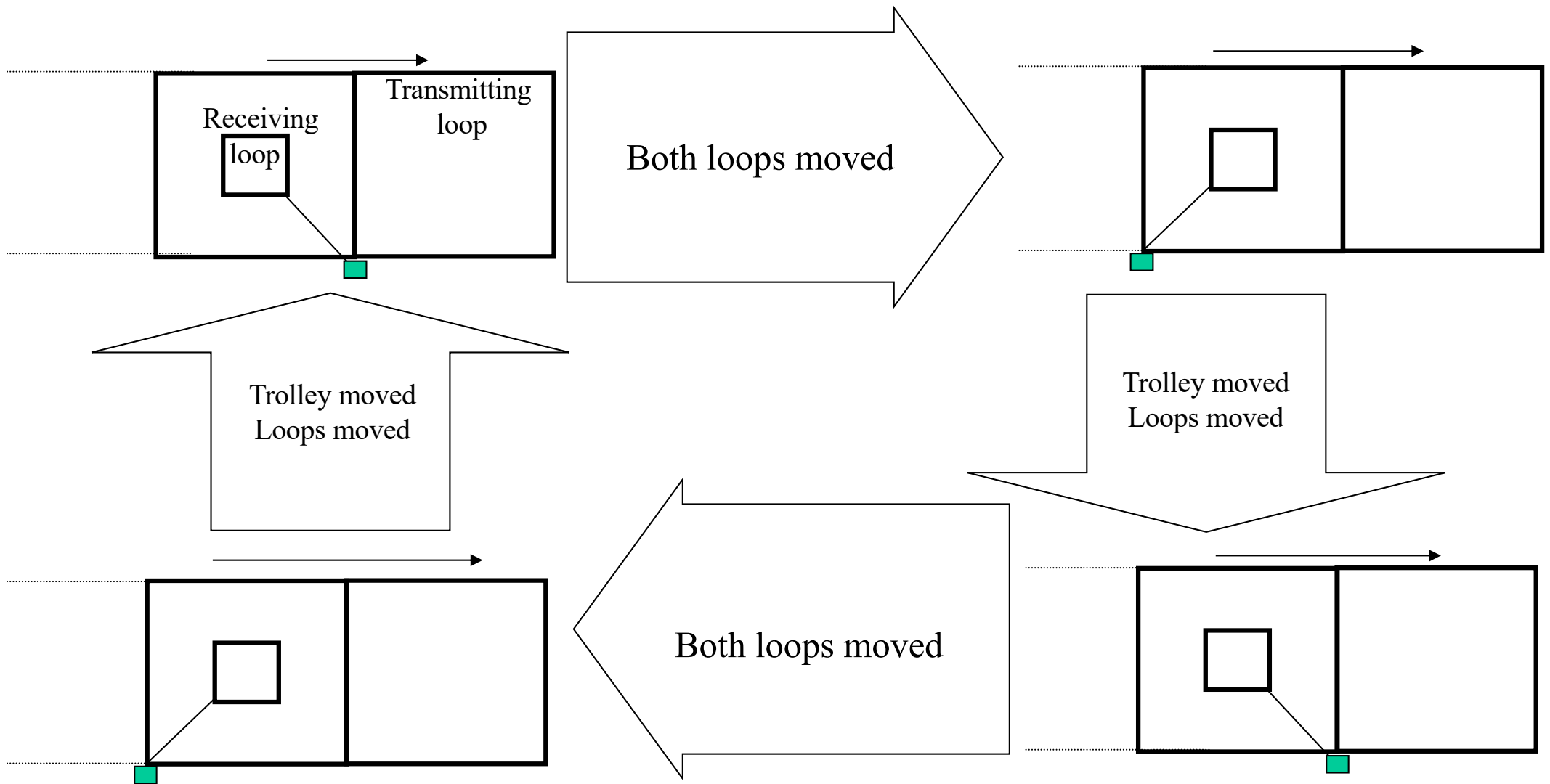
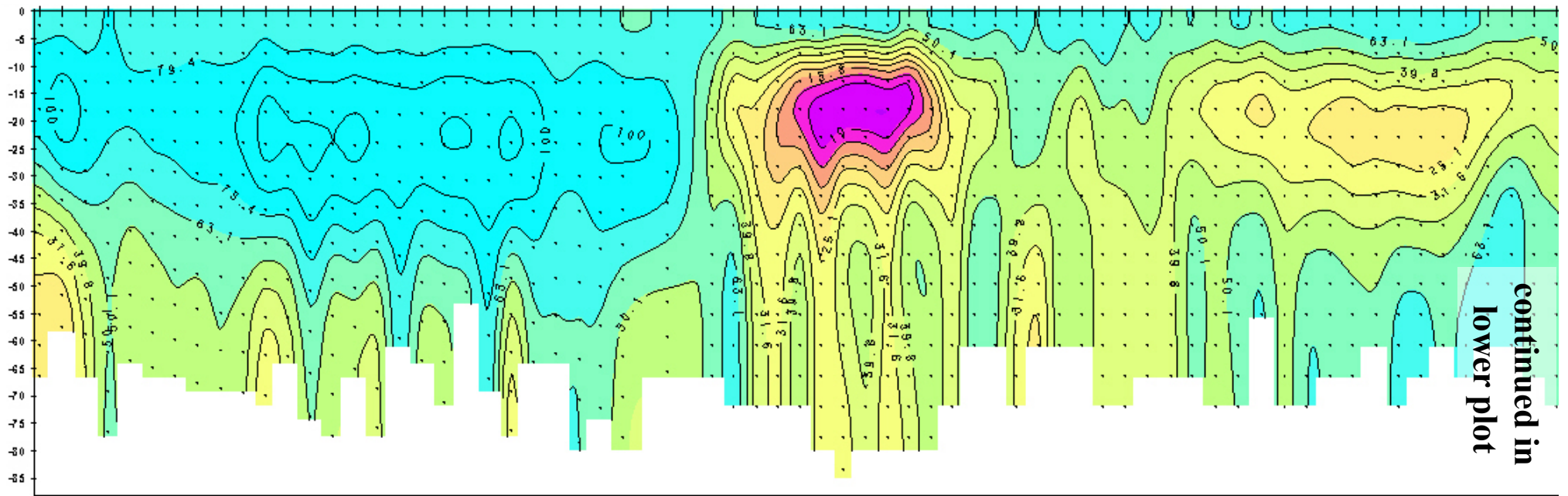
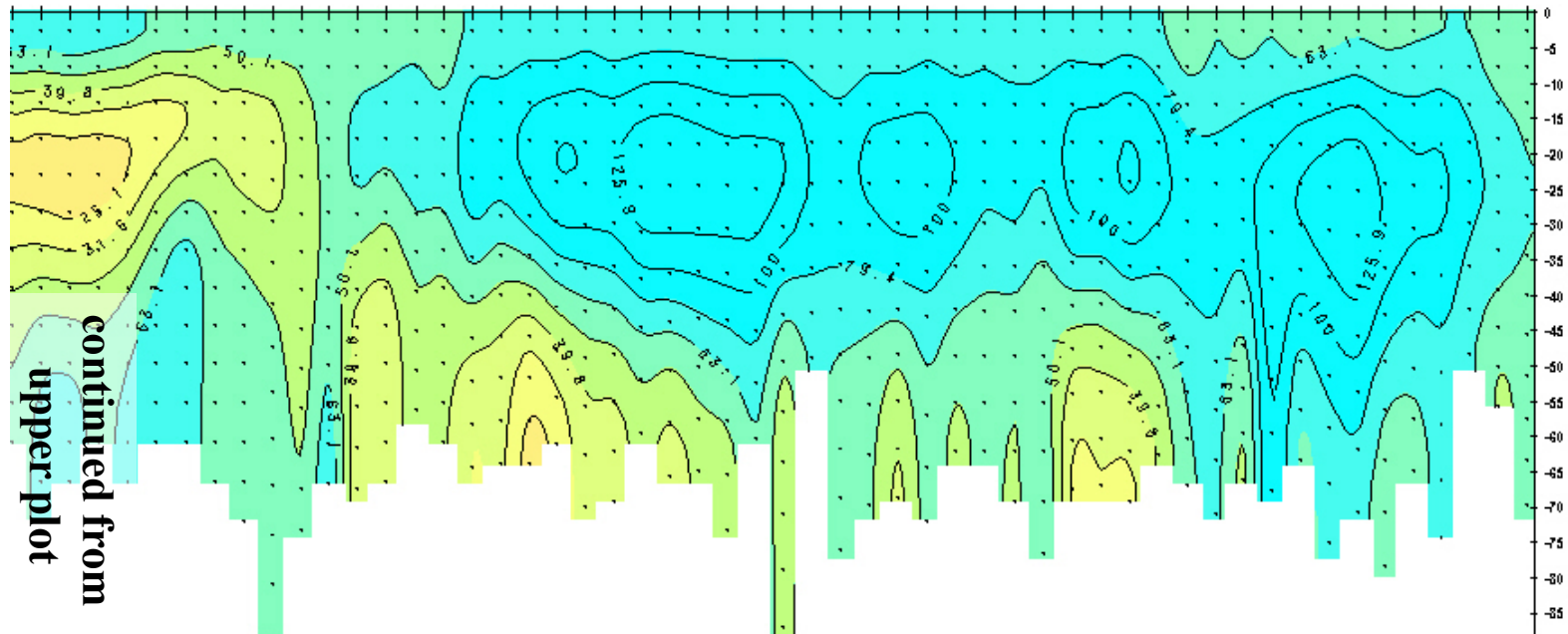


Figure 34



1000 m      ← West      10 m (Depth)

79.4  
50.1  
31.8  
20.0  
12.8  
7.8  
Resistivity  
ohm-m



Girilambone Line 1

Figure 35

# Girilambone Line 2

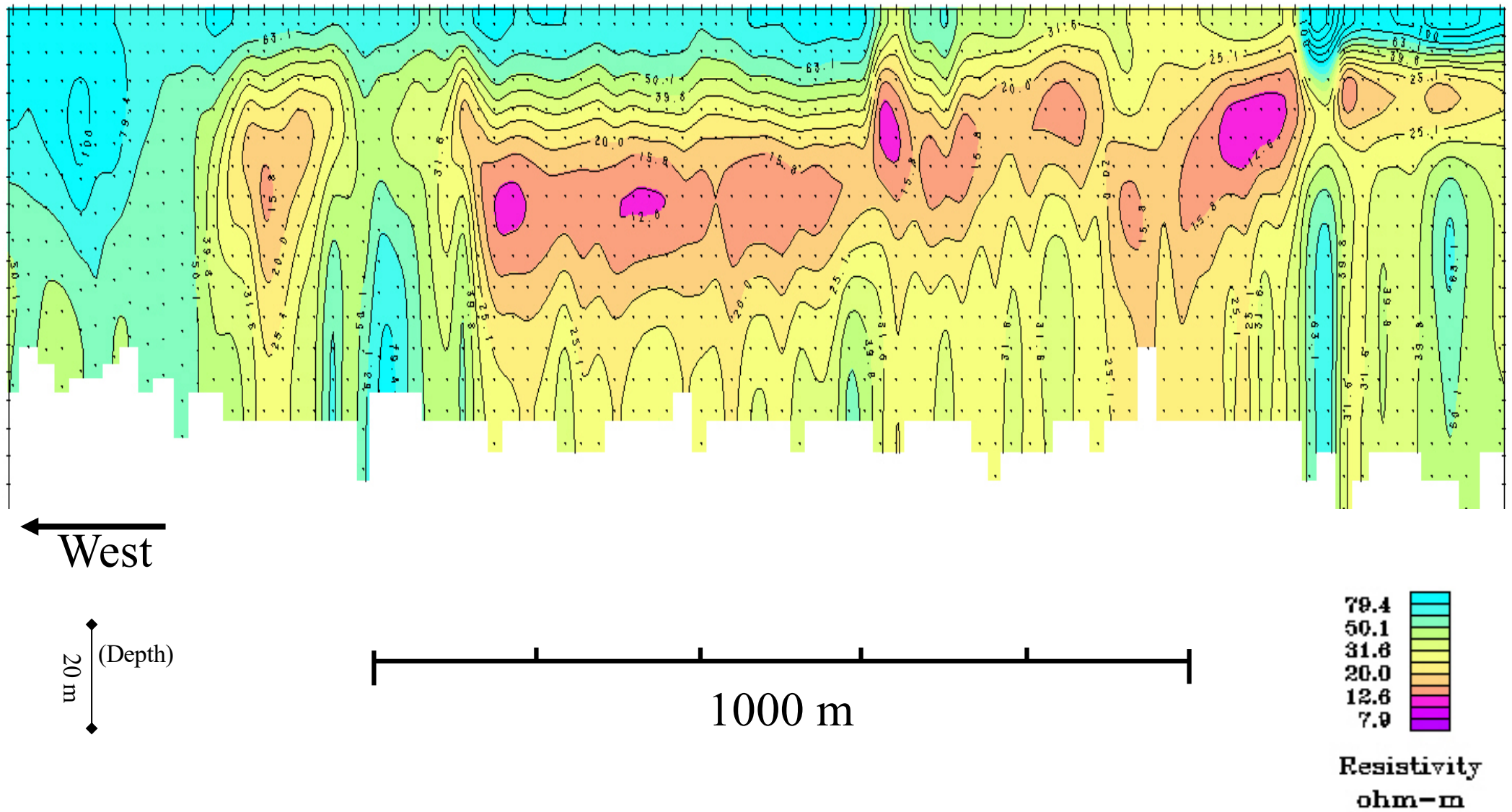
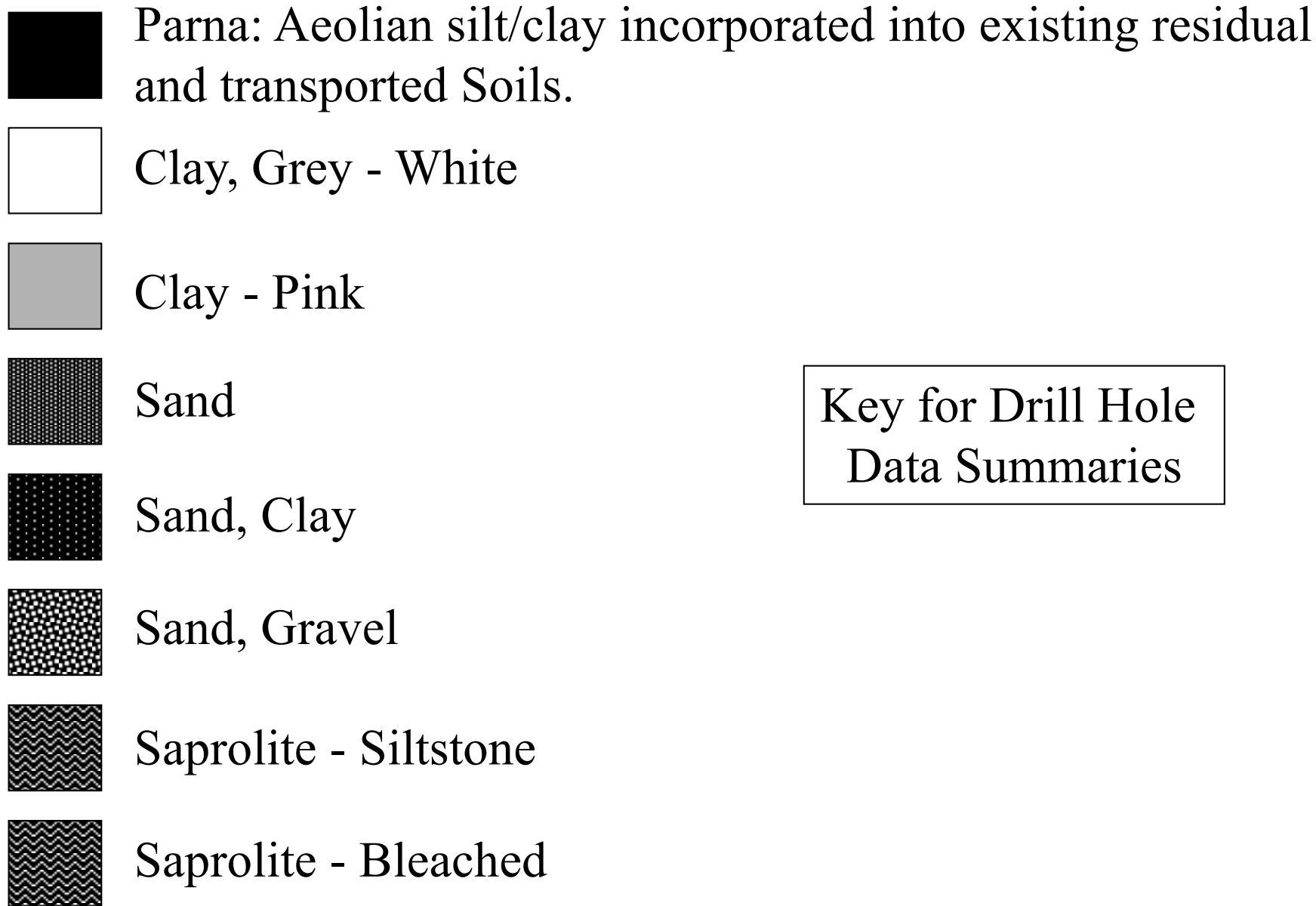


Figure 36



Key for Drill Hole Data Summaries

Figure 37a

# CBAC089

## Resistivity (Ohm m)

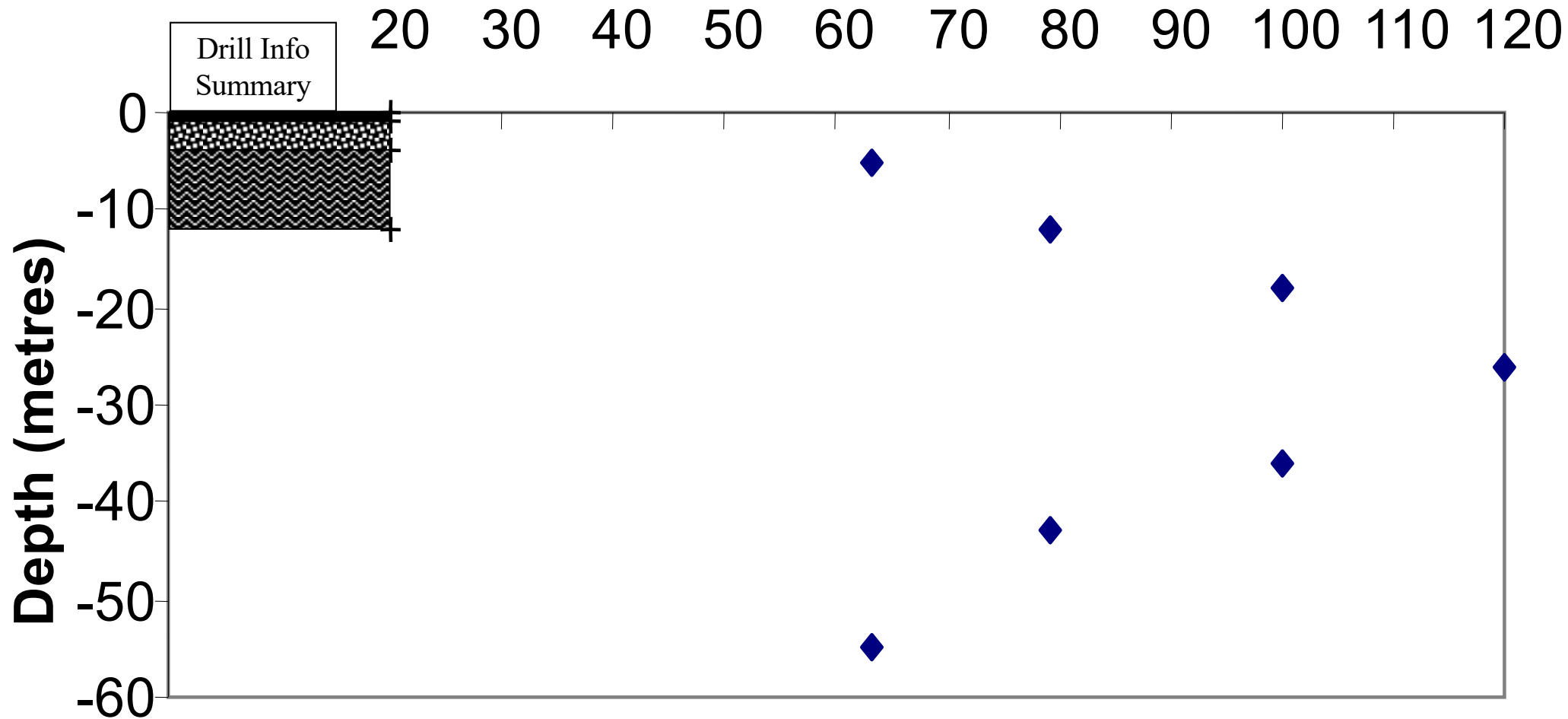


Figure 37b

# CBAC090

Resistivity (Ohm m)

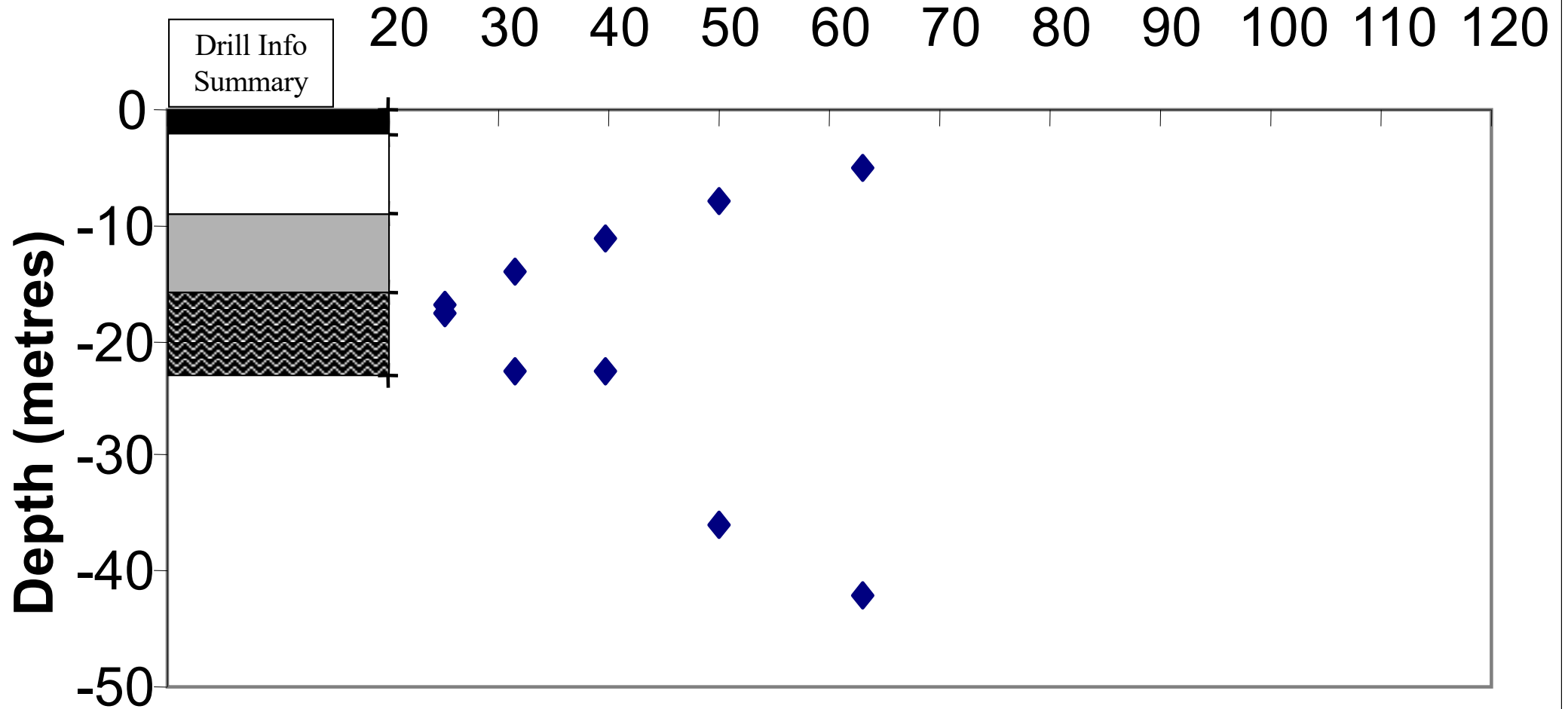


Figure 37c

# CBAC091

Resistivity (Ohm m)

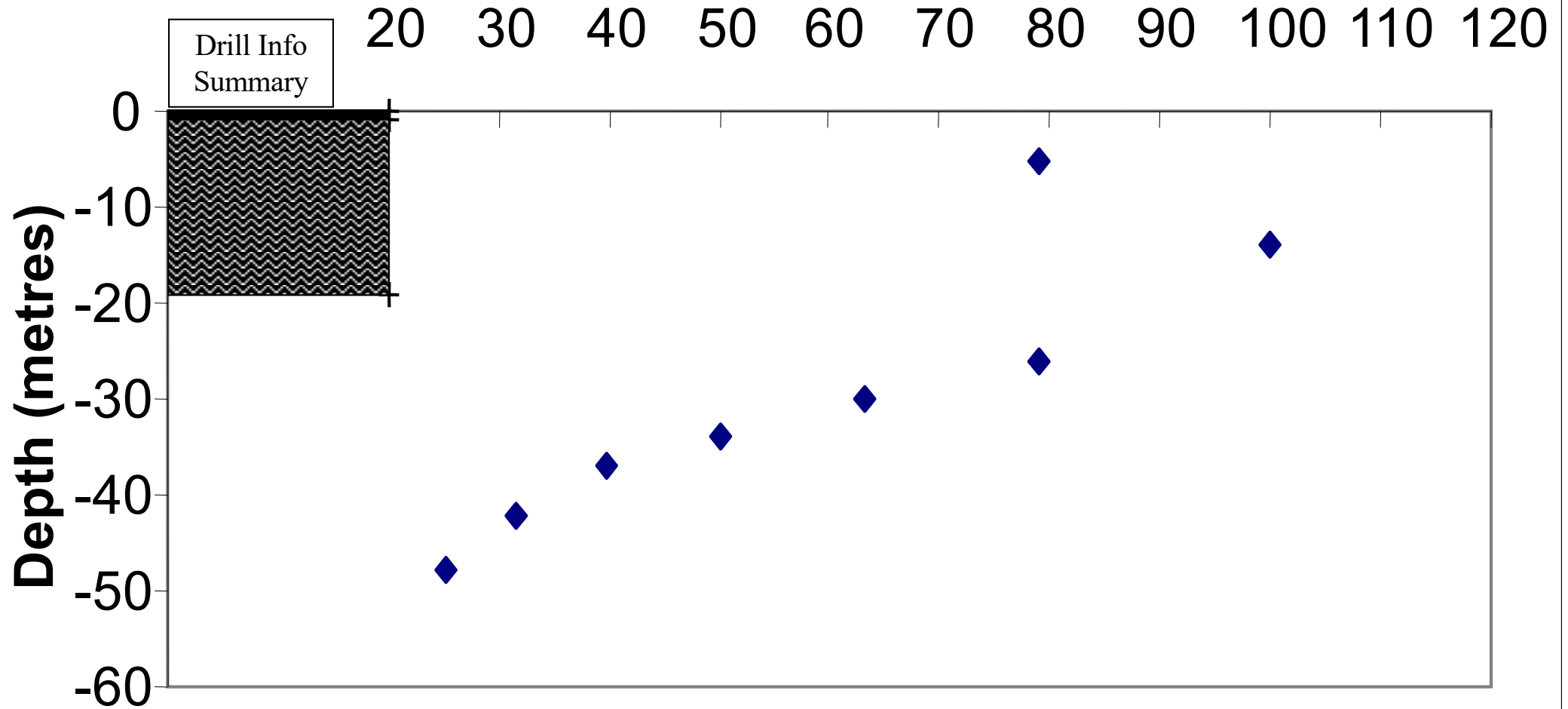


Figure 37d



# CBAC128

Resistivity (Ohm m)

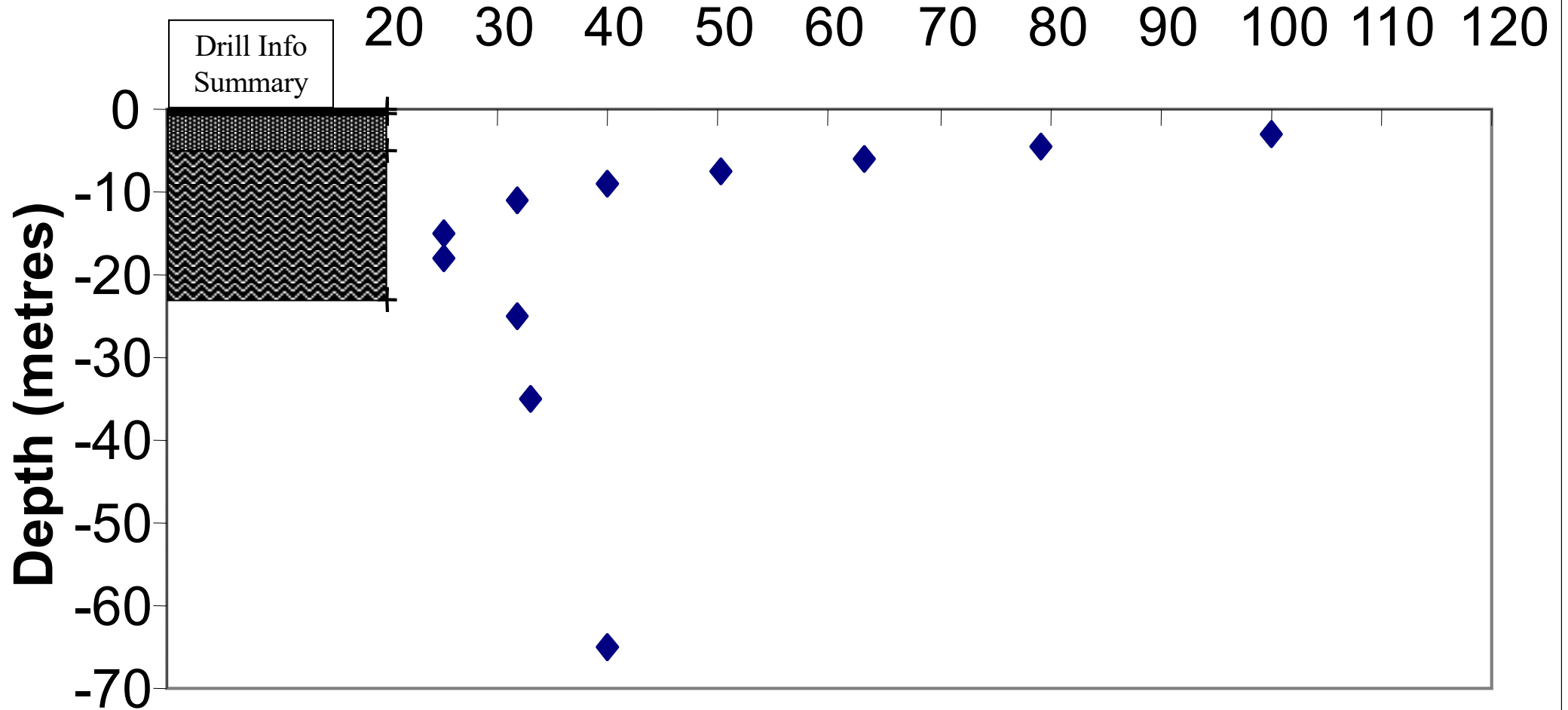


Figure 37e

# CBAC129

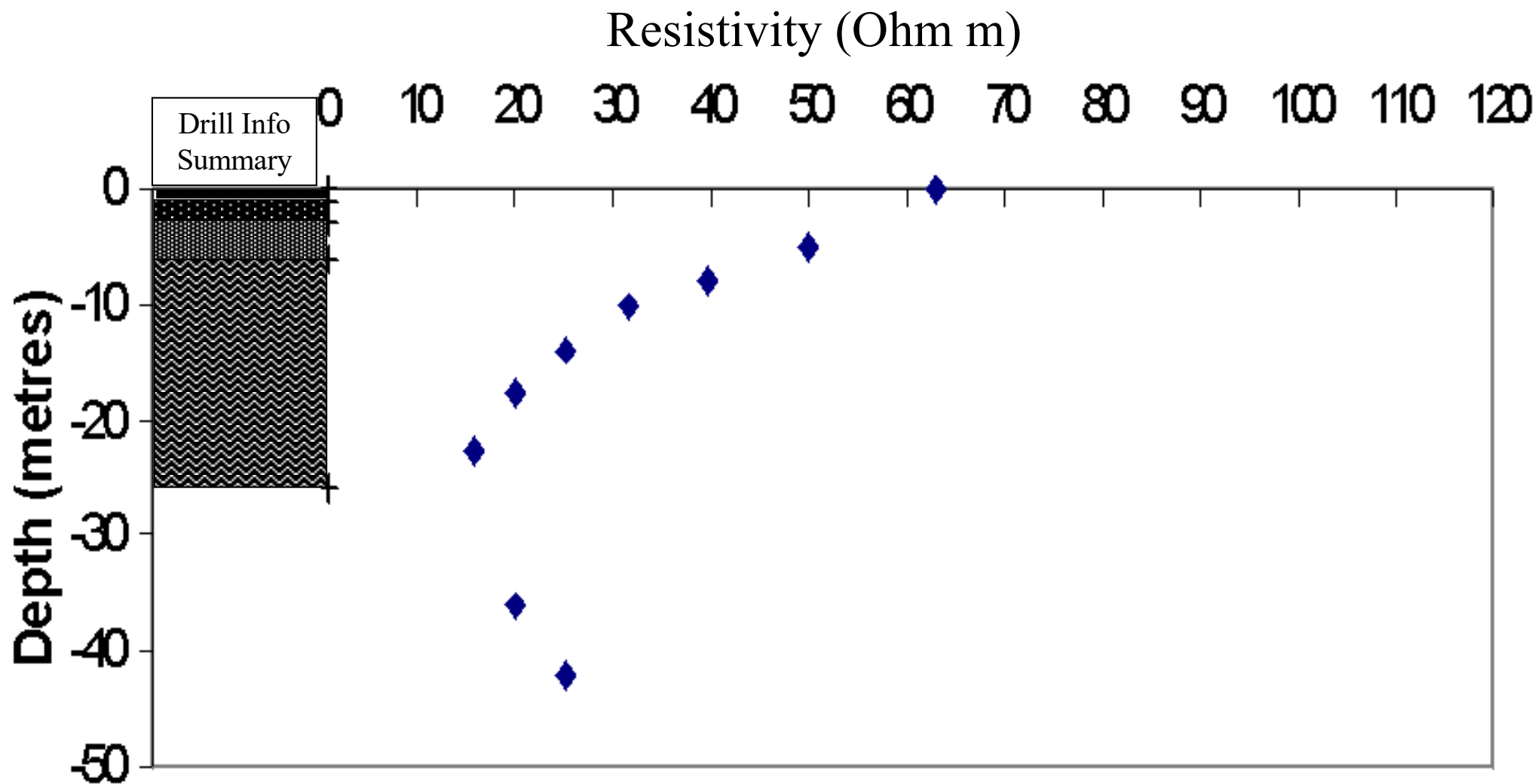


Figure 37f

# CBAC130

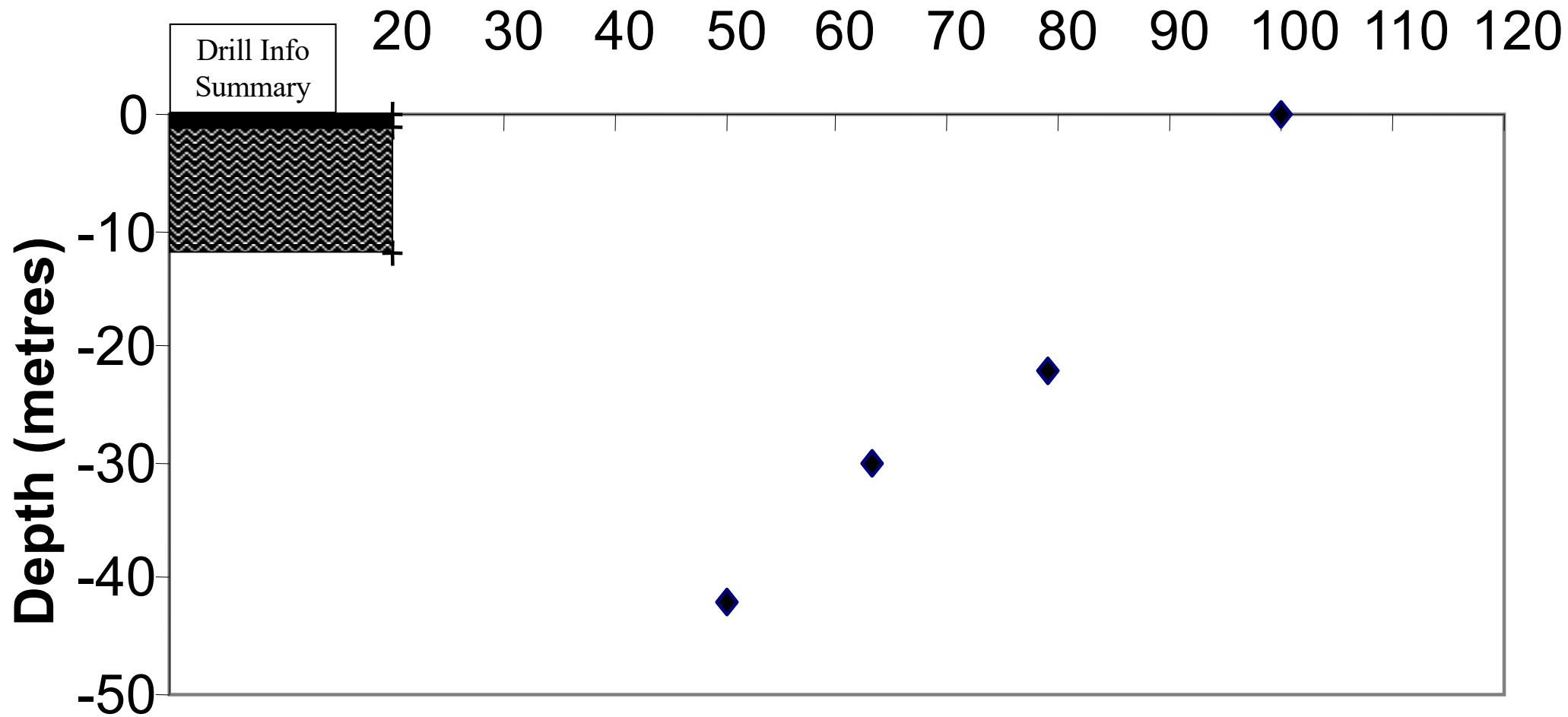


Figure 37g

### Line 1 - with Drill holes CBAC88-CBAC91

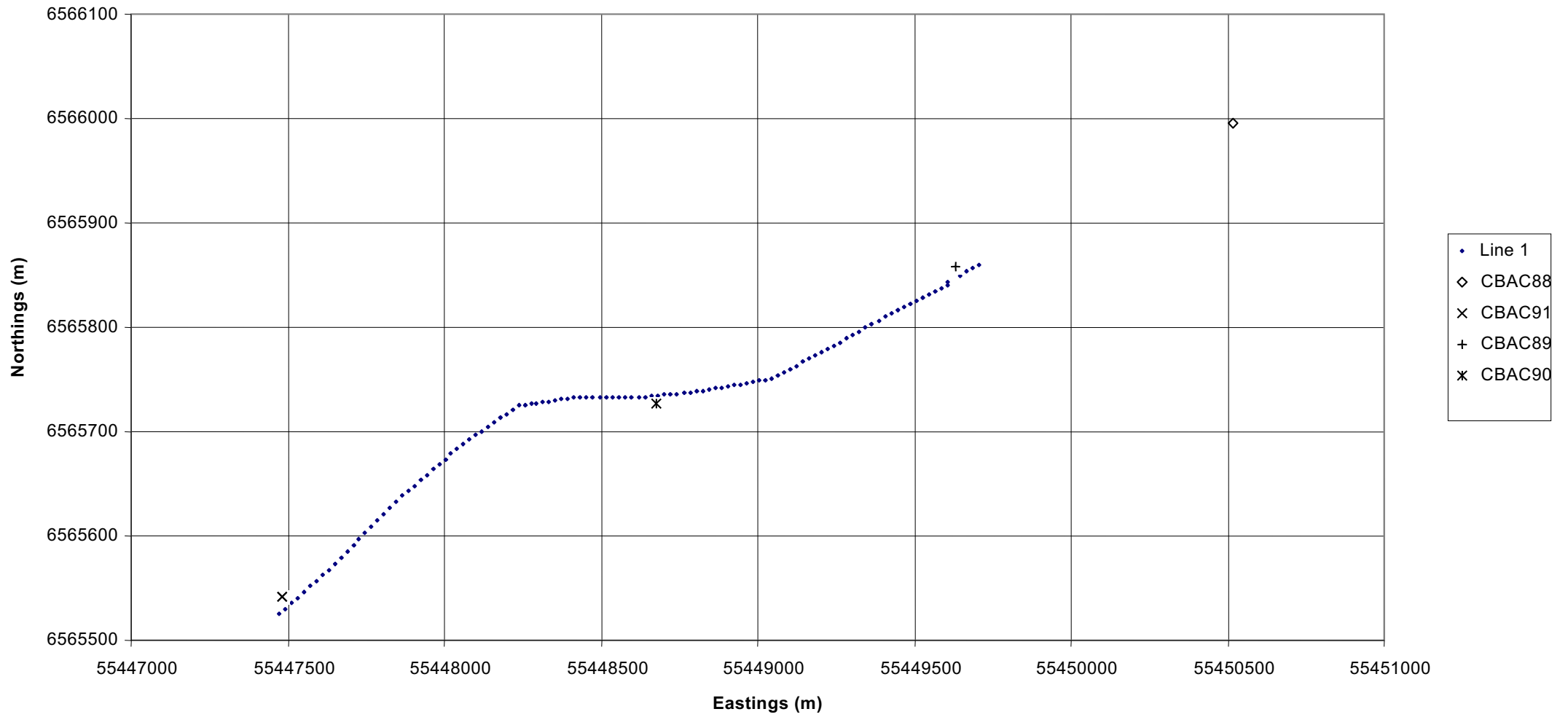


Figure 38a

Line 2, with Drill holes CBAC127-CBAC130

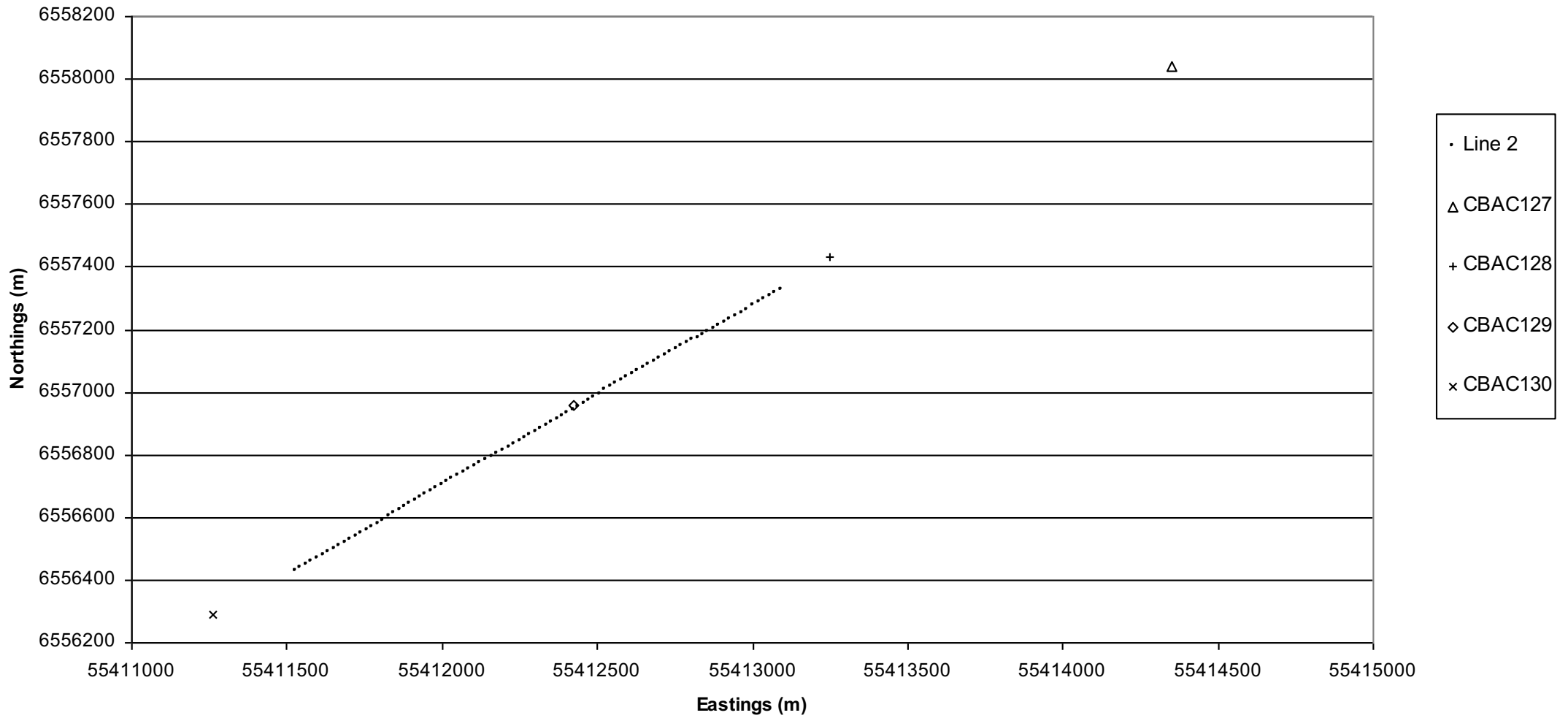


Figure 38b